Titre: Title:	Nano-Delivery System of Nitric Oxide
Auteur: Author:	Laura Karina Mireles Nunez
Date:	2019
Type:	Mémoire ou thèse / Dissertation or Thesis
Référence: Citation:	Mireles Nunez, L. K. (2019). Nano-Delivery System of Nitric Oxide [Ph.D. thesis, Polytechnique Montréal]. PolyPublie. https://publications.polymtl.ca/4148/

POLYTECHNIQUE MONTRÉAL

affiliée à l'Université de Montréal

Nano-delivery system of nitric oxide

LAURA KARINA MIRELES NUNEZ

Institut de génie biomédical

Thèse présentée en vue de l'obtention du diplôme de *Philosophiæ Doctor*

Génie biomédical

Octobre 2019

POLYTECHNIQUE MONTRÉAL

affiliée à l'Université de Montréal

Cette thèse intitulée :

Nano-delivery system of nitric oxide

présentée par **Laura Karina MIRELES NUNEZ**

en vue de l'obtention du diplôme de *Philosophiæ Doctor*

a été dûment acceptée par le jury d'examen constitué de :

Abdellah AJJI, président
L'Hocine YAHIA, membre et directeur de recherche
Edward SACHER, membre et codirecteur de recherche
Oumarou SAVADOGO, membre
Mircea-Alexandru MATEESCU, membre externe

DEDICATION

À mon père ✝

ACKNOWLEDGEMENTS

It is important to mention the gratitude that I have for Prof. L 'Hocine Yahia as my thesis director and Dr. Edward Sacher as my thesis co-director, because with all their knowledge and patience they have guided my thesis work at all times and they have forged my knowledge and professional development with invaluable tools and therefore I feel deeply grateful

Dear Dr. Yahia, I feel the luckiest student to have you as my thesis director, when I started this project I felt it was a big challenge to achieve nitric oxide attachment as no one did before, however your words of encouragement, trust and each time that you told me that you believe in me, they have made this project something attainable and tangible. I don't find enough words of thanks to say thank you, thank you for believing in me always, thanks for understanding me when I lost my father, thanks for your respect me always when I lost what I thought was my family in Montreal, no matter what, you always motivated me, always encouraged me, it has also given me opportunities for growth in the professional area within the university, teaching, participating with industrial projects, in various international collaborations and in my own projects, with you I have learned that the life in addition to being a thesis project, it is a project to grow professionally and personally, the words of support and patience can do everything, and that all objectives can be achieved. Infinite thanks for being my thesis director.

Dear Dr. Sacher, I feel deeply grateful for all the support received, for all your knowledge that has been transmitted to me related to surface characterization, thanks to your patience, for driving me to seek knowledge, to debate, to have judgment defending my points of view and grow in excellence and professionalism when explaining and demonstrating each result. I admire you, professionally and as a person. Thanks for always being for me in every question, in every explanation, demanding at the right times, correcting me, understanding, teaching me the importance of observation, and to fight to show quality work and supporting me in this project that I can say that the success has been thanks to everything I have learned with you.

I would like to thank the members of the Jury of my thesis, Dr. Andellah Ajji, Dr. Oumarou Savadogo, and Dr. Mircea A. Mateescu for their attention given to my work and the honor that this thesis work be judged by you.

Thanks to Suzie Poulin for being my first teacher of XPS and TOF-SIMs, for teaching me so much and sharing her knowledge, helping me to understand concepts and supporting me in handling characterization with all the desire to teach me.

Josianne Lefebvre thank you for everything you have taught me and helped in XPS and TOF-SIMs, for your patience and listening, for always having a moment for me, for being more than my characterization mentor, for believing in me, for always pushing me to go further and always continue with the forehead up.

Dr. Richard Massicote, without a doubt an honor to meet you, work on industrial projects and learn from you, from your simplicity and professionalism.

Thanks to chemists Denis Deschênes and Line Pepin of the University of Montreal, for opening to me the laboratory doors, listening to all the ideas of my experiments, supporting me and helping me to achieve all my goals. Always being willing to support me with a smile.

Thanks to Doris Mbeh for being the more than my college and sharing more an office, for being my friend and my teacher, teaching me biocompatibility concepts, listening me, laughing with me, supporting me and sharing many beautiful moments of my PhD.

Thank you Ghislaine Bayade for all the encouragement and support received, such beautiful details that energize our workplace that we call office.

Thanks to Insaf Hadjab, for sharing with me the experience of teaching, friendship, teamwork and collaboration.

Thanks to all the students and collegues that shared pleasant moments in LIAB with me: Taraneh Djavanbakht, Naziha Chirani, Melika Parsapour, Sylvie Lau, Rosario, Luka, Federico, Arthur Ruellan, Mohammad Tabai, who shared with me smiles, to say good morning to start every morning with energy, to share the nicest breakfasts, coffees and meal hours together, as well as the knowledge of each of their projects.

Thanks to each and every one of my summer students, students of integrator projects, and students taking Dr. Yahia's courses, because in each project I learned to be better and do my best for helping to grow in knowledge to others.

Thanks to my family, my brother and my friends for their interest in my work, for sharing their support and encouragement with me.

Thank you, Alejandra Salazar, for always having been there, always driving me and giving everything of you for supporting me to moving on.

Thank you Wassim, thanks for appearing in my life motivating me with your joy, thanks to believe in me, being by my side and show me with actions all that words cannot explain.

RÉSUMÉ

Avancées récentes en nanotechnologie ont conduit au développement de nanomatériaux magnétiques tels que des nanoparticules d'oxyde de fer (Fe3O4) utilisées comme nanoaporteurs dans des applications de libération de médicaments et considèrent ces nanoparticules comme des candidats à la libération de monoxyde d'azote (NO) pour interagir contre la formation de biofilm.

Cette thèse est constituée trois articles, décrivant la méthodologie pour développer un système de nano-libération de monoxyde d'azote avec des nanoparticules d'oxyde de fer superparamagnétique (SPION). Une étude approfondie de la modification de la surface des SPION est rapportée, où il a été montré que les nanoparticules avaient une composition chimique non uniforme et des variations d'un lot à l'autre. L'effet de lavage des SPIONs par dialyse s'est avéré être une méthode inefficace pour l'élimination des espèces chimiques indésirables sur les surfaces, en plus de l'interaction des espèces chimiques avec l'environnement et l'atmosphère a été trouvée, générant une oxydation des espèces. La PEGylation et le revêtement de nanoparticules avec de l’acide dimercaptosuccinique (DMSA) ont été proposés afin d'homogénéiser la surface et permettre à la surface avec des groupes thiol pour attacher des molécules de NO. L'utilisation de techniques de caractérisation à haute sensibilité a permis la démonstration des revêtements de SPIONs avec PEG-dithiol et DMSA, ainsi que l'existence de la liaison covalente S-NO. En tant qu'innovation et contribution à cette thèse de doctorat montre l'attachement chimique de monoxyde d'azote aux SPIONs, comme cela n'a été démontré par aucun outre article de recherche publié avant.

ABSTRACT

Recent advances in nanotechnology have led to the development of magnetic nanomaterials, such as iron oxide nanoparticles (Fe_3O_4), as nanocarriers in drug delivery applications. We consider such nanoparticles as candidates for nitric oxide (NO) release, to counter biofilm formation. Nitric oxide release is proposed because NO prevents bacterial adhesion on implant surfaces and, subsequently, inhibits biofilms formation.

This thesis contains three papers, describing the methodology to develop a nitric oxide nano-delivery system, using superparamagnetic iron oxide nanoparticles (SPIONs). An extensive study of the surface modification of SPIONs is reported, where it was shown that the nanoparticles had a non-uniform chemical composition and batch-to-batch variations. The washing of SPIONs by dialysis turned out to be an ineffective method for the elimination of unwanted surface chemical species; in addition, the interaction of these chemical species with the atmosphere was found to lead to oxidation. PEGylation of the nanoparticles with PEG dithiol, and coating them with dimercaptosuccinic acid (DMSA), were used to both make the surface uniform and provide thiol groups for anchoring nitric oxide (NO) molecules. The use of highly sensitive characterization techniques permitted the demonstration of SPION coating with both PEG-dithiol and DMSA, as well as the existence of the covalently bonded S-NO. This thesis reveals the chemical attachment of nitric oxide to SPIONs, something that not previously been demonstrated.

TABLE OF CONTENTS

DEDICATION III

ACKNOWLEDGEMENTS IV

RÉSUMÉ VII

ABSTRACT VIII

TABLE OF CONTENTS IX

LIST OF TABLES XIII

LIST OF FIGURES XIV

LIST OF SYMBOLS AND ABBREVIATIONS XVII

CHAPTER 1 INTRODUCTION 1

CHAPTER 2 LITERATURE REVIEW OF IRON OXIDE NANOPARTICLES AS VEHICLES OF NITRIC OXIDE DELIVERY 3

2.1 Why is a nano-delivery system of nitric oxide necessary? 3

2.2 Nanomaterials 3

2.3 Nanomaterials applied in the biomedical field 4

2.4 Nanoparticles as promising technology against biofilm formation on implants 5

2.5 Superparamagnetic iron oxide nanoparticles 7

2.6 Dimercaptosuccinic acid (DMSA) and polyethylene glycol (peg) as polymeric coatings 8

2.7 Nitric oxide in physiological biology and biomedical applications 9

2.8 Iron oxide nanoparticles as vehicle to release nitric oxide 10

2.9 Biocompatibility 11

2.10 Cytotoxicity 12

CHAPTER 3 OBJECTIVES, APPROACH AND HYPOTHESIS 13

3.1 Context 13

3.2 General objective....14
3.3 Specific objectives....14
3.4 Approach and hypothesis....14
3.5 Iron oxide nanoparticles....15
3.6 DMSA....15
3.7 PEG-dithiol....15
CHAPTER 4 CHARACTERIZATION TECHNIQUES....16
4.1 Transmission electron microscopy (TEM)....16
4.2 Fourier-transform infrared spectroscopy (FTIR)....18
4.3 Vibrating sample magnetometry (VSM)....19
4.4 X-ray photoelectron spectroscopy (XPS)....19
4.5 Time of flight secondary ion mass spectrometry (ToF SIMS)....22
CHAPTER 5 ARTICLE 1: A COMPARATIVE PHYSICOCHEMICAL, MORPHOLOGICAL AND MAGNETIC STUDY OF SILANE-FUNCTIONALIZED SUPERPARAMAGNETIC IRON OXIDE NANOPARTICLES PREPARED BY ALKALINE COPRECIPITATION. 25
5.1 Graphical abstract....25
5.2 Highlights....25
5.3 Abstract....26
5.4 Introduction....26
5.5 Materials and methods....28
5.6 Characterizations....29
5.7 Results....30
5.7.4 FTIR spectroscopy....37
5.7.5 TOF-SIMS....38
5.8 Discussion....40

5.8.1 Surface characterization 41

5.9 Conclusions 42

5.10 Acknowledgements 42

References 43

CHAPTER 6 ARTICLE 2: WASHING EFFECT ON SUPERPARAMAGNETIC IRON OXIDE NANOPARTICLES 46

6.1 Abstract 46

6.2 Specifications table 47

6.3 Value of the data 47

6.4 Data 48

6.5 Experimental design, materials and methods 48

6.6 Acknowledgements 51

References 52

CHAPTER 7 ARTICLE 3: NITRIC OXIDE ATTACHMENT TO SPIONS: DEMONSTRATION OF THE COVALENT S-NO BOND IN A NANODELIVERY SYSTEM 53

7.1 Graphical abstract 53

7.2 Highlights 54

7.3 Abstract 54

7.4 Introduction 54

7.5 Materials and methods 56

7.6 Physicochemical characterizations 57

7.7 Results 58

7.8 Discussion 71

7.9 Conclusions 78

7.10 Acknowledgements 78

References 79

CHAPTER 8 GENERAL DISCUSSION 83

8.1 Synthesis of nanoparticles 83

8.2 Characterization techniques 84

8.3 Washing effect – dialysis 86

8.4 Surface contaminants 87

8.5 S-NO attachment 88

8.6 Coating selection – thiolation 88

8.7 Funcionalization – covalent bonds 90

8.8 Difficulties, challenges and contributions 92

CHAPTER 9 CONCLUSIONS AND RECOMMENDATIONS 94

9.1 Conclusions 94

9.2 Recommendations 95

REFERENCES 96

LIST OF TABLES

Table 5.1 Summary of XPS deconvolution of SPIONs from the first and second batches…….39

Table 5.2 Attribution of FTIR peaks from the first batch……..……..42

Table 5.3 Masses and attributions of the fragments found in SPIONs from the first batch…….41

Table 6.1 Specifications……..……..…….…...51

Table 6.2 Summary of XPS spectral deconvolutions of SPIONs, second batch, before and after dialysis…….…….…..55

Table 7.1 XPS peak attributions of functionalized SPIONs……...67

Table 7.2 XPS peak attributions of functionalized SPIONs under a nitrogen atmosphere……75

Table 7.3 A comparison of influences of oxygen and nitrogen atmospheres…….....82

LIST OF FIGURES

Figure 4.1 Schematic diagram of TEM system……20

Figure 4.2 Schematic diagram of the IR spectroscopy……21

Figure 4.3 Absorption of a photon and resultant expulsion of a 1s level photoelectron……23

Figure 4.4 Sketch of the functional principle of a ToF-SIMS instrument……...26

Figure 5.1 TEM images of: (a) bare SPIONs (b) positive SPIONs and (c) negative SPIONs…34

Figure 5.2 Size distributions of: (a) bare, (b) positive and (c) negative SPIONs……34

Figure 5.3 Magnetization curves of SPIONs……43

Figure 5.4 High resolution XPS spectra of bare, positive and negative SPIONs (first batch)…37

Figure 5.5 High resolution XPS spectra of positive, negative and bare SPIONs (second batch)..38

Figure 5.6 HRTEM photomicrographs of (a) positive, (b) negative and (c) bare SPIONs. Each sample lacks a visible surface coating……..…..40

Figure 5.7. IR spectra of bare, positive and negative SPIONs……..…41

Figure 5.8 Positive and negative SIMS spectra of ((a) and (b)) bare, ((c) and (d)) positive and ((e) and (f)) negative SPIONs……..…..……43

Figure 5.9 High resolution SIMS comparisons of (a) NH2 peaks (M: 16.01), (b) COOH peaks (M: 44.99), of the SPIONs……44

Figure 6.1 High resolution XPS spectra of positive, negative and bare SPIONs, second batch, before dialysis……..…….53

Figure 6.2 High resolution XPS spectra of positive, negative and bare SPIONs, second batch, after dialysis……..…54

Figure 7.1 a) SPIONs, b) a thin PEG layer is visible around the SPIONs, c) PEG thickness is seen to be quite variable. The histogram d) shows the size distribution of the bare SPIONs; e) shows the size distribution of the PEGylated SPIONs and f) shows the size distribution of the PEG layer (2.7 ± 1.3 nm). The length of a PEG dithiol chain, Mn ~ 1000, is ~ 3x the size of the average thickness……..……..63

Figure 7.2 a) SPIONs, b) a thin DMSA layer is visible around the SPIONs, c) the shell thickness is seen to be quite uniform; average thickness of 3.1 nm ±1.7 nm. The histogram d) shows the size distribution of the bare SPIONs; e) shows the size distribution of the coated SPIONs and f) shows the size distribution of the DMSA layer (3.1 ± 1.7 nm). The length of a DMSA molecule is about ¼ that of the average thickness……..…..…..64

Figure 7.3 XPS peaks of SPION@DMSA (upper series), and SPION@DMSA@NO (lower series)……...….65

Figure 7.4 XPS peaks of SPION@PEGdithiol (upper series) and SPION@PEGdithiol@NO (lower series)……66

Figure 7.5 TOF-SIMS HR spectra of SPION@PEGdithiol.....68

Figure 7.6 TOF-SIMS HR spectra of SPIONs@DMSA.....69

Figure 7.7 TOF-SIMS HR spectra of SPION@PEGdithiol@NO.....70

Figure 7.8 TOF-SIMS HR spectra of SPION@DMSA@NO.....71

Figure 7.9 FTIR spectral comparisons of a) SPION@PEGdithiol and SPION@PEGdithiol@NO and b) SPION@DMSA and SPION@DMSA@NO.....72

Figure 7.10 XPS peaks of SPION@PEGdithiol (upper series) and SPION@PEGdithiol@NO (lower series) under a nitrogen atmosphere…….…….73

Figure 7.11 XPS peaks of SPION@DMSA (upper series) and SPION@DMSA@NO (lower series) under a nitrogen atmosphere……...74

Figure 7.12 ToF-SIMS HR spectra of SPION@PEG dithiol under nitrogen atmosphere……..77

Figure 7.13 TOF-SIMS HR spectra of SPION@DMSA under a nitrogen atmosphere……..…78

Figure 7.14 TOF-SIMS HR spectra of SPION@PEGdithiol@NO under a nitrogen atmosphere…….……...……..79

Figure 7.15 TOF-SIMS HR spectra of SPION@DMSA@NO under a nitrogen atmosphere…...80

Figure 7.16 XPS peak fitting of C1s and Fe2p spectra……..81

Figure 8.1 Molecular schema of PEG-dithiol and DMSA……..…93

LIST OF SYMBOLS AND ABBREVIATIONS

ATR	Attenuated total reflection
DEG	Diethylene glycol
DMSA	Dimercaptosuccinic acid
DNA	Deoxyribonucleic acid
HR	High resolution
HRTEM	High resolution transmission electron microscopy
FDA	Food and Drug Administration
FTIR	Fourier transform infrared spectrometer
FWHM	Full width at half maximum
HOPG	Highly oriented pyrolytic graphite
MRI	Magnetic resonance imaging
MNPs	Metallic nanoparticles
N_2 atm	Nitrogen atmosphere
NPs	Nanoparticles
O_2 atm	Oxygen atmosphere
PBS	Polybutylene succinate
PEG	Poly (ethylene glycol)
SAED	Selected area electronic diffraction
SF	Sensitivity factor
SIMS	Secondary ion mass spectrometry
SPION	Superparamagnetic iron oxide nanoparticle
TEM	Transmission Electron Microscopy
TEOS	Tetraethoxysilane

TEPSA	[3-(triethoxysilyl) propyl succinic anhydride]
ToF-SIMS	Time-of-Flight Secondary Ion Mass Spectrometry
TPED	[N-[3-(trimethoxysilyl) propyl] ethylenediamine]
XPS	X-ray photoelectron spectroscopy

CHAPTER 1 INTRODUCTION

I start this thesis with a question ...

Is it possible that after almost 60 years, since the beginning of the nanotechnology era, the chemical reactions and behaviors of nanomaterials are unpredictable today?

It is a known fact that Phoenicians, Etruscans, Chinese and Aztecs used gold in dental surgery, more than 2000 years ago (Duffo G., 2011), thus demonstrating knowledge through the science of biomaterials thousands of years ago. It was until 1965 that the winner of the Nobel Prize in Physics, Richard Feynman, was the first to refer to the beginning of nanoscience and nanotechnology, describing for the first time the possibility of synthesis via direct manipulation of atoms (Feynman, R. P., 1959). Later, inspired by Feynman's concepts, Eric Drexler used the term "nanotechnology" in 1986 in his book "Engines of Creation: The Coming Era of Nanotechnology" (Drexler K.E., 1986). In this way the advances in science began to open their doors to a new branch of materials science: Bio-nanomaterials, this means, interest and study by nanomaterials, (materials whose dimensions are less than 100 nm), such interest grew exponentially during the following years, especially in the medical area.

The development in the advancement of biomaterials has been inspired by the unique properties of the nano-scale materials that have been demonstrated. Despite the tremendous progress in the field of nanoscience, very little is known about the detailed mechanisms of interaction between nanoscale devices (nanodevices) and the biological system. According to some studies (Cedervall, Lynch, Foy, et al., 2007, Mahmoudi, Sant, et al., 2011), the biological responses of nano-biomaterials result from complex interactions. The latter depend mainly on the physicochemical properties of the nanoparticle surface. This PhD project whose main objective is to develop magnetic nano-vectors capable of transporting therapeutic substances, such as nitric oxide (NO), proposes the use of iron oxide nanoparticles (magnetite, Fe_3O_4), which have a superparamagnetic behavior (superparamagnetic iron oxide nanoparticles, SPIONs), and are candidates to be functionalized and adapted to attach NO molecules. The use of physico-chemical characterization techniques will be the key to the study and demonstration of chemical reactions at nano-scale and, consequently, demonstrate whether the successful use of SPIONs as nano carriers and with the possibility of manipulate such nanoparticles into localized areas.

This thesis is divided into nine chapters. In the first chapter it is described in the introduction of this thesis, giving a general idea of what will be found in this manuscript, the second chapter contains the basic literature review that will allow the reader to enter into context with the subject, the current problems and the importance of this study. The third chapter indicates the hypothesis and the approach chosen to solve the problem. This approach includes knowledge of nanoparticle surface chemistry to allow carrying out the reactions proposed in each step of the modification of the surface of the nanoparticles and establish a correlation between the chemical groups present on the surface of the SPIONs and the reactions obtained at each functionalization step. Chapter 4 describe the principles of characterization techniques used in this project to achieve the objectives. The next three chapters (5, 6 and 7) are dedicated to the results and contain three articles published in three different journals. My contribution in each article is at least 75% of the work and covers the literature review, laboratory experiments, data analysis, writing of these articles and their submission. The first article deals with the first objective of this project, which refers to the synthesis and functionalization of SPIONs. This first article, presented in Chapter 5, shows a comparison of how SPIONs surfaces differ, these comparisons are based on characterization techniques such as TEM, VSM, FTIR, XPS and ToF SIMS, where the results are compared between nanoparticles naked (bare), meaning NPs without subsequent functionalization after their synthesis, SPIONs with positive surface charge and SPIONs with negative surface charge, due to surface modification by silane surface layers. Another comparison is also made regarding the reproducibility of the synthesis, and they are evaluated as potential candidates for use as prodrugs to target the specific sites. The second article, presented in Chapter 6, aims to identify the effect of dialysis on the surfaces of nanoparticles to eliminate the existence of undesirable contaminants and discuss about the efficiency of dialysis. And finally, in the third article presented in Chapter 7, presents the results focused on the NO attachment on SPIONs based on the nanoparticle prepatarion to be usind as nanocarriers. This article presents two methods to attach NO: using dimercaptosuccinic acid (DMSA) and polyethylene glycol (PEG) dithiol as source of thiol groups to react and obtain covalent S-NO bonds. In addition, a comparison is made in the conditions of reactions taking place in N_2 atm and O_2 atm. The final characterization indicate the parameters to consider for a successful NO attachment. Finally, a general discussion is presented in Chapter 8, followed by a section dedicated to the general conclusions and futures perspectives of the PhD project in Chapter 9.

CHAPTER 2 LITERATURE REVIEW OF IRON OXIDE NANOPARTICLES AS VEHICLES OF NITRIC OXIDE DELIVERY

2.1 Why is a nano-delivery system of nitric oxide necessary?

On average, 7% of all patients in industrial countries are affected by "nosocomial" infections, which are infections caused in hospitals. In intensive care units, the risk increases even more. This can result in serious illnesses and life-threatening blood poisoning. If patients are treated with invasive medical measures, hospital microorganisms have a particularly easy time of it: if tubes are inserted into the body to ventilate it, supply it with fluids or drain urine, the infectious agents quickly gain a foothold. It is still unclear how these infections can be prevented, and it is here where new technologies that preventing biofilm formation play an important roll.

The focus lies on the analysis of biofilms, which are accumulations of microorganisms on surfaces such as implants, urinary catheters, heart valves, hip prostheses, etc. The use of antibiotics is not always a viable solution due to antibiotic resistance, which is one of the major public health challenges of our time. Each year, in the U.S., at least 2.8 million people suffer antibiotic-resistant infections, and more than 35,000 people die. Fighting this threat is a public health priority because this problem imposes great challenges for the use of conventional antimicrobials, and underlines the need for new ideas to fight against surface biofilms formation. This thesis is based on a project aimed at reducing the risk of biofilm formation through the preparation of superparamagnetic nanoparticles, taking advantage of their surface functionalization with nitric oxide molecules and, through magnetic manipulation, accessing specific targets and concentrating a desired amount of NO. The literary review in this chapter recapitulates the bases that were considered in this design.

2.2 Nanomaterials

At the end of 1959 a new area of study for science, technology on a nanometric scale emerged. Richard Feynman in his speech entitled "There is plenty of room at the botton", in which he raises the possibility of manipulating materials at an atomic and molecular scale, Freyman explained in a very visionary way for the first time the advantages that could work in the nanometric scale (a nanometer is equivalent to one billionth of a meter) (Invernizzi and Foladori, 2005). Other pioneers

in this area were Richard Smalley, Robet Curl and Harold Kroto, who discovered a type of carbon molecule previously unknown and what they called ¨fullerene¨ (buckyball) which has been essential in the development of nanotechnology. Eric Drexler, an American engineer, has suggested the possibility that robots develop specific functions and perform tasks similar to those of cellular transcription and translation machinery for protein synthesis. (Sahoo et al., 2007; Coppo, 2009).
However, these advantages did not begin to be patented until 20 years later with the appearance of new manufacturing techniques and especially with new characterization techniques that allowed us to understand and control the composition, shape, size and physical properties. It is precisely here that Nanoscience focuses on understanding and exploiting the properties of different materials as a consequence of being in the "nanodimension." In fact, a material on a nanometric scale has very different properties of the same material on a macroscopic scale. It is in these differences in the chemical-physical properties (optical, electrical and structural properties) that the growing interest in this type of materials resides.

Nanotechnology is a multidisciplinary field that includes areas such as biology, chemistry, physics, materials science, engineering, etc. At present, nanotechnology is a very fast-growing area, with thousands of existing products already on the market and it is expected that the number of products and therefore their economic and social impact will be much greater in the next years. One of the sectors with more growth prospects and that is beginning to be a reality is biotechnology and medicine, both in the development of new diagnostics techniques and imaging techniques, as in more effective therapeutic treatments, specifically aimed at tissues and organs damaged.
Probably one of the most widespread applications in the field of therapy is the use of nanoparticles as transport vehicles for controlled drug release. The encapsulation of certain drugs in nanometric systems has been shown in many cases to improve their stability, solubility and biodistribution. In some cases, one can even direct the drug to the target organ to act in an effective way.

2.3 Nanomaterials applied in the biomedical field

Within a multidisciplinary context, the primary goal of the new nanomaterals is to improve the quality of life and promote human development. Biomedical nanotechnology offers solutions in the diagnosis, prevention and treatment of diseases, ingeniously participates in biological processes of the human body, as mentioned before, in the release of drugs at specific targets and fight against a battery of infections, among others (Puurunen and Vasara 2007, Roco, 2003). In addition, it

designs and creates new products with novel features, such as motorized prostheses with movement from the detection of brain signals, and many other uses. (Yadav H.K.S et al., 2018).

A subdiscipline of nanoscience is nanomedicine and is one of the most promising aspects of the many technological advances still under study, since it offers the possibility of diagnosing and treating diseases at the cellular and molecular level (Bouwmeester et al., 2009). For example, iron oxide nanoparticles are used in cancer therapies (Carvalho et al, 2019); colloidal gold is used in the systemic administration of biological substances; Silver nanoparticles are useful in antimicrobial coatings for various implanted devices and in catheters (Romanò C.L et al., 2019);

Superparamagnetic iron oxide nanoparticles are used to mark the transplanted cells and thus follow up *in vivo* the patient recovery process (Mohanty S, et al., 2018, Etheridge et al., 2013; Kubinová and Syková, 2010). Structures such as dendrimers, nanospheres, nanopores and quantum dots, have been developed to diagnose early and effectively treat diseases that are difficult to manage, such as heart attack, cancer, diabetes, kidney failure, immunodeficiency virus infection human (Pastrana and Ávila, 2006) and in neurodegenerative pathologies such as Alzheimer's and Parkinson's (Fedorovich et al., 2010). It is anticipated that in the future nanomachines or nanorrobots may be introduced into the human organism to repair cellular damage and also to control, prevent and diagnose pathologies that cannot yet be intervened by man, although decades should probably take place until this technology is available (Freitas, 2005; Kewal, 2005; Coppo, 2009; Wang, 2009). The main areas of application of nanomedicine involve the development of pharmaceutical products, *in vivo* and *in vitro* diagnostics, regenerative medicine and device implantation (Boisseau and Loubatonb, 2011). The nanorobots on the other hand, will also be protagonists in the processes of selective distribution of drugs in the body (Laocharoensuk et al., 2008), as well as in the improvement of human physiological conditions (Lin et al., 2009).

2.4 Nanoparticles as promising technology against biofilm formation on implants

Nosocomial infections represent a serious problem accordig to statistics; it is one of the major causes of death in the world in addition to cancer, cardiovascular diseases and diabetes. (National Center for Health Statistics, 1999). Just in United States in 2001 the mortality rate of nosocomial bloodstream was estimated between 87 500 to 350 000 life lost (Wenzel R.P and Edmond M.B, 2001) and in total during the year, approximately 2 million nosocomial infections

were reported, reflecting a cost of 11 billions dollars (Schierholz J. M and Beuth J, 2001), and the mortality rate continues to increase each year. These numbers clearly indicate that we have an economic and health problem and finding a solution is urgent. Exposure to a medical device implantation increases the risk of infection and biofilm formation resulting in critical health and costly consequences to the patient in several cases.

Some strategies exist to prevent implant contamination, the most common being when the medical staff takes step by step aseptic protocols before and during implantation and prophylactic administration of antibiotics during the days following surgery. However antibiotic resistance is a problem that goes hand in hand with the contamination of implants and medical devices, a growing global health problem and is not a new phenomenon; and if no changes are made and urgent action is not taken, common infections and minor injuries could become fatal.

This resistance has been attributed to the failure of antibiotics to penetrate biofilms, and the persistent use of antibiotics by the patient (Lewis K, 2005; Mah T.F.C and O´Toole G.A, 2001). Some of the most common bacteria found in devices colonized by bacteria after implantation are *Staphylococcus aureus* and *Enterococcus*, which turn out to be more resistant to anibiotics, once the biofilm is formed on the implant surface (Dupont H, 2007; Birolini C, 2016).

Due to the necessity to stop hospital infections and biofilm formation, the science has the challenge to find solutions and develop longlasting biomaterials with antibacterial and antibiofilm surfaces (Allegranzi B, et al., 2011; Zarb P, et al., 2011).

Some studies point out that the biological response to a biomedical device depends on the structure and surface functionality of the material used, and most device-associated infections are likely to originate from material surface contamination at the time of implantation. The surface engineering of materials can enhance device biocompatibility and functionality and material properties and surfaces can be modified to reduce microbial contamination and prevent biofilm infections. Antibiotic coatings efficiently provide surface antimicrobial activity because bacteria directly bind with antibiotics and are lysed before biofilm establishment. The antibacterial activity of metal oxide nanoparticles (NPs) as Fe_3O_4, indicate antibacterial activities and low toxicity, also propose metal oxide nanoparticles as candidates for controlling or treating bacterial biofilms on indwelling medical devices and implant (Kadiyala, et al., 2019) and it is exactly the target of the problem to combat with the application the nano-delivery system of nitric oxide. Throughout this brief

introduction, this chapter has discussed key issues that involve the characteristics of nano-device, its features and design.

2.5 Superparamagnetic iron oxide nanoparticles

Magnetic nanoparticles (MNP) display outstanding properties on account of their small sizes and high surface-volume ratios, which differentiate them from larger particles and their bulk material. Superparamagnetic nanoparticles are attractive for the purpose of drug delivery and hyperthermia, as magnetization within the nanoparticle is lost as soon as the magnetic field is removed due to thermally induced spin flipping. This is beneficial, as remnant magnetization could induce MNP agglomeration and embolization of capillary vessels (Arruebo M, et al., 2007).

The most prevalent iron oxide nanomaterials are magnetite (Fe_3O_4) and its oxidised form maghemite (γFe_2O_3), and are preferentially used in medical research on account of their biocompatibility (Wahajuddin and S. Arora, 2012). Iron is ordinarily present in the human body and the liberation of free iron by the biodegradation of the MNP could be utilised in subsequent metabolic processes, thereby preventing prolonged risk from exposure (Thorek D.L, et al., 2006). While magnetite and maghemite are ferrimagnetic at room temperature (retain their magnetisation in the absence of a field), it is known that below a critical size of 30 nm, the permanent magnetism is lost and they become superparamagnetic (Baumgartner J, et al., 20113; Mahmoudi M, et al., 2012).

Superparamagnetism occurs when the nanomaterials contain a single magnetic domain, in which all magnetic moments are aligned with one another and they point in the same direction, when in the presence of an external magnetic field. The sum of all the individual magnetic moments results in a single giant magnetic moment, which align along the applied field, leading to a net magnetisation. The length of time it takes for the magnetic moment to flip, from parallel to anti-parallel orientations, is referred to as the Néel relaxation time. It is well known that size governs the magnetic properties (Dunlop D.J. and Ozdemir O.Z, 1997), and it is therefore important to have a reliable synthesis method to ensure that the nanomaterials produced maintain a core size of less than 30 nm.

There exist many methods to synthesize iron oxide nanomaterials, such as co-precipitation, thermal decomposition, microemulsion, hydrothermal synthesis, and more, including recently

green chemical synthesis methods involving the bacterium Actinobacter sp. (Magnetosomes) (Bharde A.A, et al., 2008). These methods have been explored for their ability to produce nanomaterials that are of uniform size and have suitable physicochemical properties for their required application (Laurent S, et al, 2008). While co-precipitation is the method of synthesis of NPs used in this thesis, it results in a wider size distribution and non-uniformity in population shape characteristics (quasi-espheric) (Wu W, et al., 2008).

2.6 Dimercaptosuccinic acid (DMSA) and polyethylene glycol (peg) as polymeric coatings

The biomedical application of nanoparticles also requires the optimization of parameters such as their residence time in blood, providing surfaces able to be functionalized as well as promote biocompatibility. Hence, one of the most used strategies for surface modification of nanoparticles is the coating with different materials, such as DMSA and PEG (Iijima and Kamiya, 2009). Dimercaptosuccinic acid (DMSA) and polyethylene glycol (PEG) are hydrophilic and biocompatible polymers, frequently used to coat nanoparticles in the research area. DMSA, is commonly used as a nanoparticle coating due to supporting greater stability to magnetic nanoparticles, across a broad pH range (pH 1 – 14) (Chen, Z.P., et al., 2008). The DMSA coating plays an important role in sample mono-dispersibility and has been shown to increase cellular association, compared to uncoated nanomaterials (Pisanic, T.R., et al., 2007; Wilhelm C, et al., 2003). Nanomaterials coated with DMSA have also demonstrated little to no cytotoxicity or genotoxicity in vitro (Auffan M et al., 2006; Gupta A.K, et al., 2005) and in vivo (Monge-Fuentes V, et al. 2011). In vitro cytotoxicity has been observed at concentrations greater than 100 µg/mL (Auffan M, et al., 2006), which far exceed the concentrations used with clinically implemented MNPs (Hudgins P.A, et al., 2002). DMSA coated MNPs have the capacity to reduce intracellular reactive oxygen species levels (Mou, Y., et al., 2015). This confers to DMSA acceptability to be used in drug delivery (as NO delivery), and for this project is considerated as a major option for the thiolation process.

Concerning PEG, PEGylation is one of the most favored ways of surface modification of nanoparticles for biomedical with common applications related to intracellular targeting, antitumoral delivery systems and diagnostics, among others (Tkachenko A.G, et al., 2004; Cai L.L, 2012; Illés E, et al., 2018; Dilnawaz F, et al., 2010; Na H, et al., 2009). Polyethylene glycol

solvation properties also have an effect on the efficiency of NPs used as MRI contrast agents (LaConte L.E, 2007; Wattendorf U and Merkle H, 2008). They also offer grafting sites for covalent immobilization of targeting like proteins, peptides or antibodies (Yang H.W, 2012).

2.7 Nitric oxide in physiological biology and biomedical applications

The focus of this thesis is to develop a nano-system able to release a small inorganic molecule that has received much attention in recent years: nitric oxide (NO). Nitric oxide is a diatomic free radical that has extremely short lived and widespread distribution in biological systems.

Humprey Davy did the first experiment to study the effect of nitric oxide (NO) on respiration in the late 1700's when he experienced aspiration pneumonitis and nearly died from inhalation of the gas (Sprigge J. S, 2002). In the early 1980's, NO was studied as an important gas in the atmosphere because of its role in acid rain, smog and depletion of the ozone layer. (Heywood J. B, 1988; Ignarro L. J, Donahue, N. M, 2011). In 1987, the endothelium derived relaxing factor (EDRF) was discovered to be NO responsible for vasodilatation. (Ignarro L. J, et al., 1987; Palmer R.M.J, et al., 1987). These events began he consideration of NO as an important molecule in physiological processes. (Ignarro L. J, Buga G. M, et al., 1987) However, the real interest in NO as a molecula concerned in biological functions was recognized when Furchgott Ignarro and Murad won, in 1998, the Nobel Prize in Physiology and Medicine for their work in establishing NO as a chemical signaling agent in physiology. (Davies I. R and Zhang X, et al., 2008; Saavedra J.E, et al.,2002). Robert F. Furchgott's group identified, in the vascular epithelium, a molecule responsible for mediating vasodilation. It was named endothelium-derived relaxing factor (EDRF) because of its source and for its effects on smooth muscle in blood vessel walls (Furchgott & Zawadzki, 1980). Its discovery brought Furchgott the Nobel Prize for Physiology or Medicine, an honour he shared with Louis Ignarro and Ferid Murad; their research served to confirm the function of NO as a signalling molecule in the cardiovascular system; it is a key chemical signaller for the homeostasis of the gastrointestinal (GI) tract (Lamarque et al., 1996), participate in mediating immunity (macrophages release NO upon invading pathogens, which causes their destruction) (Green et al., 1990; MacMicking et al., 1997). The low level of NO production in the skin may play a role in the maintenance of a barrier function and optimum blood flow in the microvasculature (Cals-Grierson & Ormerod, 2004).

NO and NO synthase (NOS, its synthesizing enzyme) are also found in nervous tissue in a variety of animals (Bredt et al., 1990; Dawson & Snyder, 1994; Huang et al., 1997), where NO may exert a developmental influence as well as functional importance in healthy nervous systems. NO has been found to be involved in learning and memory (Bohme et al., 1993; Estall et al., 1993) Its production has been linked to inflammatory states such as ulcerative colitis (UC) (Rachmilewitz et al., 1995), and skin conditions (Cals-Grierson & Ormerod, 2004). NO is also implicated in the processing of various pain states like chronic pain (Luo & Cizkova, 2000). Much attention has also been drawn to the role of NO in carcinogenesis: NO and its derivatives can react with DNA in inflamed tissues and cause mutations (Felley-Bosco, 1998). Indeed, NO has been implicated in the progression, invasion, metastasis and angiogenesis of different cancers (Ekmekcioglu et al., 2005), and has been associated with the suppression of tumorigenicity and the regression of already-present metastases (Xie et al., 1996); cardiovascular disorders, such as angina can readily be treated with NO-releasing drugs, and such NO-based remedies may be derived from botanicals (Achike & Kwan, 2003). In fact, such medicinal uses may have also opened up the exploration of NO activity in plants (Beligni & Lamattina, 2001). Research into nano-delivery systems, able to release NO will certainly help in the near future to deliver this endogeneus molecule into specific zones and interact with physiological functions.

2.8 Iron oxide nanoparticles as vehicle to release nitric oxide

Nowadays, research in this endogenous molecule explores its properties and possible applications, such as diagnosis, prevention, and treatment of diseases. Iron oxide nanoparticles MNPs (Fe_2O_3 and Fe_3O_4) have been explored in biomedical applications such as drug delivery, drug targeting of cancer cells, tracking target cells using labeling (Yokoyama M, 2011; Uhrich K E, 2011; Nguyen T K, 2002) and therapy (Fang B, et al., 2011; Rosen J.E, et al., 2011; Pankhurst, Q A, et al, 2004), since they are considered less toxic in comparison with metallic nanoparticles, and have been approval by the FDA for MRI application, due to their metabolization, low toxicity and biocompatibility (Bulte et al, 2004).

In vivo studies with Fe_3O_4 nanoparticles have demonstrated severe inflammatory and toxicologic responses in rats exposed through inhalation (Zhu M.T, 2008; Bhattacharya K, 2009). In contrast, other studies performed with microscale and nanoparticulate Fe_3O_4 describe them both

to be nontoxic under in vitro test conditions with human small airway epithelial and mouse fibroblast cells (Mahmoudi M, et al., 2009)

The biomedical applicability of MNPs is greatly improved by coating their surfaces with biocompatible ligands (Murray C.B, et al., 1993), and those with biocompatible ligands containing functional groups such as COOH and SH (Hong S C, 2011). The nitric oxide (NO) molecule may interact on the surface of these nanoparticles covered with biocompatible ligands. Thus, there is a great interest in the development of NO-releasing vehicles that are able to stabilize and release NO locally direct to the target site, in diverse biomedical applications.

2.9 Biocompatibility

Besides the NP size, the chemical nature of its surface appears to determine the intensity of the biological effects with significant differences between different types of coating because of their surface chemistries that vary their reactions with the components of the culture medium before reacting with the cells. (Mbeh D, Franca R, et al, 2012)

Up to now, the overwhelming majority of reports have claimed that SPIONs are biosafe because they are presumably bio-inert and/or because their metabolites are. Fe is essential for living organisms and thus is biocompatible. Many studies have also shown no adverse effects on potential cytotoxicity and cell function at low doses (10 pg Fe/cell) for optimal MRI cell tracking (Kroll A, Pillukat, 2009). The conclusion of biosafety, however, may be premature, due to lack of criteria to evaluate the safety and toxicity of these nanomaterials. (Bulte J, 2009). Therefore, the effects of SPIONs on diverse aspects of cellular activities should be carefully evaluated even though such NPs are generally considered biocompatible at present.

Previous studies in our research group (Mbeh D.A, 2014, Mbeh D.A, 2015) using the same nanoparticles used in this project affirmed that the negatively charged TEPSA SPION is more biocompatible than the positively charged TPED and the bare SPIONs, demonstrating the impact of functionalization on cell response; the nanoparticles all induced the production of reactive oxygen species. This study underlines the necessity to consider non-toxic doses of SPIONs, so that it is clear that maximum doses must be determined for each SPION used. (Mbeh D.A, Mireles L.K et al, 2015)

2.10 Cytotoxicity

The physico-chemical properties and potential cytotoxicities of nanoparticles (NPs) are significantly influenced by their interaction with proteins, which results in corona formation. It is well recognized that, on contact with a biological medium, SPION surfaces are immediately covered by various types of proteins (Mahmoudi, Lynch, et al., 2011). This adsorption confers a new "biological identity" to the SPION, which determines the subsequent cellular/tissue response (Rahman, Laurent, Tawil, Yahia, & Mahmoudi, 2013). The composition and quantity of protein coronas are strongly dependent on the surface properties of the SPIONs and the composition of the biological milieu. Therefore, the proper in vitro toxicity assessment of SPIONs requires their comprehensive physicochemical characterization.

Based on in vitro cytotoxicity assays, its known that coated SPIONs could be used in bio-applications over a broad range of concentrations (Mbeh D.A, et al., 2015). Recent cytotoxicity studies on SPIONs have demonstrated that SPIONs with various physicochemical characteristics have no cytotoxicity when used in a concentration range below 100 μg/ml (Ankamwar et al., 2010; Karlsson L.H, et al., 2008). Other studies mention that uncoated SPIONs are more toxic than the functionalized nanoparticles. In order to be used for safe and high-performance biomedical applications, the SPIONs must have a continuous coating. These coatings include polyethylene glycol, polyethylene glycol fumarate, polyvinyl alcohol, coatings based on polysaccharides, synthetic polyesters, alginate, chitosan etc. (Laurent S, et al., 2011). Thus, SPIONs@DMSA and SPIONs@PEGdithiol could be potentially safe and non-toxic in biological media.

In general, this chapter of introduction summarizes the information found in the literature review, evidencing the current problems and the necesity of new drug delivery estrategies to release drugs into specific points against biofilm formation, avoiding bacterial resistance.

Based on the literature, this project proposes to designe a nano-delivery system using SPIONs and functionalize them to release of nitric oxide against biofilms into specific place by the manipulation of magnetic field. The evidence of a well done functionalizarion (NO attachment) its the main goal in this PhD project, due to no one research team have been found an efective estrategie to design a system like this, and the need for this design is urgent. The following chapter describes the objectives, hypotesis and approach, followed by the description of the characterization techniques that have allowed to confirm the desingn of the project step by step.

CHAPTER 3 OBJECTIVES, APPROACH AND HYPOTHESIS

3.1 Context

This PhD project is focused on creating and developing a nano-system of nitric oxide (NO) release to inhibit biofilms, using superparamagnetic iron oxide nanoparticles (SPIONS) to prevent bacterial adhesion related to implants and subsequent biofilm formation. The project was divided in three stages:

1. Synthesis and functionalization of SPIONs; (article 1)
2. The characterization of the physicochemical properties of these SPIONs; (article 2)
3. Attachment of nitric oxide to SPIONs; (article 3)

Stage 1: Three differently functionalized magnetite (Fe_3O_4) spions were synthetized by alkaline coprecipitation and functionalized: a) bare spions (precursor), b) coated positively spions (- NH_2) and coated negatively spions (- COOH) by our collaborator: Sophie Laurent at the University of Mons (Belgium).

The second and third stage is the subject of this thesis. current processes of functionalization of biomaterials, omit the important part of analysis of the surface where the physicochemical interactions are developed.

It cannot be taken for granted that the chemical reactions that occur in macro-scale will occur at the nano-scale, or will occur without variations, and for this reason the characterization of nanomaterials with high sensitivity plays an indispensable role in the new technology, where reactions cannot assumed, but have to be proven.

The importance of nano-systems of nitric oxide release is evident, because the benefits that this molecule provides are of vital importance for the human being; however, there are no significant investigations of reactions and functionalization that demonstrate the molecular attachment to SPIONs, in consecuense, the characterization of physico-chemical properties of the surface of nanoparticles is emerging.

3.2 General objective

The surface characterization of SPIONs provides the necessary tools to know and understand the surface chemistry of the SPIONs and thus be able to have the basis to propose a nitric oxide attachment procedure.

Therefore, the main objective of this thesis is:

Carry out the functionalization of magnetic nanoparticles (SPIONs) to use them as prodrugs of nitric oxide; through the evaluation and physicochemical characterization of the SPIONs as nano carriers, to propose an anchoring protocol of nitric oxide and demonstrate its veracity by means of physicochemical analysis tools.

3.3 Specific objectives

1. Obtain the morphological, magnetic and physicochemical properties of superparamagnetic iron oxide nanoparticles as candidate to be use in the nano-delivery system of nitric oxide.
2. Identify the most appropriate method of functionalization, to prepare the SPION surface (by thiolation) for NO attachment.
3. Perform the anchoring of NO to the SPIONs surface by the nitrosation method and test the effectiveness of the anchoring method

3.4 Approach and hypothesis

We presume that a polymer shell around the nanoparticles will help provide thiol groups that permit NO anchoring. In this project we propose the use of dimercaptosuccinic acid (DMSA) and poly (ethylene glycol) (PEG)-dithiol to achieve thiolation and later nitrosation, which will be evaluated by characterization techniques such as X-ray Photoelectron Spectroscopy (XPS) and Time-of-Flight Secondary Ion Mass Spectrometry (TOF-SIMS), which provide accurate information on the existence of the S-NO covalent bond. Both types of shells will be compared to evaluate their effectiveness. S-nitrosation is a post-translational modification involving the covalent attachment of NO moiety to sulfhydryl residues (-SH) of proteins, resulting in the formation of S-nitrosothiols (SNOs).

3.5 Iron oxide nanoparticles

Numerous types of iron oxide exist in nature and can be prepared in the laboratory, however only maghemite (γ-Fe_2O_3) and magnetite (Fe_3O_4) are able to satisfy the necessary requirements for biomedical applications, because its biocompatibility (Figuerola A., et al 2010) with respect to other magnetic materials. These requirements include: high magnetic moments, chemical stability in physiological conditions and low toxicity, plus the easy and economical synthetic procedures available to prepare these materials (Figuerola A., et al 2010). Magnetic nanoparticles (NPs) such as Fe_3O_4 have been proposed for bio-applications such as drug delivery, nano-sensors magnetic resonance imaging (MRI) and hyperthermia (Estelrich J., et at 2015; Langer R, 1998)

3.6 DMSA

We have considered DMSA as a supplier of thiol groups for the anchoring of nitric oxide. Fe_3O_4 NPs coated with DMSA have been revealed as a very promising material due to its magnetic properties, biocompatibility and nontoxicity already been demonstrated (Garcia MP et al., 2010; Chaves SB et al., 2002; Soler M et al., 2007; Auffan M et al., 2006). In this project we wanted to support the use of DMSA-Fe_3O_4 NPs for future drug delivery against biofilm formation and biomedical applications.

3.7 PEG-dithiol

Poly (ethylene glycol) (PEG) has been extensively used in biomedical applications, especially for controlling drug delivery (Peppas NA, Hilt JZ, 2006). PEG gels, including PEG dithiol chemically-crosslinking (polymer chemically modified, joining two molecules of -SH by a covalent bond at the end of the chains) leads to relatively stable hydrogel structures with physico-chemical properties (Lin C.C and Metters A.T, 2006; Peppas N.A, et al., 2006; Drury J.L and Mooney J.D, 2003, Mellott M.B, et al., 2001)

The versatility of the PEG integrates with its excellent biocompatibility and nanoparticle dispersion (Nuttelman CR, et al., 2008), In the context of controlled delivery, PEG hydrogels play an important role for controlled delivery of many biomolecules, ranging from small molecular weight drugs to large biomacromolecules, such as nucleic acids, peptides, and proteins (Chien-Chi L, Anseth KS, 2009)

CHAPTER 4 CHARACTERIZATION TECHNIQUES

In this chapter, the basic principles of operation of the characterization techniques used throughout this project are discussed.

Nano-devices studied and used in theranostics will ultimately come into contact with protein-rich physiological fluids. Therefore, the importance of understanding the physicochemical properties of engineered nanopartciles should not be overlooked. Knowing how the properties of nanoparticles (SPIONs) are affected by dispersion in physiological medium is decisive for the success of the MNP in its specific application (Calatayud M.P, et al., 2014)

4.1 Transmission electron microscopy (TEM)

Transmission Electron Microscopy (TEM) is a powerful characterization technique in understanding both structure and composition of materials using a beam of high-energy electrons to examine objects. It plays a vital role within the fields of materials science, nanotechnology, and biotechnology. TEM was used in this thesis to study and determine parameters such as 1) Morphology: the size, shape and arrangement of the particles which make up the specimen as well as their relationship to each other on the scale of atomic diameters, 2) Compositional information: the elements and compounds present in the sample, 3) Crystallographic information: The arrangement of atoms in the specimen and their degree of order.

TEM consists of an electron source (electron gun), condenser lenses, an objective lens, imaging system (consisting of the diffraction lens, intermediate lenses, projector lenses depending on the type of microscope), a viewing screen and operate using principles similar to those used in light microscopy. The advantage of electron microscopy (EM) is that the wavelength of electrons is much smaller than the wavelength of visible light, which results in much higher achievable resolutions and allow obtaining images of nanoscale specimen (Bozzola J.J and Russell L.D, 1999). The beam of electrons is generated using an electron gun and then passes through a series of magnetic lenses and apertures in order to obtain a well-focused beam, which “illuminates” the sample. In transmission electron microscopy (TEM) the beam passes through the sample deposited on a thin metal grid and reaches the detector (See Figure 3.1). The image collected in bright field imaging mode gives contrast information about the sample, in which thicker areas or areas with

higher atomic number will be darker and vice versa. The lattice fringes can be seen in the particles, and can be used to estimate the sample crystallinity. The choice of specimen support is important for high resolution TEM, since thicker support film decreases the resolution and may make lattice fringes difficult to detect (Bozzola J.J and Russell L.D, 1999).

The JEM-2100F field emission electron microscope, with ultrahigh resolution, at a beam energy of 200 kV was the TEM equipment used in this PhD project. All the samples analyzed were diluted in water and sonicated for 3 minutes to disperse the SPIONs. One drop of each sample was spread on a copper grid with a lacey carbon film, and analyzed when the drop dried. Photomicrographs were obtained by bright-field imaging at beam energy of 200 keV. The elemental analysis was carried out by energy dispersive spectroscopy (EDS). Selected area electronic diffraction (SAED) was used to obtain crystal diffraction patterns.

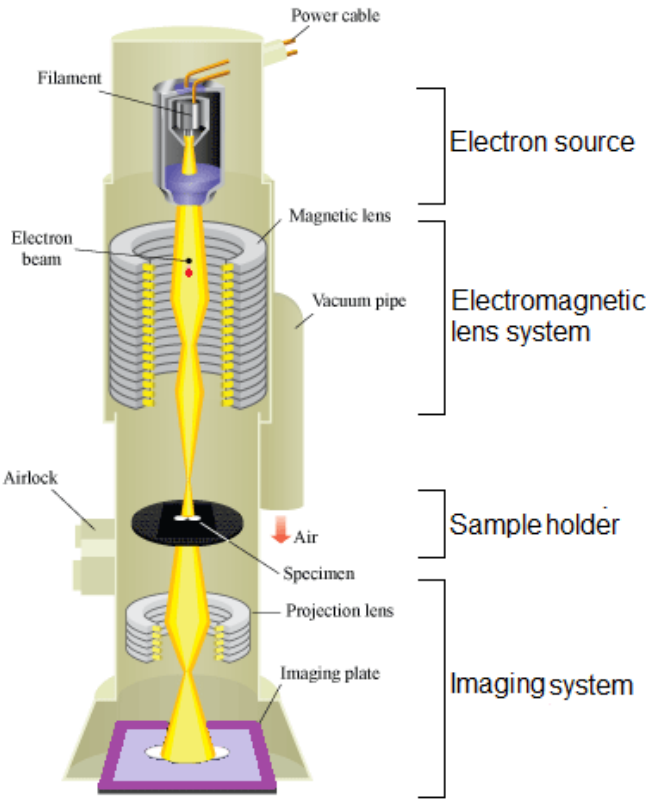

Figure 4.1 Schematic diagram of TEM system

4.2 Fourier-transform infrared spectroscopy (FTIR)

Fourier-transform infrared spectroscopy (FTIR) analysis of solid samples as SPIONs can be understand as the emitted radiation from an IR source that passes through an interferometer composed of a beam splitter, a fixed mirror, and a moving mirror. The interferometer measures the wavelength of emitted light via interference patterns that help to increase precision. IR spectrum are obtained by applying IR radiation to a sample and measuring the intensity of the passing radiation at a specific wavenumber, (Faghihzadeh F, et al., 2016) (See Figure 3.2).

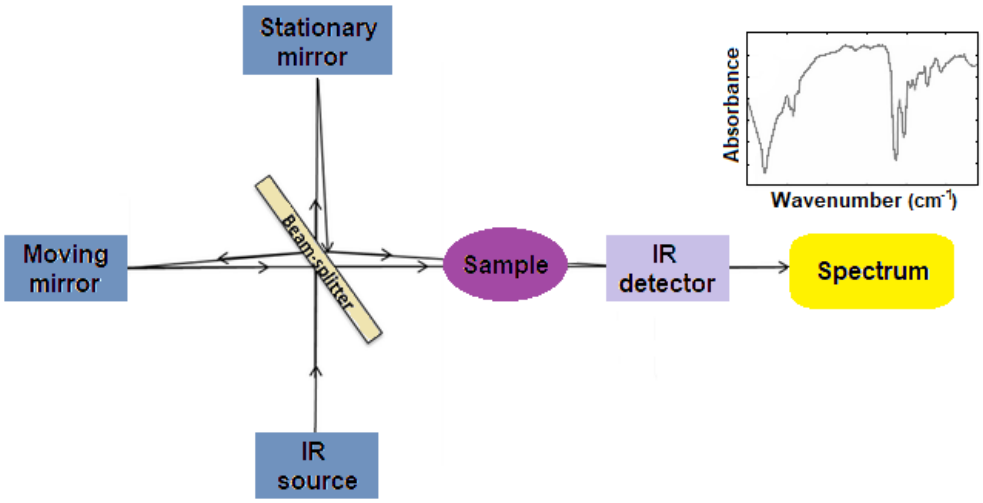

Figure 4.2 Schematic diagram of the IR spectroscopy

The number of scans can be adjusted based on the quality requirement for the sample analysis. IR radiation of certain molecular group can be detected at a specific wavenumber. The *x* axis of the spectrum represents the wavenumber while the *y* axis represents absorbance or transmittance (Faghihzadeh F, et al., 2016).

In this project the IR spectra were obtained, in the range 450-4000 cm^{-1}, using a Bruker Alpha spectrometer, at a resolution of 4 cm^{-1}; 64 scans were coadded to improve S/N and Thermo Scientific Nicolet 6700 Fouriertransform IR spectrometer, at a resolution of 4 cm^{-1}; 96 co-additions were used to increase S/N. The samples were deposited by placing several drops on a diamond

plate and silicon substrate, and drying before add the next drop; spectra were obtained after depositing three drops.

4.3 Vibrating sample magnetometry (VSM)

The Vibrating Sample Magnetometer (VSM) is a magnetic characterization instrument used to study the magnetic moments in many materials as metallic nanoparticles in function of applied magnetic field and/or temperature. Its use in studies of superconducting materials arises from the ability to perform a contactless determination of the critical current density, by measuring the magnetic moment, and hence magnetization of the sample. Characterization by vibrating sample magnetometer was used to obtain the magnetization vs magnetic field (M vs H) loop at room temperature, from H = 0-2 T, with a measurement precision of 1×10^{-6} emu. Measurements were determined on a known quantity of sample (Fiorillo F, 2010). Drops of each sample were spread onto a 10 mm × 10 mm piece of cleaned glass, and dried, and the weight of each sample

4.4 X-ray photoelectron spectroscopy (XPS)

X-ray Photoelectron Spectroscopy (XPS) also known as Electron Spectroscopy for Chemical Analysis (ESCA) is a surface characterization analysis technique that uses soft x-rays in an ultra-high vacuum exiting core and valence electrons within the atoms of a surface to determine the chemical compounds and chemical states on a sample. XPS depends on the interactions between X-rays and electrons; when the X-ray energy is large enough photoelectrons are ejected from the material and their kinetic energies (KE) are measured by the instrument. This excitation process is known as the photoelectric effect (See Figure 3.3)

The ejection of the inner core electron represents an unstable hole in the electronic shell. An electron from the valance shell then fills the newly formed hole, causing an Auger electron to be emitted from the valance shell to conserve energy. Then, the kinetic energy of the emitted electron is directly related to the binding energy of the electron to the atom.

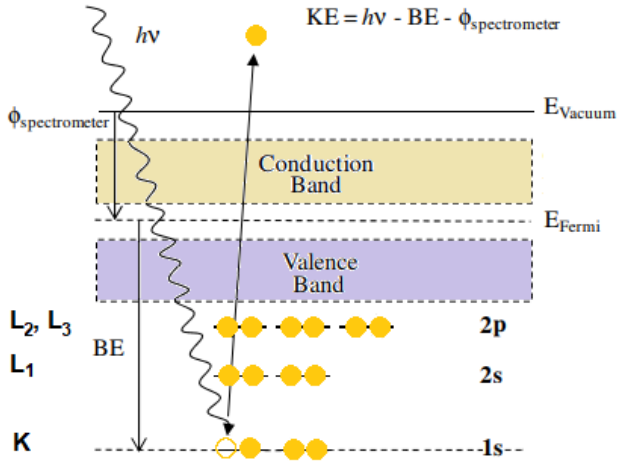

Figure 4.3 Absorption of a photon and resultant expulsion of a 1s level photoelectron

The differences in chemical elements within the near surface region are identified on the basis of their binding energy (BE), which is measured relative to the Fermi level (E_{Fermi}) of the individual atoms. To determine the binding energies, we first need to collect the kinetic energies of the electrons, once the detector collects the data, we can calculate the binding energies of the electrons if we know the wavelength of the incident x-rays, the KE and BE of the photoelectron are related via the following equations:

$$BE = h\nu - KE - \phi_{spectrometer} \quad \text{(Eq. 1)}$$

$$\nu = c / \lambda \quad \text{(Eq. 2)}$$

(KE) is the kinetic energy of the emitted electron and (BE) the binding energy of thatparticular electron to the atom. The frequency of the incident x-ray (ν) is related to the wavelength (λ) of the x-ray and the speed of light (c), lastly, $\phi_{spectrometer}$ is a correction factor that is unique to the spectrometer (Grant J.T and Briggs, 2003; Seah M.P and Briggs D, 1992).

The data collected are the kinetic energies of the electrons. This is because the kinetic energy of the electron is related to the energy of the incident x-ray. Since not all systems will have the same incident x-ray energy, it is not as convenient to compare kinetic energies. Binding energies, however, are unique to the element and not the system. Since the energy of the incident x-ray will be known for the system, the binding energies can easily be found and the data can be

transferred onto a binding energy scale. This will also make it more convenient when comparing data from different XPS systems (Grant J.T and Briggs, 2003).

The emitted electrons penetrate only 1-10 nm without interaction and energy loss, allowing for surface specific analysis. As an atom absorbs the x-rays the energy of the x-ray will cause an electron ejected (See Figure 2.3). The ejected electron has a kinetic energy (KE) that is related to the energy of the incident beam (hν), the electron binging energy (BE) and the work function of the spectrometer (Grant J.T and Briggs D, 2003; Seah M.P and Briggs D, 1992). In order for the resultant photoelectrons to be detected they first must escape from the surface without interacting with overlaying atoms; which may lead to loss of KE (inelastic scattering). The probability that a photoelectron will reach the surface without losing any of its KE can be approximated using the equation:

$$I_d = I_0 e^{-d/\lambda} \qquad \text{(Eq. 3)}$$

I_d is the photoelectron intensity originating from atoms at depth d, I_0 is the signal emanating from the surface atoms, and λ is the electron inelastic mean free path (IMFP).

The IMFP represents the average distance a photoelectron can travel before undergoing inelastic scattering and is dependent on both the material properties (i.e., density) and electron KE. If a Gaussian probability distribution is assumed, then 95% of the photoelectrons detected would have been produced within a depth of 3λ (Crist B.V, 2004).

A phenomenon seen in XPS analysis is the effect of electronegativity. This effect is predominantly seen in oxide samples due to the strong electronegative oxygen atoms. The electronegative atom attracts electron density in addition to the electron's host atom. This causes the energy needed to emit the electron from the host atom to increase. Since the electron is being attracted by both the host atom and electronegative atom, it requires more energy to be emitted. Therefore, the binding energy for the host atoms is shifted to a slightly higher energy. Lastly, an important aspect of XPS is determining the composition of the sample. This can be determined from the electron binding energy peaks. The area under the binding energy curve is proportional to the number of atoms that emit the electrons at that binding energy. Therefore, if we take the ratio of the area under the binding energy curve for each element, we can determine the composition of the samples surface (Crist B.V, 2004, Watts J.F and Wolstenholme J, 2003). However, a sensitivity factor must be introduced for each element in this ratio. All XPS systems have different sensitivity

factors, making it difficult to obtain a precise composition without knowing the exact sensitivity factors. In this project XPS was performed with a VG ESCALAB 3 MK II (Thermo VG Scientific). VG ESCALAB 3 MK II is equipped with a non-monochromatic Al Kα X-ray source having wavelength of 8.3386 Å which corresponds to a phonon energy of 1486.7 eV and Mg Kα X-ray source having wavelength of 9.89 Å which corresponds to a phonon energy of 1253.6 eV. All the measurements in this project used non-monochromated Mg Kα X-rays (hν = 1253.6 eV). The instrument resolution was 0.7 eV, and a perpendicular take-off angle was used. The analysis chamber pressure was < 10^{-9} torr. After Shirley background removal, the component peaks were separated by the VG Avantage software. To account for this during analysis, we calibrate the data by setting the C1s C-C peak, to 285 eV. FWHM values were those previously established in our laboratory. The depths probed by this technique, for elements of present interest, range from 3-5 nm and, with proper peak intensity sensitivity factors, the relative atomic percentages determined are highly quantitative (± 5%).

4.5 Time of flight secondary ion mass spectrometry (ToF SIMS)

Time of Flight Secondary Ion Mass Spectrometry (ToF SIMS) is another surface characterization technique that is extremely sensitive and uses a variety of pulsed ion beams as excitation sources to remove molecules from the outermost surface layer. The high energy primary beam is typically between 1 and 25 keV. These can be monoatomic, e.g., Ga^+, Cs^+, and Xe^+ (Grams J, 2007; Appelhans A.D and Delmore J.E, 1989). In order to minimize scattering, a pressure of at least 10^{-5} Torr is required (Briggs D, 1998). The energy from the primary ion beam is transferred to the surface layer of a sample with sufficient energy to disrupt inter-atomic attraction and covalent bonds, resulting in a collision cascade (Briggs D, et al., 1989), which can knock out non-volatile secondary ions, molecular ion fragments and neutral atoms that are accelerated in to a Time of Flight (ToF) mass analyzer called a “flight tube” by a constant electric field; the velocity at which the ions travel through the analyzer is dependent on their mass to charge ratio. Approximately 1% of material sputtered from a sample surface is charged (Briggs D, 1998). These ions are drawn into the time-of-flight analyzer for mass analysis by applying an extraction voltage to the bottom of the tube and keeping the sample at earth (Grams J, 2007). An accelerating voltage of 3 keV is applied to the ions as they enter the field free region of the flight tube. Therefore, ions enter this tube with

velocities (v) according to their mass (m) as shown in the following equation, where KE is the kinetic energy of the ion:

$$KE = \frac{1}{2} mV^2 \qquad \text{(Eq. 4)}$$

As the ions pass through the time of flight tube they are separated as the lower mass (m) ions have higher velocities (V). At the top of the flight tube a reflectron (ion mirror) is employed to compensate for any secondary ion energy distribution which occurs when ions with the exact same mass arrive at the detector at different times. The reflectron is designed to compensate for differences in velocity and path length by applying an increasing potential in an ion mirror located at the top of the reflectron, prior to the ions reaching the multi-channel plate (MCP). The MCP detects the end of the ion trajectory; using known hydrocarbon fragments or small atoms, the resulting time spectrum can be calibrated to a mass spectrum. This is achieved by computer software calculating a constant mass proportionality between the arrival time of two masses used for calibration and then using linear regression with further calibration masses to reduce chromatic aberration effects from the reflectron. Time resolution is absolutely key as the accuracy of the system and its detector determine both mass scale exactness and mass resolution (Briggs D and Seah M, 1992) (See Figure 3.4).

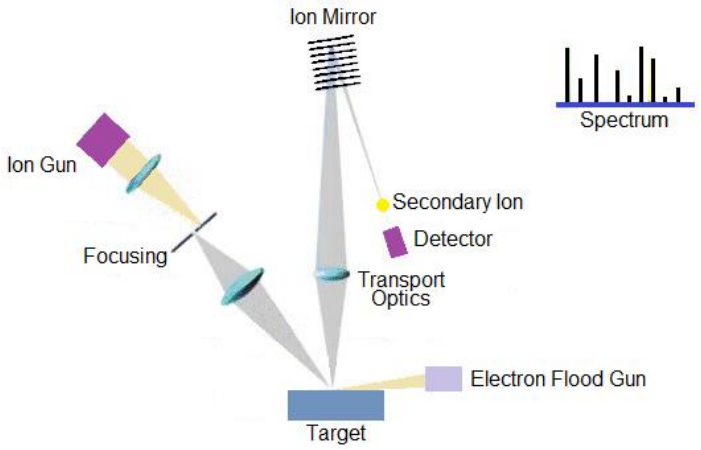

Figure 4.4 Sketch of the functional principle of a ToF-SIMS instrument

The detection limit of ToF SIMS is much lower than that of XPS and is on the order of ppm and ppb and typically the analysis areas using ToF SIMS range in size from 500 µm x 500 µm to 50 µm x 50 µm. Unlike XPS, SIMS is able to detect all elements in the periodic table and thus the location of H within an oxide film can be examined. The destructive nature of SIMS allows for in-

depth profiles of the surface to be collected, and when used in conjunction with XPS, a detailed distribution of the oxide/hydroxide phases within a surface can be obtained (Vickerman J.C and Briggs, 2013).

ToF-SIMS is a highly sensitive technique, capable of detecting fractions of a monolayer or sub-ppm elemental concentration at a surface (Passchier C.W and Trouw R.A.J 2005). It offers certain advantages over other techniques in terms of chemical specificity and surface sensitivity. These advantages include its excellent chemical sensitivity, the ability to distinguish between two isotopes of the same element and the ability to obtain information on chemical bonding at the surface by analyzing molecular ions (O'Connor D.J et al., 2003); what is really interesting to be able to verify the existence of the covalent S-NO link, which is be the main goal of the experiment in this thesis. TOF-SIMS was carried out on an ION-TOF TOF-SIMS IV mass spectrometer, using a mono-isotopic Bi^+ beam, generated by a liquid metal gun mounted on the instrument. The beam current was 1.5 pA. Positive and negative ion spectra were calibrated using H^+, C^+, $C_xH_y^+$ (x = 1-5 and y = 1-12) and H^-, C^-, $C_xH_y^-$ (x = 1-5 and y = 1-12) peaks. The depths probed by this technique range from 1-1.5 nm but the peak intensities are qualitative.

CHAPTER 5 ARTICLE 1: A COMPARATIVE PHYSICOCHEMICAL, MORPHOLOGICAL AND MAGNETIC STUDY OF SILANE-FUNCTIONALIZED SUPERPARAMAGNETIC IRON OXIDE NANOPARTICLES PREPARED BY ALKALINE COPRECIPITATION.

Laura-Karina Mireles, [a*] Edward Sacher, [a, b] L'Hocine Yahia, [a] Sophie Laurent, [c,d] and Dimitri Stanicki [d]

[a] Laboratoire d'Innovation et d'Analyse de Bioperformance, École Polytechnique de Montréal, C.P. 6079, Succursale Centre-ville, Montréal, Québec H3C 3A7, Canada.

[b] Département de Génie physique, École Polytechnique de Montréal, C.P. 6079, Succursale Centre-ville, Montréal, Québec H3C 3A7, Canada.

[c] Department of General, Organic, Biomedical Chemistry, NMR and Molecular Imaging Laboratory, Université de Mons, 19 Avenue Maistriau, B-7000 Mons, Belgium.

[d] Center for Microscopy and Molecular Imaging (CMMI), B-6041 Gosselies, Belgium.

Contact e-mail: karina.mireles@polymtl.ca Telephone: (514) 340-4711, ext. 2838

Published in the Journal: The International Journal of Biochemistry & Cell Biology 75 (2016) 203–211

5.1 Graphical abstract

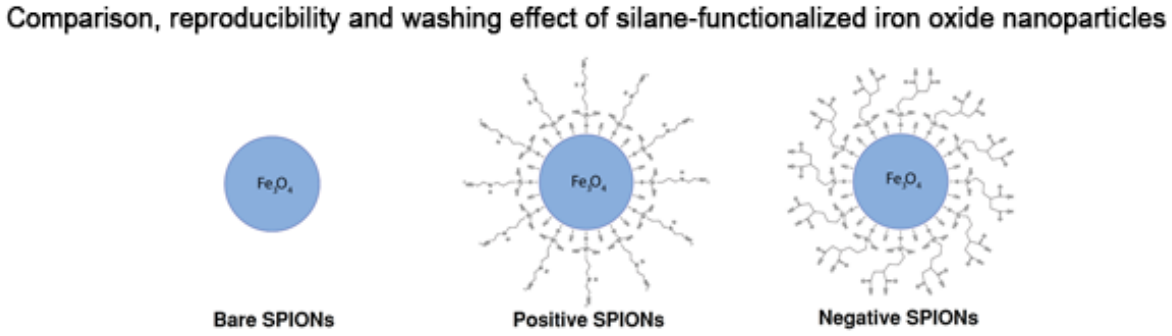

5.2 Highlights

- Detailed surface characteri5.3zations of core-shell superparamagnetic magnetite nanoparticles to probe the chemistry of the surface, predict future functionalization for drug delivery, and understand batch-to-batch repeatability, protein corona formation and cytotoxicity effects

- Comparison of product reproducibility and washing effect by dialysis on surfaces
- Batch-to-batch variation of surface chemistry is found in all the samples

5.3 Abstract

The characterization of synthetic superparamagnetic iron oxide nanoparticle (SPION) surfaces prior to functionalization is an essential step in the prediction of their successful functionalization, and in uncovering issues that may influence their selection as magnetically targeted drug delivery vehicles (prodrugs). Here, three differently functionalized magnetite (Fe_3O_4) SPIONs are considered. All were identically prepared by the alkaline coprecipitation of Fe2+and Fe3+salts. We use X-ray photoelectron spectroscopy, electron microscopy, time-of-flight SIMS, FTIR spectroscopy and magnetic measurements to characterizetheir chemical, morphological and magnetic properties, in order to aid in determining how their surfacesdiffer from those prepared by Fe $(CO)_5$ decomposition, which we have already studied, and in assessing their potential use as drug delivery carriers.

Key words*:* Drug delivery; magnetite; superparamagnetic nanoparticles; surface analysis; surface reproducibility; washing effect.

5.4 Introduction

Advances in the technology of nanoparticles used in drug delivery applications herald a promising future for their use in medicine. Currently many research teams are investigating targeted drug delivery for the treatment of cancers, (Davydov et al., 2014) and pulmonary, (Pham et al., 2015) cardiovascular (Rao et al., 2014) and infectious diseases, (Davydov et al., 2014; Pham et al., 2015; Rao et al., 2014; Mbeh et al., 2012) among others. Our group, for example, is interested in nanocarriers that act against bacteria and are capable of preventing biofilm formation on implant surfaces, because nosocomial infections represent a huge health problem around the world: just in Canada, a quarter of a mil-lion cases of associated infections are reported annually. This fact results in 8500–12,000 deaths, and the rate is rising (Healthcare - associated Infections, 2009). Infections caused by *Staphylococcus epidermidis* and *Staphylococcus aureus* are the most common, and are present in 70–90% of reported cases of implant-related infections (Dickinson and Bisno., 1989). Our approach to the prevention of the

bacterial adhesion is to develop functional coatings that are capable of destroying adhering bacteria (Nablo et al., 2005). Antibiotics, (Trampuz and Widmerm, 2001; Wilcox et al., 2001) silver ions (Yamanaka et al., 2005) and nitric oxide (NO), (Nablo et al., 2005) among others, have all shown antibacterial proper-ties, reducing the amount of bacterial adhesion. Various vehicles have been proposed for use as prodrugs; these include nanoparticles, (Franc¸ a et al., 2013; Zhang et al., 2012) micelles (Zhang et al., 2012) and polymers (Franc¸ a et al., 2013; Zhang et al.,2012). We propose to use functionalized SPIONs to target the infected site. SPIONs are considered to be excellent candidates for drug delivery, (Franc¸ a et al., 2013) since they can be directed in vivo to the specific target sites using external magnetic fields, when their diameters are smaller than 100 nm (Frankel et al., 1997; Felfoulet al., 2010; Brosseau et al., 2003).

On attaining the target, they function as advanced medical tools. As examples, they may be used as prodrugs, (Franc¸ a et al., 2013;Zhang et al., 2012; Felfoul et al., 2010; Afkhami et al., 2011) as contrast agents, (Felfoul et al., 2010; Afkhami et al., 2011) in hyperthermia (Felfoul et al., 2010; Afkhami et al., 2011; Liu et al., 2012) and in cancer treatment (Afkhami et al., 2011; Liu et al., 2012;Sawant et al., 2009). They possess low cytotoxicity and high bio-compatibility, (Mbeh et al., 2012) and have been accepted by the United States Food and Drug Administration (FDA), both as pro-drugs and for clinical MRI applications (Gupta and Wells, 2004; Tassa et al., 2011). In vivo, SPIONs are converted to ferric ions, which are assimilated into the biological iron storage pool, as erythrocytes, indicating their acceptable use in humans (Li and Chen, 2011).In a previous paper, we considered SPIONs manufactured by the thermal decomposition of $Fe(CO)_5$, whose mechanism is obscure: the nominally zero-valent Fe must oxidize to Fe^{2+} and Fe^{3+}, in the correct 1:2 ratio, before obtaining O, and forming Fe_3O_4 SPIONs. Their surfaces were found to be heavily contaminated during fabrication, (Franca et al., 2013) and they were found to have batch-to-batch variations of the surface chemistry, extensive enough to remove them from consideration as prodrugs. In fact, the general reproducibility of nanoparticle surface chemistry may presently be unfeasible. This presents a serious challenge for new biomedical applications, with their safety related issues (protein corona formation, and the resultant bio and hemocompatibilities) that depend on the control of the chemical and physical properties of the surfaces. In the present paper, we characterize SPIONs made in a more conventional manner: the alkaline coprecipitation of Fe^{2+} and Fe^{3+}, in the correct 1:2 ratio; the precipitate loses water and forms Fe_3O_4 on annealing. SPIONs fabricated in this manner have been the subjects of several

recent papers (Forge et al., 2008; Bridot et al., 2013). It is our purpose to thoroughly characterize them, to determine to what extent their surfaces differ from those made by the thermal decomposition of Fe $(CO)_5$, which we previously studied, (Franca et al., 2013) to what extent their synthesis is reproducible, and, through this, if they can be considered as potential candidates for use as prodrugs to target the infected sites.

5.5 Materials and methods

5.5.1 Synthesis

5.5.1.1 Bare SPIONs

Bare SPIONs were synthesized by the alkaline coprecipitation of iron salts in diethylene glycol (DEG), according to a published protocol. (Forge et al. 2008, Bridot et al. 2013) Briefly, a mixture of $FeCl_2.4H_2O$ (45 mmol; 8.9 g) and $FeCl_3$ (45% solution; 37 mmol; 9.1 ml) in DEG (250 ml) was heated under N_2 at 170°C, with stirring. After 15 min, solid NaOH (15 g) was added. After stirring for 1 h at 170°C, the solution was cooled and the magnetic particles were isolated by magnetic decantation (B_0 = 0. 5 T). The black precipitate was washed five times with aqueous HNO_3 (200 ml, 1 M) and the SPIONs were dispersed in deionized water, sonicated (45 min), and centrifuged (16, 500 G; 45 min) to remove aggregates (eq. (1)).

(1) $$2Fe^{3+} + Fe^{2+} + 8OH^- \longrightarrow Fe_3O_4 + 4H_2O$$

5.5.1.2 Positive SPIONs

TPED [N-[3-(trimethoxysilyl)propyl] ethylenediamine] (50 mmol; 10.8 ml) was slowly added to an aqueous suspension of bare SPIONs (200 ml; [Fe] = 25 mM) at 50°C and the mixture was heated at reflux for 2 h. On cooling, the suspension was purified by membrane filtration (membrane cut-off: 30 kDa), and centrifuged (16, 500 g; 45 min).

5.5.1.3 Negative SPIONs

Bare SPIONs were treated with TEPSA [3-(triethoxysilyl) propyl succinic anhydride] in organic medium, as previously described. (Bridot et al. 2013, Stanicki et al. 2014) Briefly, TEPSA (25 mmol; 7.1 ml) was slowly added to a suspension of SPIONs in dimethylformamide (50 ml; [Fe] = 100 mM). Water was then added (4.3 ml), followed by an aqueous solution of $(CH_3)_4NOH$ (1 M; 2.5 mmol; 2.5 ml) at room temperature while stirring. After heating at 100°C for 24 h under continuous stirring, the SPIONs were collected by pouring the suspension into an acetone/diethyl ether mixture, followed by magnetic decantation. After washing with acetone, the black precipitate was dispersed in water and purified by membrane filtration (membrane cut-off: 30 kDa) before centrifuging (16, 500 g; 45 min).

5.6 Characterizations

5.6.1 Transmission electron microscopy (TEM)

Photomicrographs were obtained by bright-field imaging, using a JEM-2100F electron microscope, at beam energy of 200 keV. The elemental analysis was carried out by energy dispersive spectroscopy (EDS). Selected area electronic diffraction (SAED) was used to obtain crystal diffraction patterns. All the samples were diluted in water before preparation, and sonicated for 3 minutes to disperse the SPIONs. One drop of each sample was spread onto a copper grid and covered with a microscope cover glass until dry.

5.6.2 Vibrating sample magnetometry

Vibrating sample magnetometry was used to obtain the magnetization vs. magnetic field (M vs H) loop at room temperature, from H= 0 - 2 T, with a measurement precision of $1x10^{-6}$ emu. Measurements were determined on a known quantity of sample. Drops of each sample were spread onto a 10 mm x 10 mm piece of cleaned glass, and dried, and the weight of each sample was obtained before the measurement.

5.6.3 Transmission ir spectroscopy

Transmission IR spectra were obtained, in the range 400 - 4000 cm^{-1}, using a Thermo Scientific Nicolet 6700 Fourier transform IR spectrometer, at a resolution of 4 cm^{-1}; 96 co-

additions were used to increase S/N. The samples were deposited by placing a drop on a diamond plate, and drying before adding the next drop; spectra were obtained after depositing three drops.

5.6.4 X-ray photoelectron spectroscopy

X-ray photoelectron spectroscopy (XPS) was performed with a VG ESCALAB 3 MK II (Thermo VG Scientific), using non-monochromated Al Kα X-rays (hν = 1486.6 eV) at an instrument resolution of 0.85 eV and a perpendicular take-off angle. The analysis chamber pressure was < 10^{-9} torr. Following Shirley background removal, the component peaks were separated by the VG Avantage software. The energy was calibrated by setting the C1s C-C peaks of all but the negative SPIONs to 285 eV; the energy of the negative SPIONs was calibrated by setting the more prominent C-Si peak to 284.1 eV. FWHM values were those previously established in our laboratory. Drops were deposited onto highly oriented pyrolytic graphite (HOPG) and permitted to dry.

5.6.5 Time-of-flight SIMS

ToF-SIMS was carried out on an ION-TOF TOF-SIMS IV mass spectrometer, with a mono-isotopic Bi^+ beam, generated by a liquid metal gun mounted on the instrument. The beam current was 1.5 pA. Drops of the samples were deposited onto a silicon substrate, covering an area greater than 2 mm x 2 mm, and permitted to dry. Positive ion spectra were calibrated using H^+, H_2^+, and $C_xH_y^+$ peaks, and negative ion spectra used C^-, CH^-, C_2^-, C_2H^-, C_3^- and C_3H^- peaks.

5.7 Results

5.7.1 TEM (Size distribution and morphology)

ToF-SIMS photomicrographs are found in Fig. 1, all SPIONs (Figure 5.1a-c) had well-defined shapes; their selected area electron diffraction patterns correspond to Fe_3O_4.The size distributions can be observed in the histograms (Figure 5.2), where the average diameters of bare, positive and negative SPIONs (Figure 5.2a-c) are 9.2 ± 1.3, 9.7 ± 1.8 and 9.9 ± 1.1 nm, respectively.

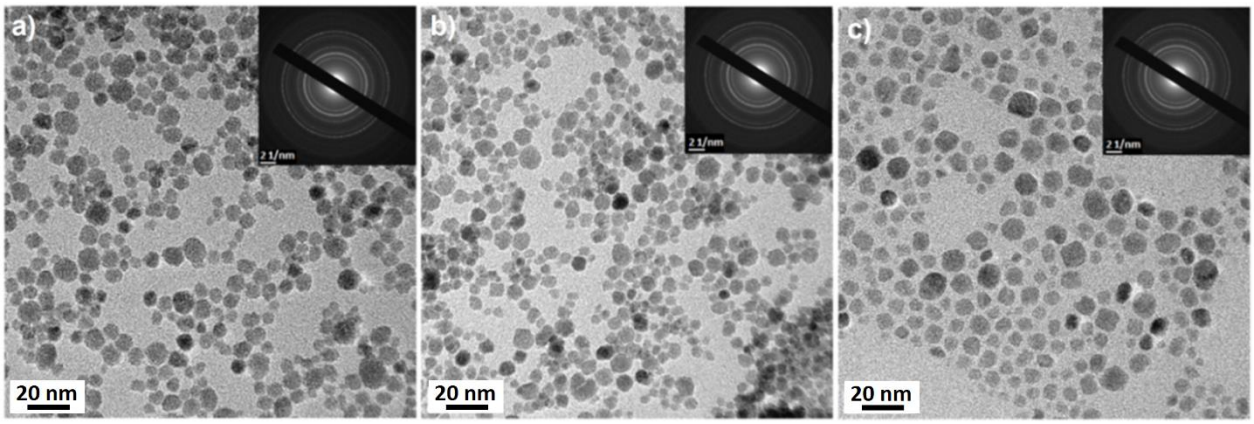

Figure 5.1 TEM images of: (a) bare SPIONs (b) positive SPIONs and (c) negative SPIONs

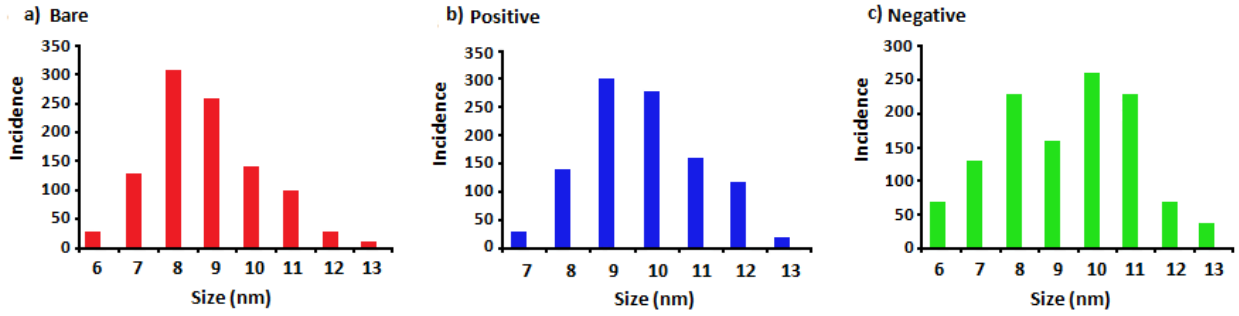

Figure 5.2 Size distributions of: (a) bare, (b) positive and (c) negative SPIONs

5.7.2 VSM

Figure 5.3 contains the magnetization curves of the samples at room temperature. The absence of hysteresis loops confirms that the three SPIONs have superparamagnetic behavior. The saturation magnetization (M_s) values were 27 emu/g for the bare SPIONs, 28 emu/g for the positive SPIONs and 24 emu/g for the negative SPIONs, all at ~ 10 000 Oe.

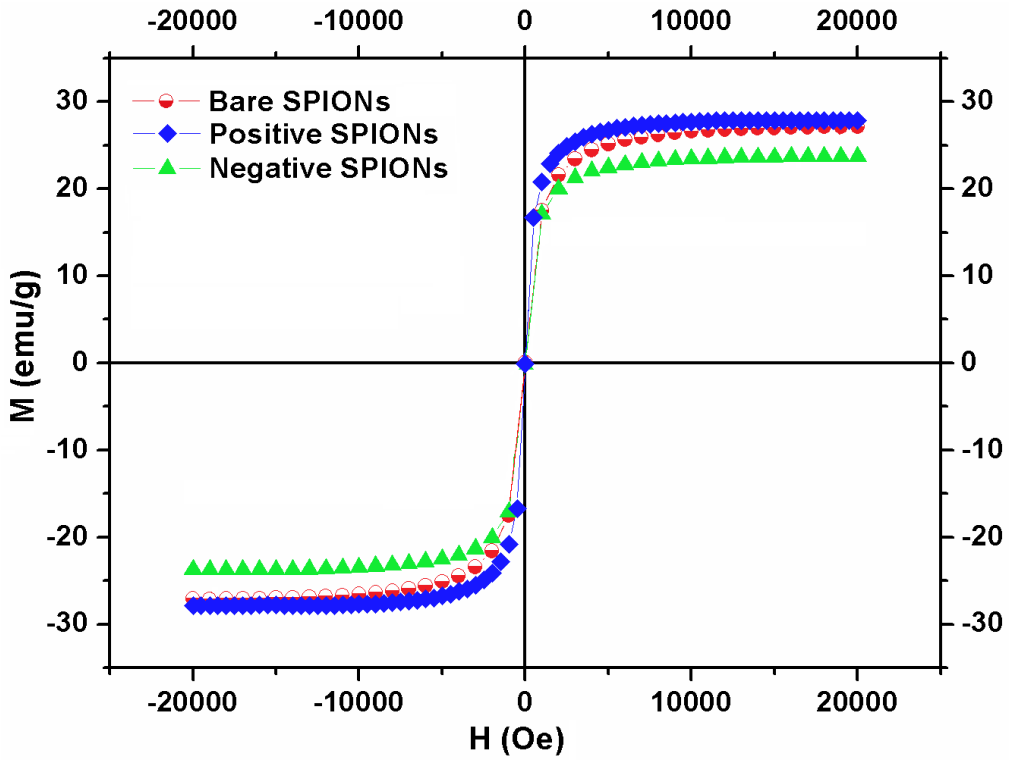

Figure 5.3 Magnetization curves of SPIONs

5.7.3 XPS

In this section, the results of two batches of SPIONs are presented. A second batch was characterized because (1) the analysis of the first batch showed the presence of surfaces contaminantes and (2) we wished to determine whether there were batch-to-batch inconsistencies.

SPION survey spectra, seen in the upper row of Figure 5.4 (first batch) and Fig. 5 (second batch), revealed the presence of carbon, oxygen, iron, nitrogen and silicon. For pure Fe_3O_4, the chemical distribution of Fe ions would correspond to 1:1:1 Fe^{II} octahedral: Fe^{III} octahedral: Fe^{III} tetrahedral. (Poulin et al.2010) In the spectra of all the SPIONs in Figure 5.4 and 5.5, it is clear that none of the Fe^{II} octahedral (~ 709.6 eV): Fe^{III} octahedral (~ 710.2-711.7 eV): Fe^{III} tetrahedral (~ 712.9-713.7 eV) peaks of the SPIONs correspond to this ratio, probably due to incomplete surface oxidation, as well as chemical modifications that occurred during manufacture and functionalization.

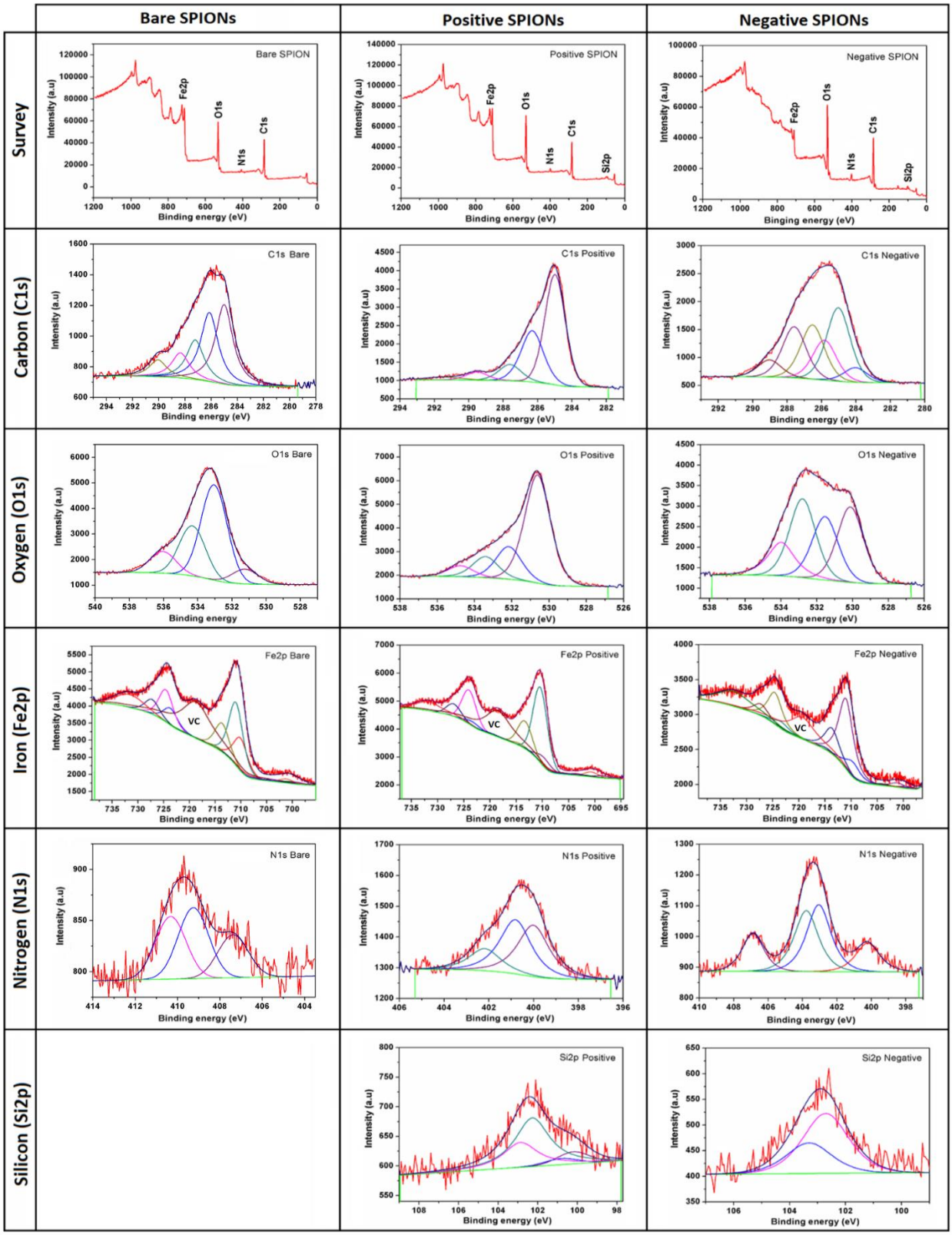

Figure 5.4 High resolution XPS spectra of bare, positive and negative SPIONs (first batch)

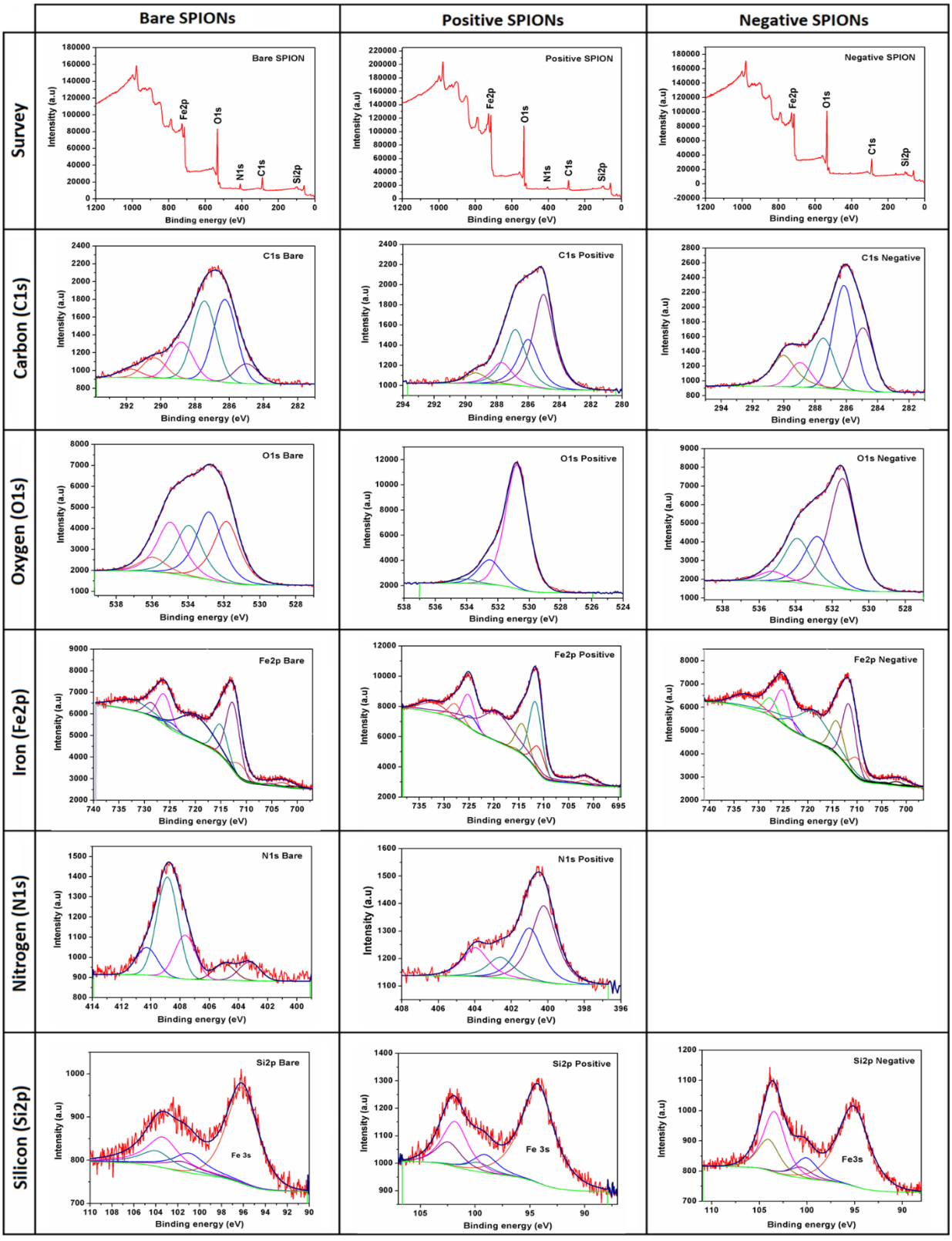

Figure 5.5 High resolution XPS spectra of positive, negative and bare SPIONs (second batch)

5.7.3.1 Bare SPIONs

The spectra of the bare SPIONs, in Figure 5.4 and 5.5, contain several contaminant peaks, such as oxidized C and NO_3^-, present even before functionalization. While peak attributions are found in Table 5.1, some peaks could not be attributed with certainty, due to contaminant interference, SPION catalysis and peak overlap.

Table 5.1 Summary of XPS deconvolution of SPIONs from the first and second batches

Comparison first and second batches—peak positions						
Suggested attribution	Bare SPIONs (eV)		Positive SPIONs (eV)		Negative SPIONs (eV)	
	First batch	Second batch	First batch	Second batch	First batch	Second batch
C—Si			284.1 (~0)		284.1	
C—C	285.0	285.0	285.0	285.0	285.0	285.0
C—N			285.8	286.0	285.8	
C—O	286.1	286.3	286.1	286.8	286.5	286.2
C═O	287.2	287.5	287.5	287.7	287.6	287.5
COOH	288.4 (***)	288.8	289.5	289.4	289.2	288.9
COO—	290.1	290.4				290.0
***		291.8				
Fe—O	531.0		530.6	530.8 + Fe—OH	530.1	
Fe—OH					531.5 + O—Si	
C═O	532.9 + Fe—OH	531.8 + Fe—OH	532.2 + O—Si	532.5	532.8	531.4 + Fe—OH
C—O	534.1 + C—OH	532.8	533.4		533.9 + C—OH	532.8
C—OH/O—N			534.7	534.1		533.9
***	536.8	535.0				535.3
***		536.0				
NH_2			400.1	400.2	400.2	
NH_3^+			400.8	401.0		
NO			402.2	402.6		
***						
NO_2		403.3			403.0	
***		405.0		404.0	403.8	
NO_3 organic	407.2	407.7			406.8	
NO_3 inorganic	408.3	408.8				
***	409.5	410.3				
Fe II octa	710.1	711.1	709.7	711.0	709.7	710.0
Fe III octa	711.0	712.6	710.4	711.8	711.0	711.6
Fe III tetra	713.7	715.0	713.4	714.2	713.7	714.1
Si—C				99.2		100.1
Si—O		101.0	100.2 + Si—C			
$Si—O_2$			102.3	101.9		
$Si—O_3$		103.4			102.7	103.4

*** correspond to unattributed peaks (***) at 288.4 eV on the first batch corresponds to peak with low energy to be attributed to COOH.

5.7.3.2 Positive SPIONs

The pK_as of amines lie near 9, so that, in water (pH = 7), they are protonated ($-NH_3^+$) and, thus, positively charged. The deposition of aminosilanes, such as the TPED used here, is self-catalyzed (Kaas et al.1971) and, on deposition onto *flat plates*, results in surface layers several nm thick. However, HRTEM photomicrographs of all the SPIONs (Figure 5.6) show the absence of

such a layer, as does the absence of C1s peak components attributable to C-Si and C-N. Despite this, the presence of N1s and Si2p spectra indicates that at least *some* aminosilane molecules were deposited, probably as a monolayer or less. This lack of an expected silane layer is surely due to the fact that the Fe_3O_4 SPION is itself, a catalyst (Agnihotri et al. 2013) of certain reactions and, as the XPS component peaks in Table 1 indicate, is capable of causing unexpected reactions, such as the C and N oxidations and Si fragmentation, previously reported by us. (França et al. 2013, Zhang et al. 2012)

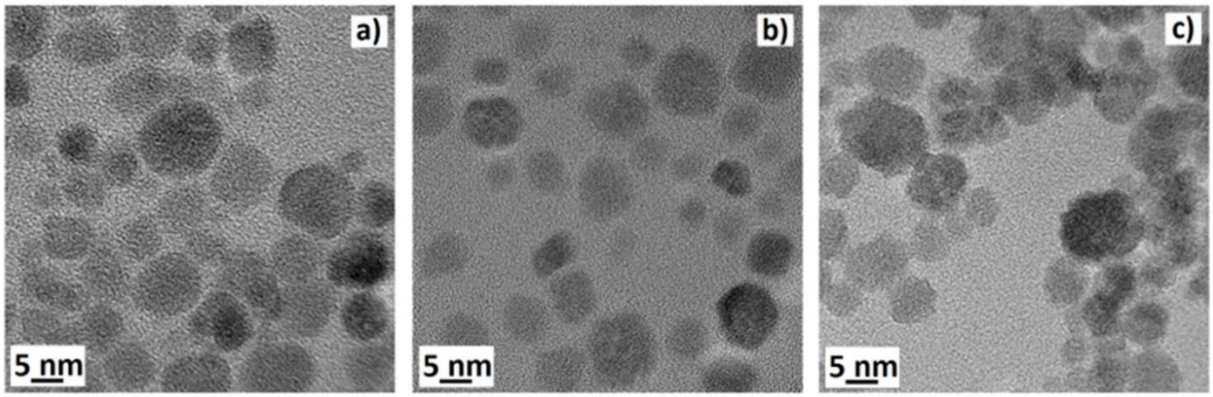

Figure 5.6 HRTEM photomicrographs of (a) positive, (b) negative and (c) bare SPIONs. Each sample lacks a visible surface coating

5.7.3.3 Negative SPIONs

The pK_as of carboxylic acids, obtained when the anhydride of the presently used TEPSA is hydrolyzed, lie near 4, so that, in water, they are ionized ($-COO^-$), and, thus, negatively charged. As noted earlier, HRTEM photomicrographs indicate the absence of a noticeable surface layer (Figure 5.6), although this may be due, in part, to the omission of a deposition catalyst. (Kaasand Kardos, 1971) The presence of a Si2p spectrum and the subdued presence of the C1s carboxylic acid component indicate that only some anhydride was deposited, as previously found, (Stanicki et al. 2014) again as a monolayer or less. The unexpected presence of the various N1s components indicates contamination, probably by the HNO_3 used in the sample preparation. The peak attributions are found in Table 5.1.

In an effort to understand the presence of impurities on the surface, particularly as to which can affect the functionalization of the nanoparticles as prodrugs, and whether they can be removed by washing, we carried out a study of the surfaces of the nanoparticles from the second batch, subsequent to dialysis (Mireles et al, 2016). As seen in Table 1 of the accompanying Data in Brief (article 2), while some contaminants can, indeed, be removed by washing, the washing process introduces others.

5.7.4 FTIR spectroscopy

Figure 5.7 shows the IR spectra of the three SPIONs. The bands and their attributions are found in Table 5.2, and corroborate the species found by XPS. The presence of oxidized N is attributed to the trace of HNO_3, as well as to oxidized amine (positive SPIONs). The presence of silica demonstrates the attachment of silane chains to the surface (positive and negative), only a monolayer or less, as already noted. In confirmation, the sizes of all the types of SPIONs are, within experimental error, identical.

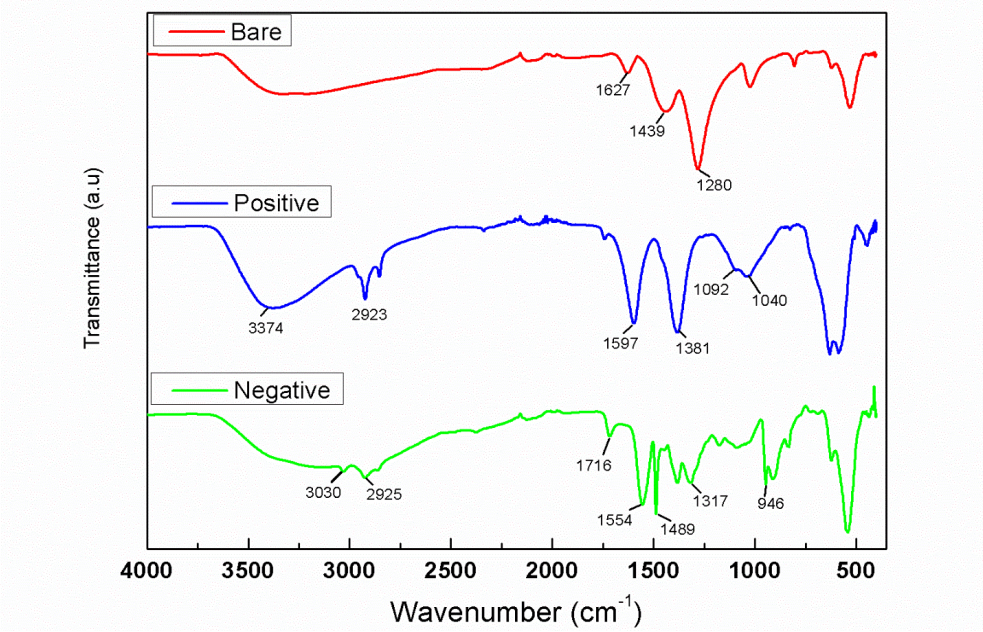

Figure 5.7. IR spectra of bare, positive and negative SPIONs

Table 5.2 Attribution of FTIR peaks from the first batch

Sample	Wavelength (cm^{-1})	Attribution
Bare	1627	R—O—NO_2
	1280	NO_3^-
Positive	3374	NH_n
	1741	C=O
	1597	RNH_2, R_2NH
	1381	R_2NH, RNO_2, NO_3^-
	1092	Si—O—Si
	1040	Si—O—C
Negative	3030	OH
	2925	C–H
	1716	C-O
	1554	COO^-
	1489	COO^-
	1374	RNO_2, NO_3^-
	1317	C–O
	1175	Si–O–Si
	1090	Si—O—C
	946	OH
	911	OH

5.7.5 TOF-SIMS

TOF-SIMS spectra of the SPIONs, in Figure 5.8, confirm the presence of amine groups in positive SPIONs. Na^+ appears in positive spectra, with elevated peak intensity, because Na^+ has a very large ion yield but a low XPS sensitivity, where it is far more difficult to see. While the C1s spectrum of the negative SPIONs was anticipated to be rich in carboxylic acid groups, the intensity found was very low, again supporting the XPS results.

Although it is important to note that TOF-SIMS is not quantitative, a comparison of the high resolution amine peaks in positive SIMS (Figure 5.9a) and the carboxylic acid peaks in negative SIMs (Figure 5.9b) show that all three types of SPIONs contain both amine and carboxylic acid groups. While the positive SPIONs have the most intense amine peak, both positive and bare SPIONs have more intense carboxylic acid peaks than the negative SPIONs. A summary of the principal peaks is found in Table 5.3.

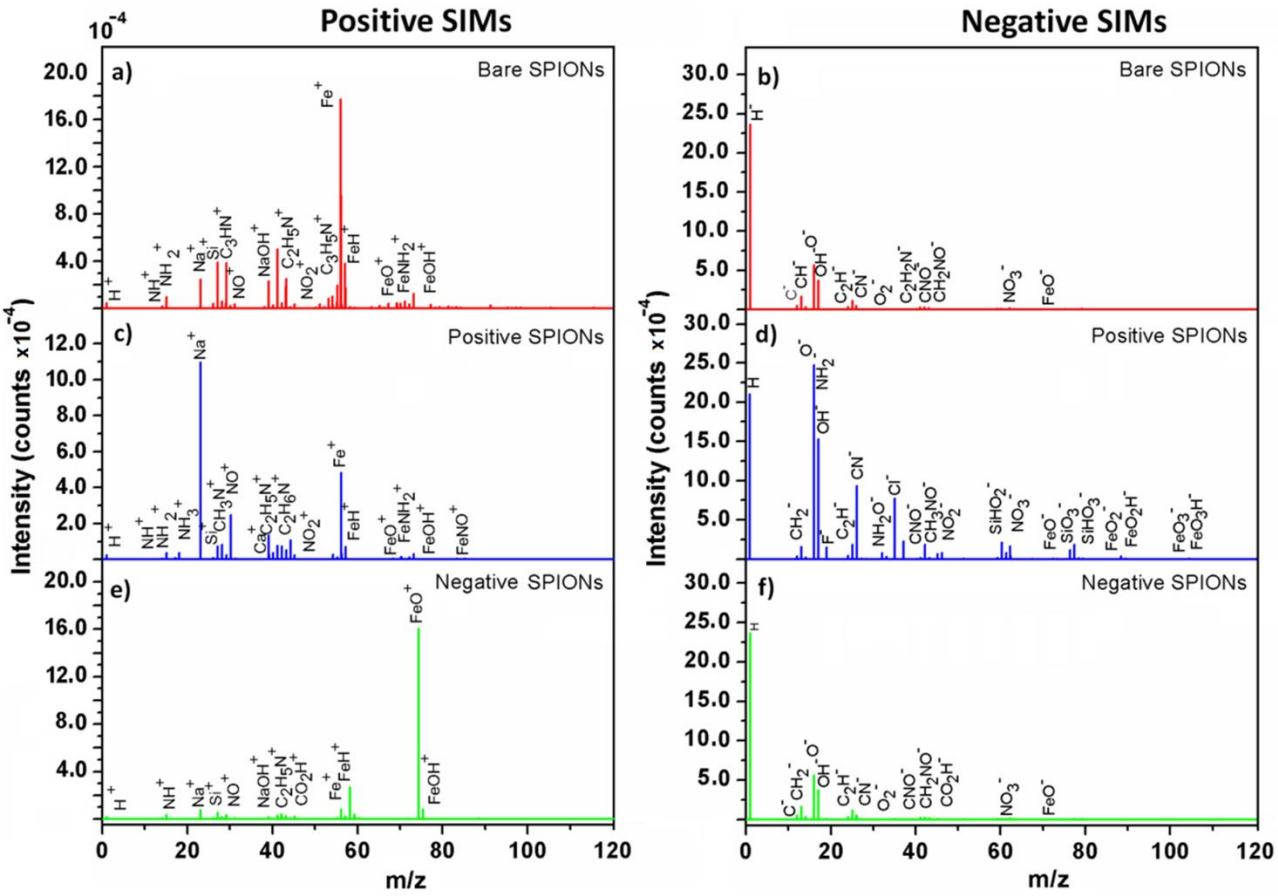

Figure 5.8 Positive and negative SIMS spectra of ((a) and (b)) bare, ((c) and (d)) positive and ((e) and (f)) negative SPIONs

Table 5.3 Masses and attributions of the fragments found in SPIONs from the first batch

Species	Mass (D)	Species	Mass (D)
C	12.00	CO_2H	44.99
NH	15.02	NO_2	45.99
O	15.99	Fe	55.93
NH_2	16.01	FeH	56.94
OH	17.00	FeO	71.92
NH_3	17.02	FeOH	72.93
Na	22.98	FeNO	85.93
NO	29.99	FeO_2	87.92

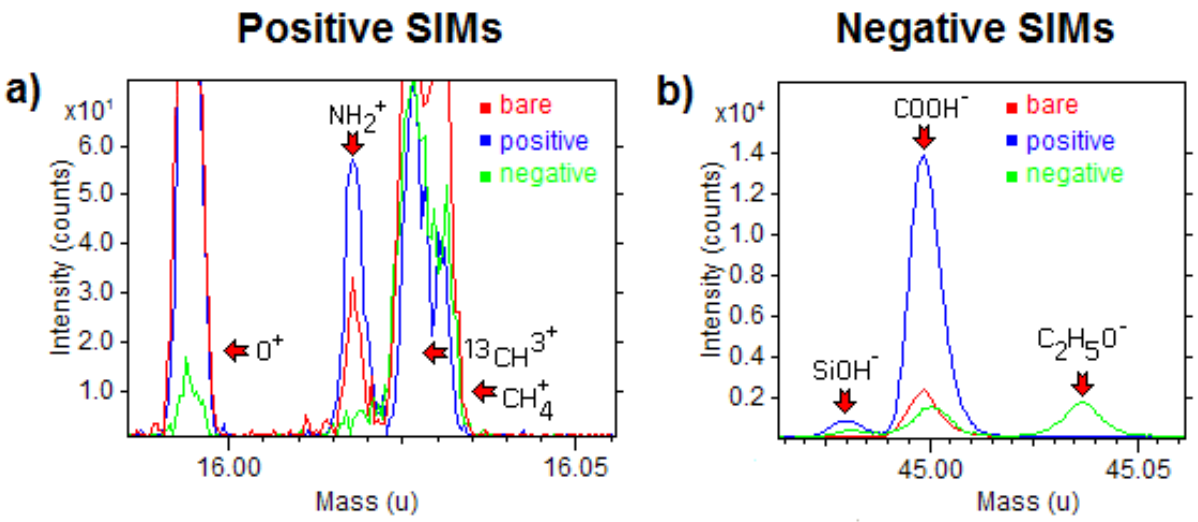

Figure 5.9 High resolution SIMS comparisons of (a) NH2 peaks (M: 16.01), (b) COOH peaks (M: 44.99), of the SPIONs

5.8 Discussion

Surface analysis plays an extremely important research role as a fundamental technique in characterizing functionalized SPIONs proposed as drug delivery vehicles. This is because low resolution techniques (e.g., FTIR), cannot satisfactorily confirm that functionalization has occurred, as opposed to the high-resolution techniques used in the present paper.

As mentioned earlier, our goal is the characterization of the surface functionalization of SPIONs produced by alkaline coprecipitation, and its reproducibility. In contrast, results found in the literature often lack surface analytical characterizations that confirm the attachment of drugs onto ostensibly functionalized nanoparticles. Further, a lack of reproducibility in nanomaterial fabrication creates a worrisome situation for the research community, as well as for companies that produce and develop products and processes, destined for use in the human body, that use them. One crux of the problem is surely a lack of standards and techniques for surface characterization, and their use in quantifying reproducibility.

5.8.1 Surface characterization

Our SPIONs showed relatively uniform sizes around 10 nm (Figure 5.1 and 5.2), and spherical shapes (Figure 5.1). The increases in average sizes of our positive and negative SPIONs, compared to our bare SPIONs, are around 0.5 and 0.7 nm, respectively (Figure 5.6). These results are comparable with hydrodynamic diameters of 9.3 ± 1.4 nm for bare SPIONs, 10.1 ± 1.3 nm for positive SPIONs and 10.4 ± 1.6 nm for negative SPIONs, previously published by us (*Mbeh DA* et al. 2015); both techniques confirm the essentially identical sizes of our SPIONs, and their small size differences; since both of the silanes used have lengths of > 1 nm, this implies possible silane fragmentation [11] on deposition, and/or only partial functionalization, too low for self-assembly.

The XRD patterns of our SPIONs (Figure 5.1) indicate magnetite cores. Their magnetic properties (Figure 5.3) indicate reasonably high magnetization (around 26 emu/g), and the absence of a hysteresis loop confirms them to be SPIONs.

The presence of -NH_2 and -COOH were confirmed by our XPS (Table 5.1), FTIR (Table 5.2) and TOF-SIMS (Table 5.3) results. These three techniques also showed traces of residual contaminants, as well as cross-contamination; since precautions were taken to avoid cross-contamination, its presence appears to be unavoidable and can affect the chemical surface analysis, as seen in the XPS attributions in Tables 1 and in the accompanying second article in Data in Brief (Mireles et.al., 2016). Examples of contamination abound, such as both positive and bare SPIONs containing amine groups, and negative SPIONs being the least rich in carboxylic acid groups.

Our previous studies (França et al. 2013) on SPIONs manufactured by the thermal decomposition of Fe $(CO)_5$ showed the same characteristics found in the present case: batch-to-batch differences in Tables 5.1 and 5.2, and in the accompanying Data in Brief (Mireles et.al., 2016), hydrocarbon-contaminated surfaces, the absence of a silane layer (although a silane layer may be deposited over a silica layer from the alkaline decomposition of TEOS), amine oxidation and silane fragmentation. The absence of a substantial silane layer deposited onto the bare SPIONs has been found by others using other fabrication schemes, (França et al. 2013, Agnihotri et al. 2013, Boon et al. 2014) making it improbable that this is due to our manufacturing process. Zeta potential measurements, for the SPIONs considered here, were determined previously (*Mbeh DA* et al. 2015) in water, PBS and culture media containing fetal bovine serum; they were found to have potentials of -25 mV for bare SPIONs, +35 mV for positive SPIONs and -40 mV for negative

SPIONs. The negative potential of the bare SPIONs supports our contention of unavoidable contamination during synthesis, and such contamination can be persistent even after dialysis (Mireles et. al., 2016), as our results demonstrate.

5.9 Conclusions

The surfaces of our SPIONs are only weakly functionalized by direct reaction with silanes, probably due to the catalytic effect of the magnetite core. Further, their manufacture appears to involve unavoidable contamination that can cause problems impacting biomedical applications. In this context, the determination of the presence of contaminants produced by the various manufacturing processes, and the extent of reproducibility are important in monitoring SPION purity and eventual use as prodrugs for use in the human body. Finally, based on the unavoidable presence of unexpected chemical groups, it may well be that bare SPIONs, when PEGylated with functionalized PEGs, offer the best opportunity as prodrugs because of the ability to control reproducibility.

5.10 Acknowledgements

We thank the Fonds de recherche du Québec (FQRNT) and the Groupe de recherche en sciences et technologies biomédicales (GRSTB) for support. We thank Josianne Lefebvre for assistance in processing the XPS and TOF-SIMs data, and Rafaella Oliveira do Nascimento, for contributions during discussions.

The ARC (research contract AUWB-2010—10/15-UMONS-5), the FNRS, the Walloon Region, the COST TD1004 and TD1402, the UIAP VII program and the Center for Microscopy and Molecular Imaging (CMMI, supported by the European Regional Development Fund and the Walloon Region) are thanked for their support.

References

Afkhami, F., Taherkhani, S., Mohammadi, M., Martel, S., 2011. Encapsulation ofmagnetotactic bacteria for targeted and controlled delivery of anticanceragents for tumor therapy. Conf. Proc. IEEE Eng. Med. Biol. Soc., 6668–6671.

Agnihotri, S., Mukherji, S., Mukherji, S., 2013. Immobilized silver nanoparticlesenhance contact killing and show highest efficacy: Elucidation of themechanism of bactericidal action of silver. Nanoscale 5, 7328–7340.

Boon, M.S., Mariatti, M., 2014. Silane treatment of magnetite filler and its effect onthe properties of magnetite-filled epoxy thin-film composites. Polym. Bull. 71, 3333–3346.

Bridot, J.L., Stanicki, D., Laurent, S., Boutry, S., Gossuin, Y., Leclère, P., Lazzaroni, R., Vander-Elst, L., Muller, R.N., 2013. New carboxysilane-coated iron oxidenanoparticles for nonspecific cell labelling. Contrast Media Mol. Imaging 8,466–474.

Brosseau, C., Youssef, J.B., Talbot, P., Konn, A.M., 2003. Electromagnetic andmagnetic properties of multicomponent metal oxides heterostructures: nanometer versus micrometer-sized particles. J. Appl. Phys. 93 (11),9243–9256.

Davydov, V., Rakhmanina, A., Kireev, I., Alieva, I., Zhironkina, O., et al., 2014. Solidstate synthesis of carbon-encapsulated iron carbide nanoparticles and theirinteraction with living cells. J. Mater. Chem. B 2, 4250–4261.

Dickinson, G.M., Bisno, A.L., 1989. Infections associated with indwelling devices: concepts of pathogenesis; infections associated with intravascular devices. Antimicrob. Agents Chemother. 33 (5), 597–601.

Felfoul, O., Mokrani, N., Mohammadi, M., Martel, S., 2010. Effect of the chain ofmagnetosomes embedded in magnetotactic bacteria and their motility onmagnetic resonance imaging. Conf. Proc. IEEE Eng. Med. Biol. Soc., 4367–4370.

Forge, D., Roch, A., Laurent, S., Tellez, H., Gossuin, Y., Renaux, F., Vander-Elst, L., Muller, R.N., 2008. Optimization of the synthesis of superparamagneticcontrast agents by the design of experiments method. J. Phys. Chem. C 112, 19178–19185.

Franca, R., Zhang, X.F., Veres, T., Yahia L'H, Sacher, E., 2013. Core–shellnanoparticles as prodrugs: possible cytotoxicological and biomedical impactsof batch-to-batch inconsistencies. J Colloid Interface Sci. 1 (389), 292–297.

Frankel, R.B., Bazylinski, D.A., Johnson, M.S., Taylor, B.L., 1997. Magneto-aerotaxisin marine coccoid bacteria. J. Biophys. J. 73, 994–1000.

Gupta, A.K., Wells, S., 2004. Surface-modified superparamagnetic nanoparticles fordrug delivery: preparation, characterization, and cytotoxicity studies. IEEETrans. Nanobiosci. 3 (1), 66–73.

Kaas, R., Kardos, J.L., 1971. The Interaction of alkoxysilane coupling agents withsilica surfaces. Polym. Eng. Sci. 11, 11–18.

Li, Y.F., Chen, C., 2011. Fate and toxicity of metallic and metal-containingnanoparticles for biomedical applications. Small 7, 2965–2980.

Liu, R-t, Liu, J., Tong, J.-Q., Tang, T., Kong, W.C., Wanga, X-w, Lib, Y., Tang, J-t., 2012.Heating effect and biocompatibility of bacterial magnetosomes as potentialmaterials used in magnetic fluid hyperthermia. Prog. Nat. Sci.: Mater. Int. 22(1), 31–39.

Mbeh, D.A., Franc¸ a, R., Merhi, Y., Zhang, X.F., Veres, T., Sacher, E., Yahia, L'H., 2012.In vitro biocompatibility assessment of functionalized magnetitenanoparticles: biological and cytotoxicological effects. J. Biomed. Mater. Res. A100 (6), 1637–1646.

Mbeh, D.A., Mireles, L.K., Stanick, D., Tabet, L., Maghni, K., Laurent, S., Sacher, E., Yahia, L'H., 2015. Human alveolar epithelial cell responses to core–shellsuperparamagnetic iron oxide nanoparticles (SPIONs). Langmuir 31, 3829–3839.

Mireles, L.K., Sacher, E., Yahia, L'H, Laurent, S. Stanicki, D. Washing effect onsuperparamagnetic iron oxide nanoparticles. Data in Brief7 (2016)1296–1301

Nablo, B.J., Prichard, H.L., Butler, R.D., Klitzman, B., Schoenfisch, M.H., 2005.Inhibition of implant associated infections via nitric oxide release. Biomaterials26 (34), 6984–6990.

Pham, D.-D., Fattal, E., Tsapis, N., 2015. Pulmonary drug delivery systems fortuberculosis treatment. Int. J. Pharm. 478, 517–529.

Poulin, S., Franca, R., Moreau-Bélanger, L., Sacher, E., 2010. Confirmation of X-rayphotoelectron spectroscopy peak attributions of nanoparticulate iron oxides.Using symmetric peak component line shapes. J. Phys. Chem. C 114 (24), 10711–10718.

Rao, S., Tan, A., Thomas, N., Prestidge, C.A., 2014. Perspective and potential of orallipid-based delivery to optimize pharmacological therapies againstcardiovascular diseases. J. Controlled Release 193, 174–187.

Sawant, R.M., Sawant, R.R., Gultepe, E., Nagesha, D., Papahadjopoulos-Sternberg, N., Sridhar, S., Torchilin, V.P., 2009. Nanosized cancer cell-targeted polymericimmunomicelles loaded with superparamagnetic iron oxide nanoparticles. J. Nanopart. Res. 11, 1777–1785.

Stanicki, D., Boutry, S., Laurent, S., Wacheul, L., Nicolas, E., Crombez, D., Vander Elst, L., Lafontaine, D.L.J., Muller, R.N., 2014. Carboxy-silane coated iron oxidenanoparticles: a convenient platform for cellular and small animal imaging. J. Mater. Chem. B 2, 387–397.

Tassa, C., Shaw, S.Y., Weissleder, R., 2011. Dextran-coated iron oxide nanoparticles: a versatile platform for targeted molecular imaging, molecular diagnostics, andtherapy. Acc. Chem. Res. 44 (10), 842–852.

Trampuz, A., Widmerm, A.F., 2001. Infections associated with orthopedic implants. Clin. Infect. Dis. 2 (33), S94–S106.

Wilcox, M., Kite, P., Mills, K., Sugden, S., 2001. In situ measurement of linezolid andvancomycin concentrations in intravascular catheter-associated biofilm. J. Antimicrob. Chemother. 47, 171–175.

Yamanaka, M., Hara, K., Kudo, J., 2005. Bactericidal actions of a silver ion solutionon Escherichia coli, studied by energy-filtering transmission electronmicroscopy and proteomic analysis. Appl. Environ. Microbiol. 71 (11), 7589–7593.

Zhang, X., Mansouri, S., Mbeh, D.A., Yahia L'H, Sacher, E., Veres, T., 2012. Nitricoxide delivery by core/shell superparamagnetic nanoparticle vehicles withenhanced biocompatibility. Langmuir 28 (35), 12879–12885.

Healthcare-associated Infections, January 2009. A Backgrounder, Online Availablefrom _http://cupe.ca/updir/healthcare-associated-infections-cupe-backgrounder.pdf_.

CHAPTER 6 ARTICLE 2: WASHING EFFECT ON SUPERPARAMAGNETIC IRON OXIDE NANOPARTICLES

Mireles LK[a], Sacher E[b], Yahia L[a], Laurent S[c], Stanicki D[d]

[a] Laboratoire d'Innovation et d'Analyse de Bioperformance, École Polytechnique de Montréal, C.P. 6079, Succursale Centre-ville, Montréal, Québec H3C 3A7, Canada.

[b] Département de Génie physique, École Polytechnique de Montréal, C.P. 6079, Succursale Centre-ville, Montréal, Québec H3C 3A7, Canada.

[c] Department of General, Organic, Biomedical Chemistry, NMR and Molecular Imaging Laboratory, Université de Mons, 19 Avenue Maistriau, B-7000 Mons, Belgium.

[d] Center for Microscopy and Molecular Imaging (CMMI), B-6041 Gosselies, Belgium.

Contact email: karina.mireles@polymtl.ca

Published in the Journal: Data in Brief 7 (2016) 1296–1301

6.1 Abstract

Much recent research on nanoparticles has occurred in the biomedical area, particularly in the area of superparamagnetic iron oxide nanoparticles (SPIONs); one such area of research is in their use as magnetically directed prodrugs. It has been reported that nanoscale materials exhibit properties different from those of materials in bulk or on a macro scale (Vaseashta, 2015). Further, an understanding of the batch-to-batch reproducibility and uniformity of the SPION surface is essential to ensure safe biological applications, as noted in the accompanying article (Mireles et. al., 2015), because the surface is the first layer that affects the biological response of the human body. Here, we consider a comparison of the surface chemistries of a batch of SPIONs, before and after the supposedly gentle process of dialysis in water.

6.2 Specifications table

Table 6.1 Specifications

Subject area	*Chemistry, Physics, Biology*
More specific subject area	*Surface characterization*
Type of data	*Table, figure*
How data was acquired	*X-ray photoelectron spectroscopy (XPS) was performed with a VG ESCALAB 3 MK II (Thermo VG Scientific), using non-monochromated Al Kα X-rays (hv = 1486.6 eV), at an instrument resolution of 0.85 eV and a perpendicular take-off angle. The analysis chamber pressure was < 10^{-9} torr. Following Shirley background removal, the component peaks were separated by the VG Avantage software.*
Data format	*Analyzed, etc.*
Experimental factors	*The energy was calibrated by setting the C1s C-C peaks of all but the negative SPIONs to 285 eV; the energy of the negative SPIONs was calibrated by setting the more prominent C-Si peak to 284.5 eV. FWHM values were those previously established in our laboratory.*
Experimental features	*Drops were deposited onto highly oriented pyrolytic graphite (HOPG) and permitted to dry*
Data source location	*École Polytechnique, Montréal, QC, Canada.*
Data accessibility	*Data are available with this article*

6.3 Value of the data

- Demonstration that the symmetric peak analysis of XPS data can characterize the surface chemistry of SPIONs, and their modifications.
- Demonstration of batch-to-batch variations in SPION surface chemistry.
- Demonstration that the water dialysis of SPIONs causes changes in SPION surface chemistry.

6.4 Data

SPIONs, treated with both aminosilane and carboxylic acid silane, were dialyzed to remove con- taminants. This apparently mild process was found to modify the SPION surface chemistry. See Table 1 on "A comparative physicochemical, morphological and magnetic study of silane-functionalized superparamagnetic iron oxide nanoparticles prepared by alkaline coprecipitation" (L.K. Mireles et.al., 2015).

6.5 Experimental design, materials and methods

Using a membrane with a 14 kD cutoff, the three SPIONs were each dialyzed for three days, with deionized water being changed several times a day. The peak comparisons of the XPS spectra, before (Figure 6.1) and after (Figure 6.2) dialysis, are found in Table 6.2 on "A comparative physicochemical, morphological and magnetic study of silane-functionalized superparamagnetic iron oxide nanoparticles prepared by alkaline coprecipitation" (L.K. Mireles et.al., 2015), which demonstrates the continued presence of impurities, despite the efforts made to clean the apparatus used, as well as the occurrence of unexpected reactions. These results indicate other sources of batch-to-batch inconsistencies in the manufacture of SPIONs, as we recently noted (L.K. Mireles et.al., 2015, R. Franca et.al, 2013). Such inconsistencies become important because they determine whether, and to what extent, the surface can be functionalized for use in the human body. The surprising new peaks that appear on dialysis suggest that even this process may provoke some reactions (recall that Fe_3O_4 SPIONs are catalysts (A.Z. Moshfegh, et.al, 2009)). In summary, we have used XPS to characterize the surface chemistry of SPIONs destined for use as prodrugs. The unexpected appearance and disappearance of component peaks demonstrates the apparently unavoidable batch-to-batch differences found on the nanoscale, as well as the usefulness of the XPS technique in determining them. This information is needed even before hemo and cytotoxicological testing occurs, and demonstrates the serious challenges facing manufacturers of prodrugs

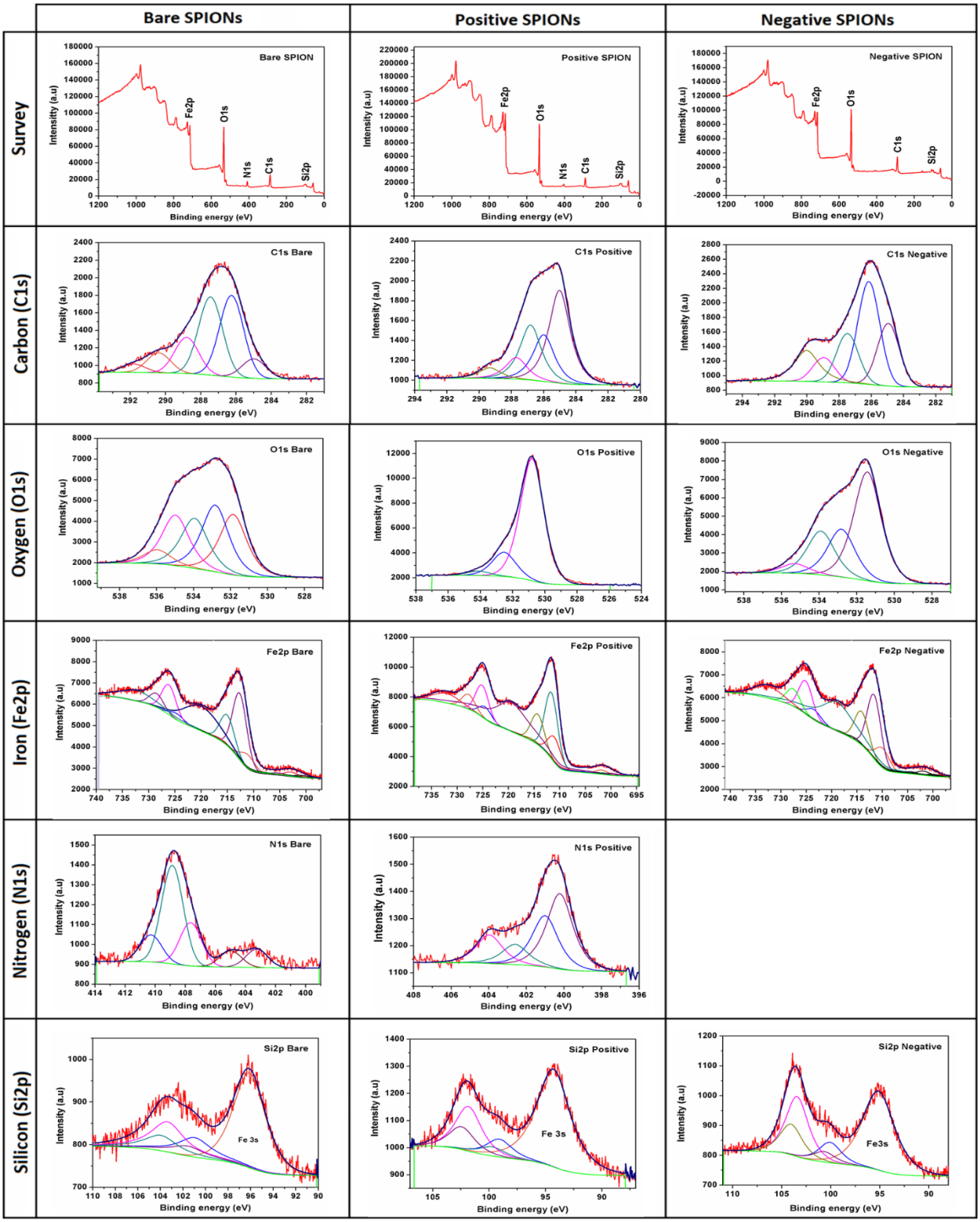

Figure 6.1 High resolution XPS spectra of positive, negative and bare SPIONs, second batch, before dialysis

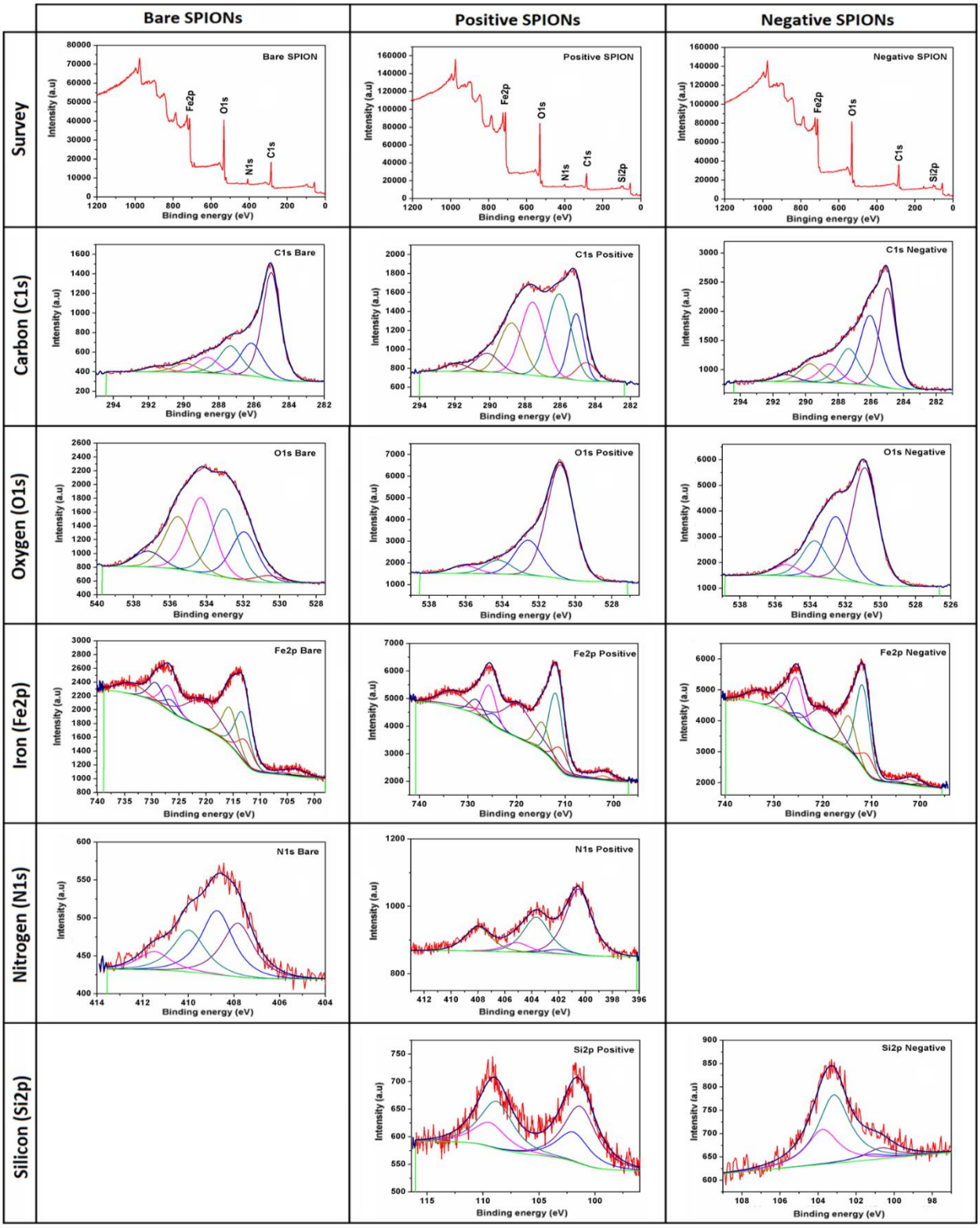

Figure 6.2 High resolution XPS spectra of positive, negative and bare SPIONs, second batch, after dialysis

Table 6.2 Summary of XPS spectral deconvolutions of SPIONs, second batch, before and after dialysis

SECOND BATCH – peak position						
Suggested attribution	**Bare SPIONs (eV)**		**Positive SPIONs (eV)**		**Negative SPIONs (eV)**	
	BEFORE DIALYSIS	**AFTER DIALYSIS**	**BEFORE DIALYSIS**	**AFTER DIALYSIS**	**BEFORE DIALYSIS**	**AFTER DIALYSIS**
C–Si				284.5		
C–C	285.0	285.0	285.0	285.0	285.0	285.0
C–N			286.0			
C–O	286.3	286.1	286.8	286.1	286.2	286.1
C=O	287.5	287.3	287.7	287.6	287.5	287.4
COOH	288.8	288.6 (?)	289.4	288.8	288.9	288.6 (?)
COO-	290.4	289.9		290.1	290.0	289.7
***	291.8	291.5		291.9		291.2
Fe–O		530.6	530.8+Fe–OH	530.8+Fe–OH		530.9+Fe–OH
C=O	531.8+Fe–OH	531.9+Fe–OH	532.5	532.6+O–Si	531.4+Fe–OH	532.5+O–Si
C–O	532.8	533.0			532.8	
C–OH/ O–N		534.3	534.1	534.2	533.9	533.7
***	535.0	535.6		536.1	535.3	535.4
***	536.0	537.2				
NH_2			400.2	400.5		
NH_3^+			401.0			
NO			402.6	402.1		
NO_2	403.3			403.7		
***	405.0		404.0	405.1		
NO_3 organic	407.7	407.8				
NO_3 inorganic	408.8	408.7		408.0		
***	410.3	410.0				
***		411.5				
Fe II octa	711.1	711.7	711.0	710.9	710.0	710.7
Fe III octa	712.6	713.6	711.8	711.9	711.6	711.8
Fe III tetra	715.0	716.4	714.2	714.7	714.1	714.6
Si–C			99.2		100.1	
Si–O	101.0			101.3		100.7
$Si–O_2$			101.9			
$Si–O_3$	103.4				103.4	103.2
***				108.8		

6.6 Acknowledgements

We thank the Fonds de recherche du Québec (FQRNT) and the Groupe de recherche en sciences et technologies biomédicales (GRSTB) for support. We thank Josianne Lefebvre for assistance in processing the XPS and TOF-SIMs data, and Rafaella Oliveira do Nascimento, for contributions during discussions.

The ARC (research contract AUWB-2010—10/15-UMONS-5), the FNRS, the Walloon Region, the COST TD1004 and TD1402, the UIAP VII program and the Center for Microscopy

and Molecular Imaging (CMMI, supported by the European Regional Development Fund and the Walloon Region), are thanked for their support.

References

Vaseashta A. Life Cycle Analysis of Nanoparticles, DEStech Publications, Inc., (2015).

Mireles L. K, Sacher E, Yahia L'H, Laurent S and Stanicki D. Acomparative physico chemical morphological and magnetic study of silane-functionalize superparamagnetic iron oxide nanoparticles prepared by alkaline coprecipitation. Int. J. Biochem. Cell Biol., 75 (2016) 203–211.

França R, Zhang X.F, Veres T, Yahia L'H and Sacher E. Core–shell nanoparticles as prodrugs: possible cytotoxicological and biomedical impacts of batch-to-batch inconsistencies, J. Colloid Interface Sci. 389 (1) (2013) 292–297.

Moshfegh Z. Nanoparticle catalysts, J. Phys. D: Appl.Phys. 42 (2009) 233001.

CHAPTER 7 ARTICLE 3: NITRIC OXIDE ATTACHMENT TO SPIONS: DEMONSTRATION OF THE COVALENT S-NO BOND IN A NANODELIVERY SYSTEM

L. K. Mireles[1], D. Stanicki[2], S. Laurent[2], D. Deschênes[3], E. Sacher[1,4] and L'H. Yahia[1]

[1]Laboratoire d'Innovation et d'Analyse de Bioperformance, Département de Génie mécanique École Polytechnique de Montréal C.P. 6079, Succursale Centre-ville Montréal, Québec H3C 3A7 Canada

[2]General, Organic and Biomedical Chemistry Unit, Nuclear Magnetic Resonance and Molecular Imaging Laboratory, University of Mons. Avenue Maistriau 19, B7000 Mons, Belgium

[3]Département de Chimie, Université de Montréal C.P. 6128, Succursale Centre-ville, Montréal, Québec H3C 3J7, Canada

[4]Département de Génie physique École Polytechnique de Montréal C.P. 6079, Succursale Centre-ville, Montréal, Québec H3C 3A7, Canada

Submitted to the journal: Applied Surface Science on June 19th 2019 Manuscript ID: APSUSC-D-19-09020

7.1 Graphical abstract

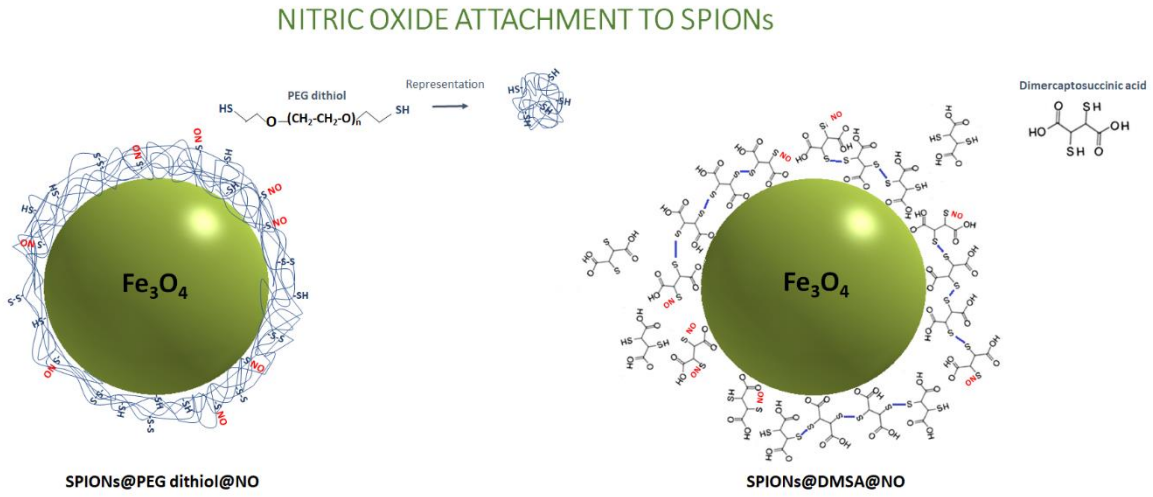

7.2 Highlights

1. Successful PEGdithiol and DMSA coating around superparamagnetic iron oxide nanoparticles (SPIONs), leading to free thiol groups at the SPION surface.

2. NO functionalization of the free thiol groups, under O_2 atmosphere, leads to SNO.

3. NO functionalization of the free thiol groups, under N_2 atmosphere, leads to unexpected oxidation.

7.3 Abstract

We demonstrate the successful functionalization of magnetite (Fe_3O_4) nanoparticles, using PEGdithiol and dimercaptosuccinic acid (DMSA). Following functionalization, TEM images show increased sizes, due to the presence of well-defined polymeric coatings. On subsequent nitrosation, X-ray photoelectron spectroscopy (XPS) and time-of-flight secondary ion mass spectroscopy (TOF-SIMS) show the presence of S-NO bonds.

Key words: Mercaptonitrosation, SPION, surface analysis.

7.4 Introduction

Nitric oxide (NO) is a diatomic free radical and endogenous antimicrobial agent, active in many physiological processes. In the human body, it is produced by macrophages, prompted by the immune response to bacterial infection (MacMicking J, Xie QW, Nathan C, 1997). In 1983, Mancinelli *et al*. (Mancinelli RL, McKay CP, 1983) demonstrated its antimicrobial efficacy, destroying colonies of bacteria. Recently, several investigations focused on NO as an effective endogenous molecule against pathogens, due to its antibacterial properties (Howlin RP, et al., 2017; Friedman A, Friedman , 2009).

At low concentrations, NO acts as a potent nitrosating agent that promotes the growth and activity of immune cells; at higher concentrations, it alters DNA replication, and regulates protein and cell function, thus inhibiting or killing target pathogens (Friedman A, Friedman J, 2009, Gow

AJ, Farkouh CR, et al., 2004). The bacteriostatic and bactericidal properties of NO, and its platelet activation, wound healing and host defense against infections (Nablo BJ, Prichard HL, 2005; Trampuz A, Widmerm AF, 2001; Wilcox M, Kite P, Mills K, Sugden S, 2001), suggest that, incorporated as an antimicrobial agent into biomaterials, it would inhibit bacterial growth and, therefore, avoid common infections, such as those induced by *S. aureus*, *E. coli* and others commonly found at hospitals (Jardeleza C, Thierry B, 2015; Laverty G, Gorman SP, Gilmore BF; 2014; Privett BJ, Broadnax AD, 2012). Our ultimate aim is to develop a NO nanodelivery system against biofilms on implant surfaces, based on superparamagnetic iron oxide nanoparticles (SPIONs).

Inorganic nanoparticles have been studied as vehicles for the controlled delivery of drugs such as NO (Saraiva J, Marotta-Oliveira SS, et al., 2011; Zhang X, Mansouri S, Mbeh DA, et al., 2012). Several of these NO-containing nanoparticle platforms have been synthesized and used specifically for antibiofilm applications, highlighting the feasibility and importance of developing these technologies to prevent contamination of prosthetic devices (Worley BV, Schilly KM, Schoenfisch MH, 2015; Friedman AJ, Han G, et al., 2008).

Currently, the use of SPIONs in the biomedical field is increasing because, when used as nanocarriers, they can be guided to the specific target sites, *in vivo*, by external magnetic fields *(*Afkhami F, Taherkhani S, et al., 2011; Liu R-t, Liu J, et al., 2012). They possess low cytotoxicity *(*Mbeh DA, França R, et al., 2012) and high biocompatibility *(*Mbeh DA, Mireles LK, et al., 2015), and have been approved, by the United States Food and Drug Administration (FDA), as prodrugs for clinical MRI applications *(*Gupta AK,Wells S, 2004; Tassa C, Shaw SY, Weissleder R, 2011). *In vivo*, SPIONs are metabolized to ferric ions, which are incorporated into the biological iron storage pool, such as erythrocytes, indicating their acceptable use in humans (Li YF, Chen C, 2011). Here, magnetite nanoparticles were functionalized by coatings of both dimercaptosuccinic acid (DMSA) and poly (ethylene glycol) dithiol (PEGdithiol); both coatings formed shells containing free thiol (-SH) ligands on the SPION surface, subsequently used as reactive groups for nitrosation, forming mercaptonitroso (S-NO) groups for NO release.

The efficacy of DMSA in drug delivery was previously demonstrated (Mejias R, Perez-Yague S et al., 2011), as were its minimal cytotoxic effects (Naqvi S, Samim M, et al., 2010). PEG has been widely used as a coating material for magnetic nanoparticles; it is easily metabolized,

having nonimmunogenic and nonantigenic properties, and can interact with cell membranes, resulting in an enhanced cellular response (Gölander CG, Herron JN, et al., 1992). However, it is not biodegradable, and its repeated dosage and accumulation can give rise to accelerated blood clearance. Del Puerto *et al*. (Ruiz A, Morais PC, et al., 2014) and others (Ikeda Y and Nagasaki Y, 2011; Wattendorf U and Merkle HP, 2008), note that the use of PEG and DMSA, as magnetic nanoparticle coatings, reduces surface charge density, achieves long circulation times and maintains hydrodynamic sizes under 100 nm, avoiding agglomeration.

Here, as in our previous studies of SPION surfaces (Mireles LK, Sacher E, et al., 2016; França R, Zhang XF, et al., 2013; Mireles LK, Sacher E, et al., 2016b; Mbeh DA, Mireles LK, et al., 2015), we use highly surface-sensitive X-ray photoelectron spectroscopy (XPS) and time-of-flight secondary ion mass spectroscopy (TOF-SIMS) to study the NO functionalization of DMSA- and PEGdithiol-coated SPIONs, carried out under both nitrogen and oxygen atmospheres, and demonstrate the capabilities of these techniques to identify S-NO bond formation.

7.5 Materials and methods

All experiments were replicated five times.

7.5.1 SPION synthesis

Bare SPIONs, prepared by alkaline precipitation, as previously described (Bridot JL, Stanicki D, et al., 2013), were treated with TEPSA [3-(triethoxysilyl) propyl succinic anhydride] in organic medium. Briefly, TEPSA (25 mmol; 7.1 mL) was slowly added to a suspension of SPIONs in dimethyl formamide (50 mL; [Fe] = 100 mM). Water was added (4.3 mL), followed by an aqueous solution of tetramethylammonium hydroxide (2.5 mL; 1 M = 2.5 mmol) at room temperature, under stirring. The solution was heated at 100°C for 24 h under continuous stirring. The SPIONs were collected by pouring the suspension into an acetone/diethyl ether mixture, followed by magnetic decantation. After washing with acetone, the black precipitate was dispersed in water and purified by membrane filtration (membrane cut-off: 30 kDa) before centrifuging (16,500 g; 45 minutes).

7.5.2 Thiolation

7.5.2.1 DMSA coating

One hundred mg of DMSA were dissolved in 5 mL of ethanol and mixed, under magnetic stirring at room temperature, with 1 mL of previously prepared SPIONs and 5 mL of milli-q water. The reaction time was 24 hours, under either an oxygen or a nitrogen atmosphere; both gases were 99.99999 % pure.

7.5.2.2 PEGdithiol coating

Five mg of PEG dithiol (M_n = 1000) were dissolved in 10 mL of milli-q water, using magnetic stirring at room temperature, with 1 mL of previously prepared SPIONs and 2 mL of milli-q water. The reaction time was 4 hours under either an oxygen or a nitrogen atmosphere.

7.5.3 Nitrosation

Two mL of 60 mM $NaNO_2$ were added to the thiolated nanoparticles and mixed under magnetic stirring, at room temperature, for 3 h under either an oxygen or a nitrogen atmosphere. The solutions were centrifugated and filtrated three times, to remove contaminants.

7.6 Physicochemical characterizations

7.6.1 TEM

The samples were diluted in water and sonicated for 3 minutes to disperse the SPIONs. One drop of each sample was spread on a copper grid with a lacey carbon film, and analyzed on drying. The samples were bright-field imaged by transmission electron microscopy (TEM), using a JEM-2100F field emission electron microscope, with ultrahigh resolution, at a beam energy of 200 kV.

7.6.2 FTIR

FTIR spectra were obtained, in the range 450-4000 cm^{-1}, using a Bruker Alpha spectrometer, at a resolution of 4 cm^{-1}; 64 scans were coadded to improve S/N. The samples were deposited by placing several drops on a silicon substrate; ATR spectra were obtained using a diamond plate.

7.6.3 XPS

XPS was performed with a VG ESCALAB 3 MK II (Thermo VG Scientific), using non-monochromated Mg Kα X-rays (hν = 1253.6 eV). The instrument resolution was 0.7 eV, and a perpendicular take-off angle was used. The analysis chamber pressure was < 10^{-9} torr. After Shirley background removal, the component peaks were separated by the VG Avantage software. The energy was calibrated by setting the C1s C-C peak, to 285 eV. FWHM values were those previously established in our laboratory. The depths probed by this technique, for elements of present interest, range from 3-5 nm and, with proper peak intensity sensitivity factors, the relative atomic percentages determined are highly quantitative (± 5%).

7.6.4 TOF-SIMS

TOF-SIMS was carried out on an ION-TOF TOF-SIMS IV mass spectrometer, using a mono-isotopic Bi^+ beam, generated by a liquid metal gun mounted on the instrument. The beam current was 1.5 pA. Drops of the samples were deposited onto a silicon substrate, covering an area greater than 2 mm x 2 mm, and permitted to dry. Positive and negative ion spectra were calibrated using H^+, C^+, $C_xH_y^+$ (x = 1-5 and y = 1-12) and H^-, C^-, $C_xH_y^-$ (x = 1-5 and y = 1-12) peaks. The depths probed by this technique range from 1-1.5 nm but the peak intensities are qualitative.

7.7 Results

7.7.1 Thiolation and nitrosation under an oxygen atmosphere

7.7.1.1Transmission electron microscopy

TEM images of bare SPIONs (Figure 7.1a and 7.2a), ~ 10 nm in diameter, may be compared with nanoparticles functionalized with PEGdithiol (SPIONs@PEGdithiol, Figure 7.1b and 7.1c) and DMSA (SPIONs@DMSA, Figure 7.2b and 7.2c); the PEGdithiol layer is seen to have an average thickness of 2.7 ± 1.3 nm (Figure 7.1e), while that of the DMSA is 3.1 ± 1.7 nm (Figure 7.2e). In the case of PEGdithiol, the PEG chain is ~ 3x that of the thickness, indicating that the chains lie parallel to the SPION surface, as suggested by Figure 7.1c; in the case of DMSA, the molecular length is ~ ¼ that of the thickness, indicating chain extension, as suggested by Figure 7.2c.

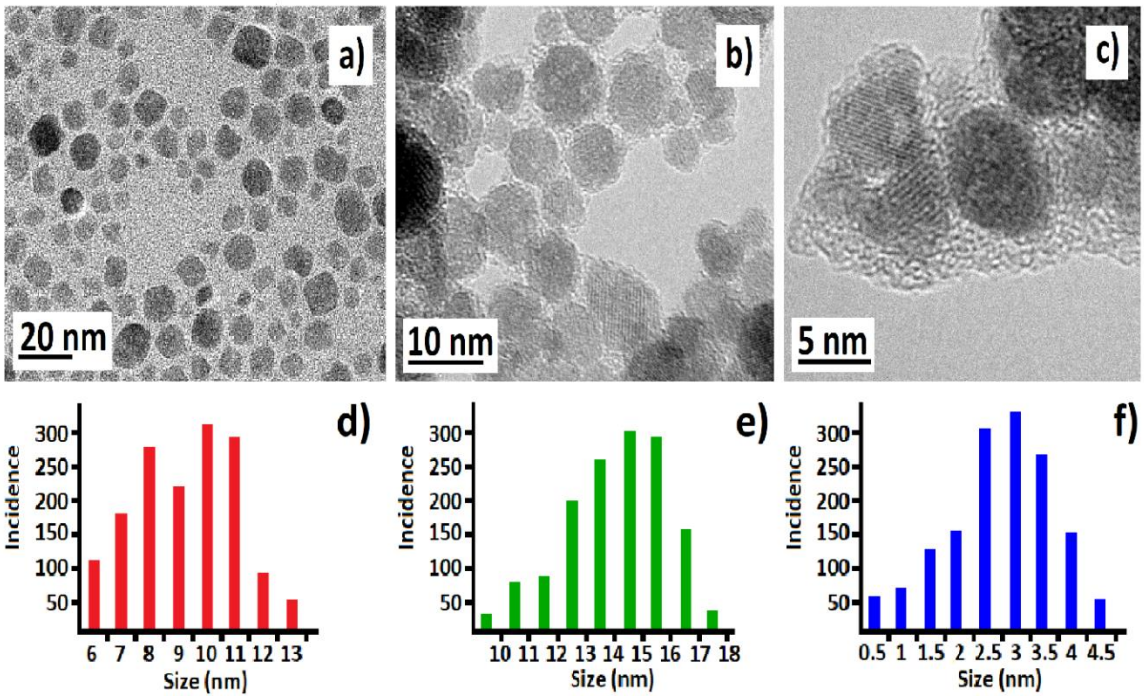

Figure 7.1 a) SPIONs, b) a thin PEG layer is visible around the SPIONs, c) PEG thickness is seen to be quite variable. The histogram d) shows the size distribution of the bare SPIONs; e) shows the size distribution of the PEGylated SPIONs and f) shows the size distribution of the PEG layer (2.7 ± 1.3 nm). The length of a PEG dithiol chain, Mn ~ 1000, is ~ 3x the size of the average thickness

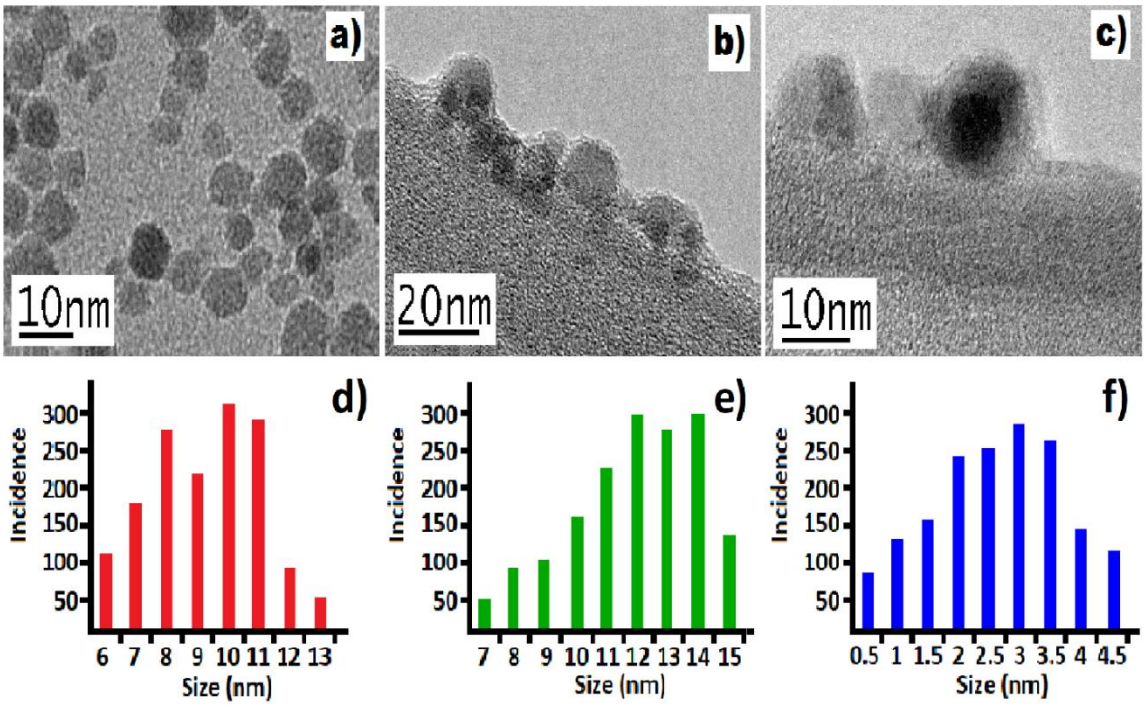

Figure 7.2 a) SPIONs, b) a thin DMSA layer is visible around the SPIONs, c) the shell thickness is seen to be quite uniform; average thickness of 3.1 nm ±1.7 nm. The histogram d) shows the size distribution of the bare SPIONs; e) shows the size distribution of the coated SPIONs and f) shows the size distribution of the DMSA layer (3.1 ± 1.7 nm). The length of a DMSA molecule is about ¼ that of the average thickness

7.7.1.2 X-ray photoelectron spectroscopy

Thiolation

The survey spectra of SPION@PEGdithiol (Figure 7.3, upper series) and SPION@DMSA (Figure 7.4, upper series) reveal the presence of $S2p_{3/2}$, C1s, O1s and $Fe2p_{3/2}$ spectra. The $S2p_{3/2}$ peak, which we shall discuss, was found at ~ 164.0 eV in both series, and is attributed to the presence of SH and SS.

Nitrosation

It is known that some reactions carried out under an O_2 atmosphere generate S-S bonds (Koval IV, 1994), which, in the present case, would preclude the successful attachment of NO. For both SPION@PEGdithiol-NO and SPION@DMSA-NO, nitrosation produces a N1s spectrum (lower series of Figure 7.3 and 7.4). The peaks, and their attributions, are found in Table 7.1. Subsequent to nitrosation, an additional shoulder appears in the $S2p_{3/2}$ spectrum, at ~ 161.5 eV, attributed to Fe-S; the $S2p_{3/2}$ peak at ~ 164 eV, which persists, may also be attributable to the formation of SN, seen in the N1s spectrum at 403 eV (0.3 at%) for SPION@PEGdithiol-NO and 403.4 eV (1.8 at%) for SPION@DMSA-NO. The N1s spectrum also contains a peak found at ~ 399.8 eV, attributed to amine, apparently generated as a byproduct during nitrosation. These peak attributions will be confirmed by the TOF-SIMS results presented below.

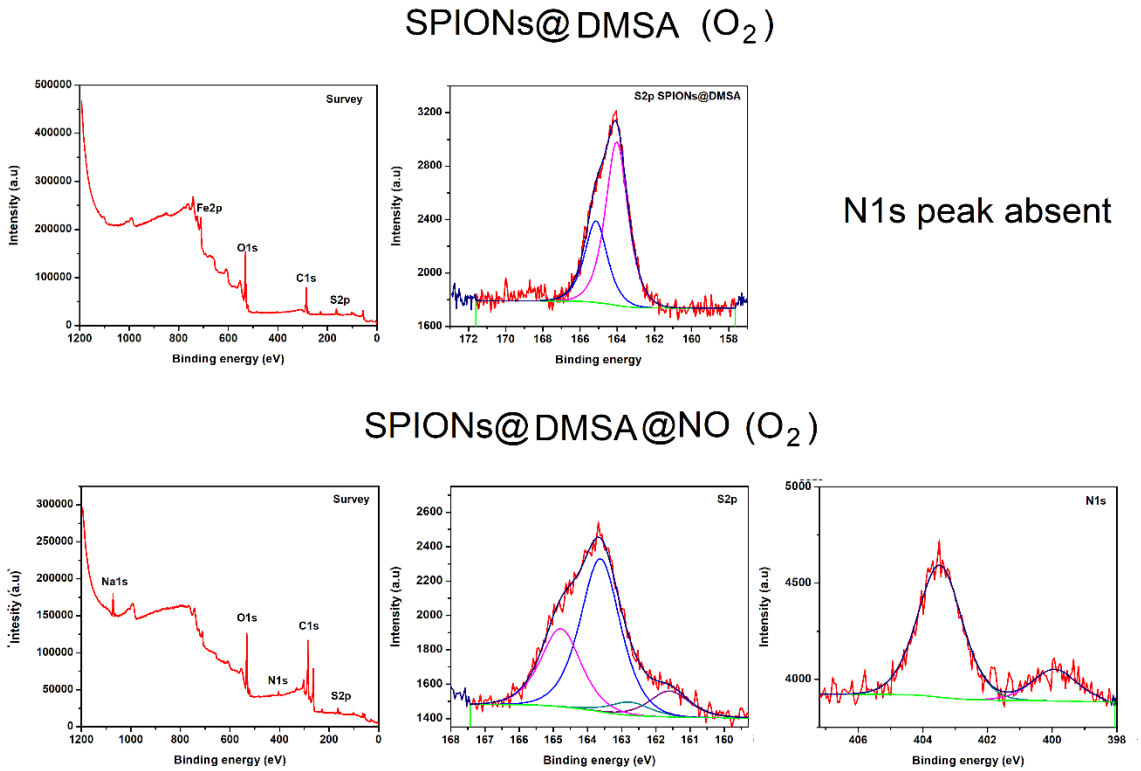

Figure 7.3 XPS peaks of SPION@DMSA (upper series), and SPION@DMSA@NO (lower series)

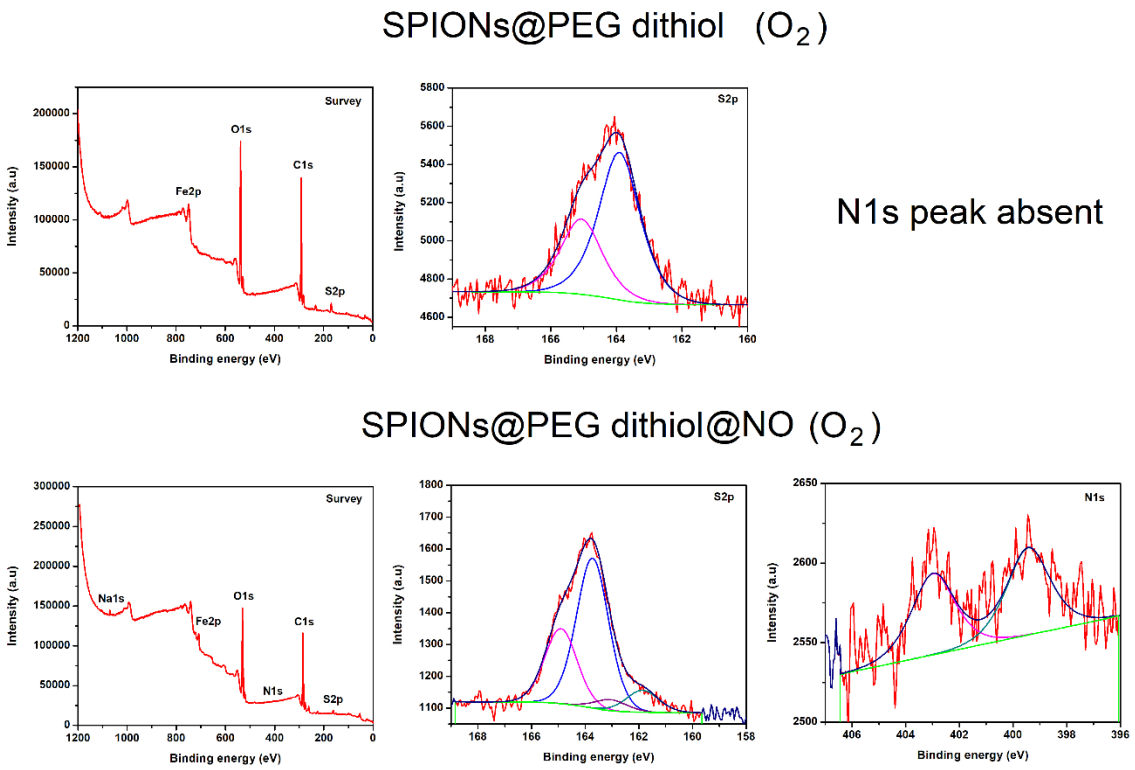

Figure 7.4 XPS peaks of SPION@PEGdithiol (upper series) and SPION@PEGdithiol@NO (lower series)

7.7.1.3 Time-of-flight secondary ion mass spectrometry

Thiolation

The TOF-SIMs spectra of SPION@PEGdithiol (Figure 7.5) and SPION@DMSA (Figure 7.6) both indicate the presence of SH, showing peaks at both 32.98 Da (SH) and 44.98 Da (C-SH), as well as peaks at both 63.94 Da (SS) and 75.95 Da (C-SS), confirming the XPS attributions of thiols and disulfides.

Nitrosation

On nitrosation, both SPION@PEGdithiol-NO (Figure 7.7) and SPION@DMSA-NO (Figure 7.8) still display peaks at 32.98 Da (SH) and 44.98 Da (C-SH), and at 63.94 Da (SS) and 75.95 Da (C-SS), indicating that not all the thiols groups underwent nitrosation. However, the

successful nitrosation of some thiol groups was shown by peaks at 57.98 Da (C-SN) and 61.97 Da (SN-O), again supporting the XPS attributions.

Table 7.1 XPS peak attributions of functionalized SPIONs

XPS characterizations of PEG dithiol and DMSA functionalizations				
Attribution	PEGdithiol		DMSA	
	SPION@PEGdithiol (eV)	SPION@PEGdithiol @NO (eV)	SPION@DMSA (eV)	SPION@DMSA @NO (eV)
NH_2		399.4 (0.2 at%)		399.8 (0.4 at%)
SNO		403.0 (0.3 at%)		403.4 (1.8 at)
Fe-S		161.9 (0.3 at%)		161.5 (0.4 at%)
SH, S-S, S-N	163.9 (1.7 at%)	163.7 (1.0 at%)	164.0 (3.3 at%)	163.8(2.1 at)

7.7.1.4 FTIR spectroscopy

FTIR (Figure 7.9) was used to determine spectral differences before and after nitrosation. The S-H stretch, expected at 2500-2600 cm^{-1}, was not displayed in any of the spectra. This is probably due to both the low extinction coefficient of the peak and the low concentration of S-H. In a similar fashion, neither S-NO (700-750 cm^{-1}) nor N-O (1320-1360 cm^{-1}) were in evidence, probably for the same reasons.

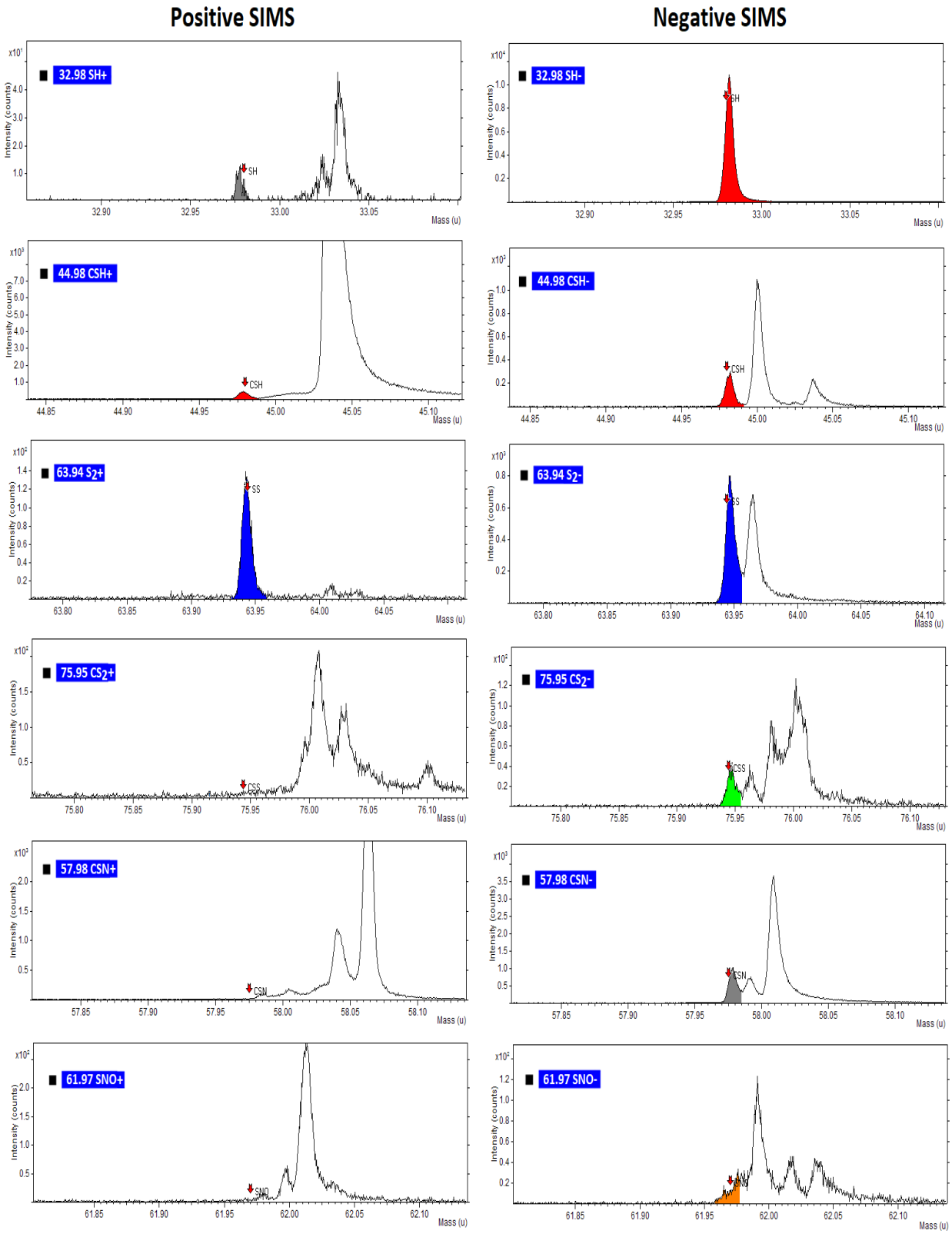

Figure 7.5 TOF-SIMS HR spectra of SPION@PEGdithiol

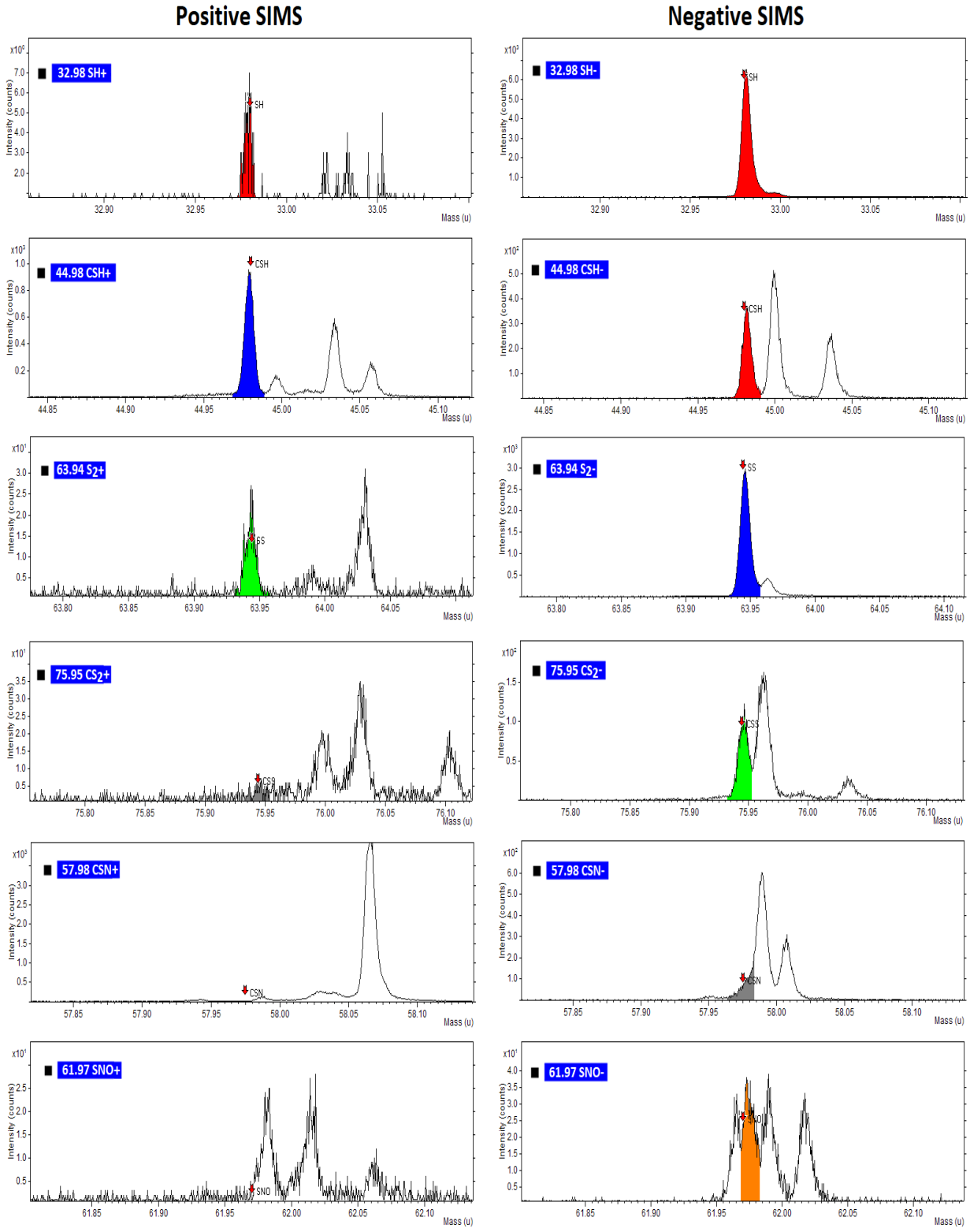

Figure 7.6 TOF-SIMS HR spectra of SPIONs@DMSA

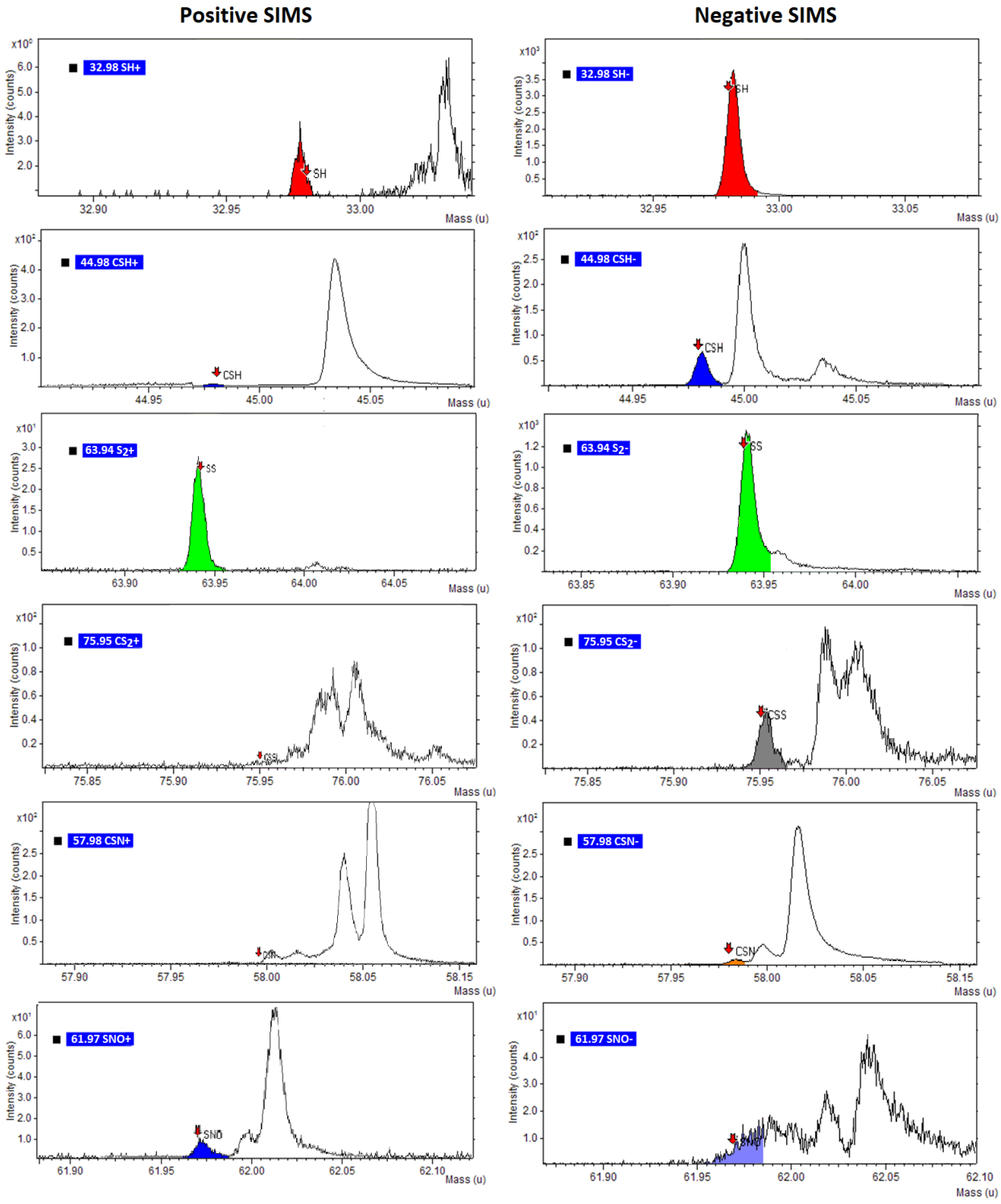

Figure 7.7 TOF-SIMS HR spectra of SPION@PEGdithiol@NO

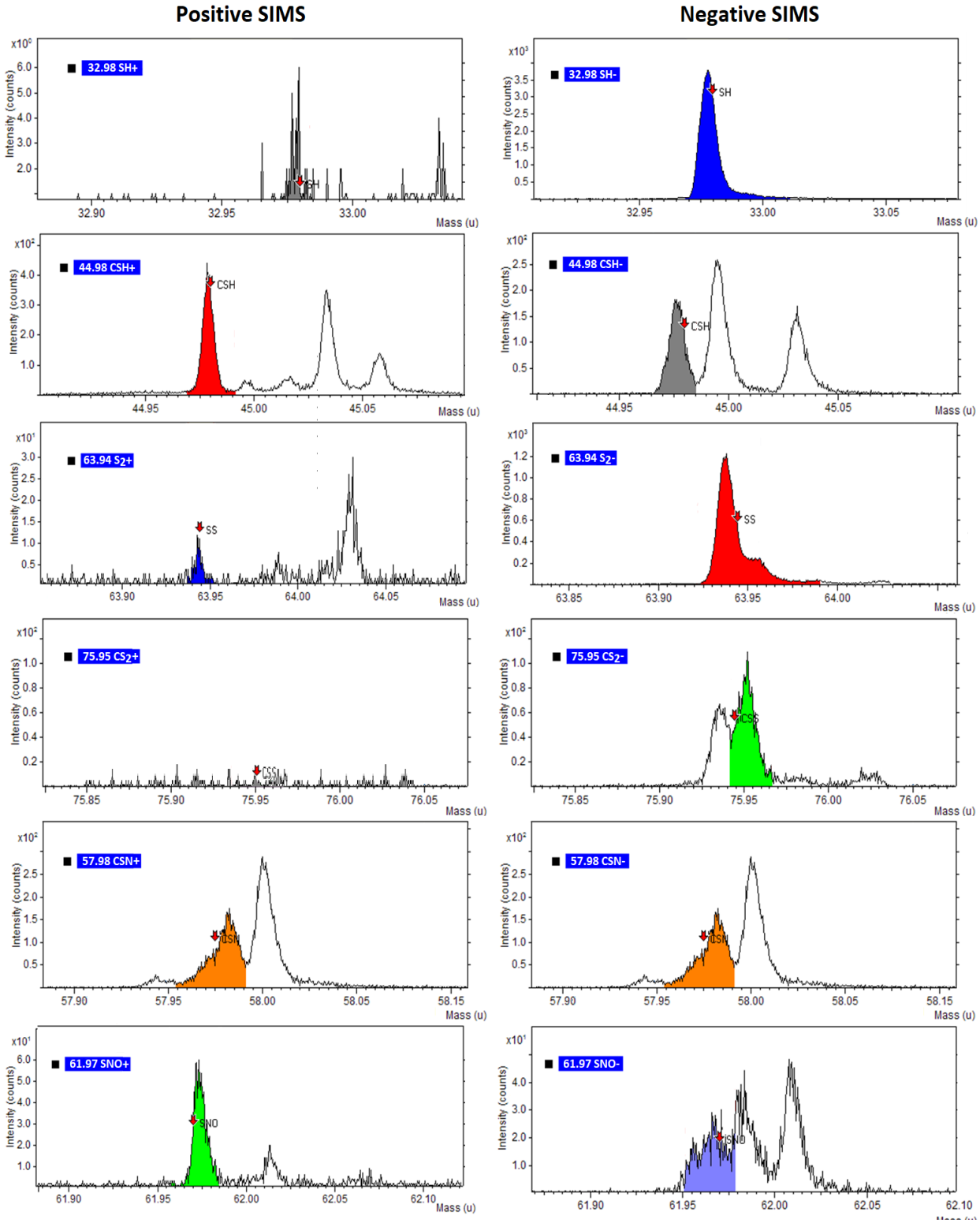

Figure 7.8 TOF-SIMS HR spectra of SPION@DMSA@NO

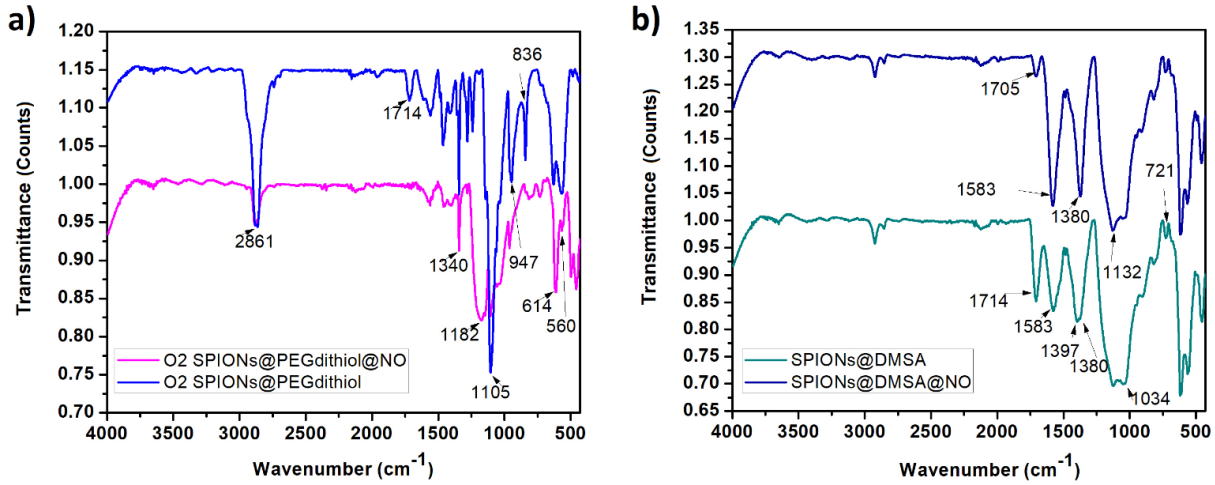

Figure 7.9 FTIR spectral comparisons of a) SPION@PEGdithiol and SPION@PEGdithiol@NO and b) SPION@DMSA and SPION@DMSA@NO

7.7.2 Thiolation and nitrosation under a nitrogen atmosphere

7.6.2.1 XPS

Thiolation

The XPS spectra of SPIONs@PEGdithiol (Figure 7.10) shows $S2p_{3/2}$ peaks at 163.7 and 167.8 eV, attributed to SH and SO_3, respectively. N1s peaks appear, even when nitrosation was not carried out, at 399.0 (NH), 400.2 (NH_2) and 407eV (NO_3), indicating an unexpected reaction with the nitrogen atmosphere, since the subsequent use of an oxygen atmosphere gave no hint of glassware contamination. Similarly, SPIONs@DMSA (Figure 7.11) shows free thiol at 164.2 (S-H), and unexpected N1s peaks at 402.0 and 403.1 eV. Clearly, the species introduced by the presence of a nitrogen atmosphere are reactive, subsequently oxidizing on exposure to air.

Nitrosation

Subsequent to SPIONs@PEG dithiol-NO nitrosation (Figure 7.10, lower series), oxidation has increased, as evidenced by peaks at 168.6 eV (SO_4), 403.8 eV (NO_2) and 407.6 eV (NO_3), found in Table 7.2. On SPIONs@DMSA-NO nitrosation, the thiol peak at 163.7eV remains and a new peak appears at 403.9 eV, attributed to SNO_2; the absence of a peak attributable to SNO indicates its oxidation. XPS attributions are found in Table 7.2.

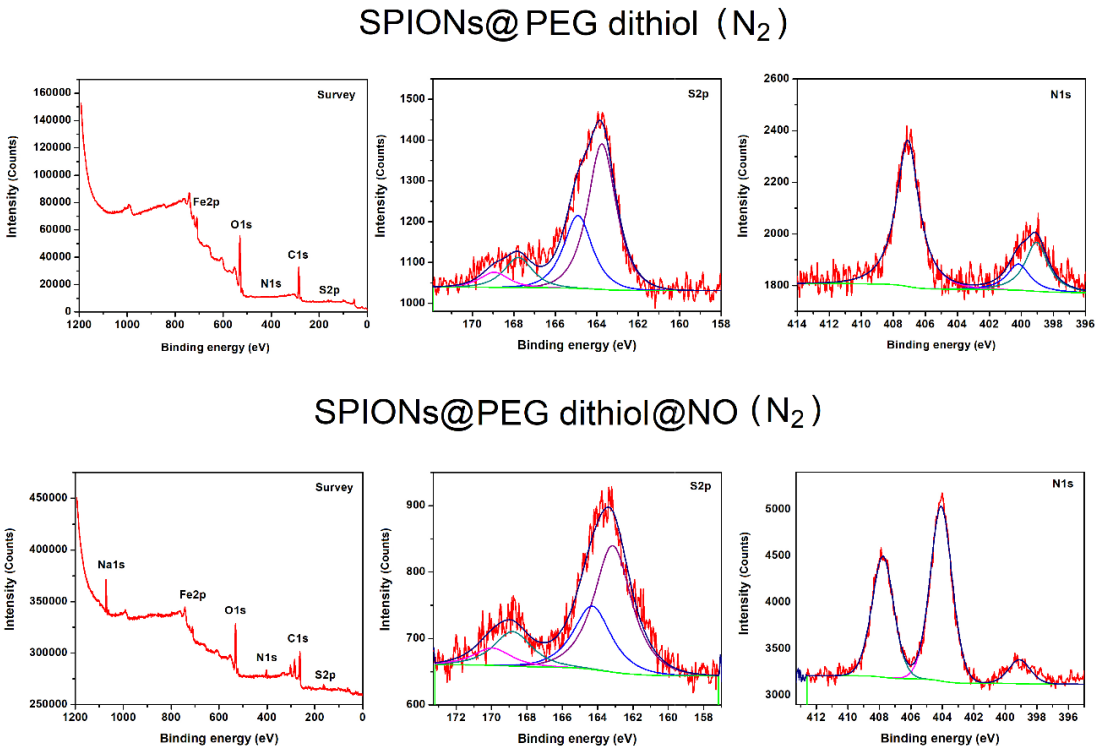

Figure 7.10 XPS peaks of SPION@PEGdithiol (upper series) and SPION@PEGdithiol@NO (lower series) under a nitrogen atmosphere

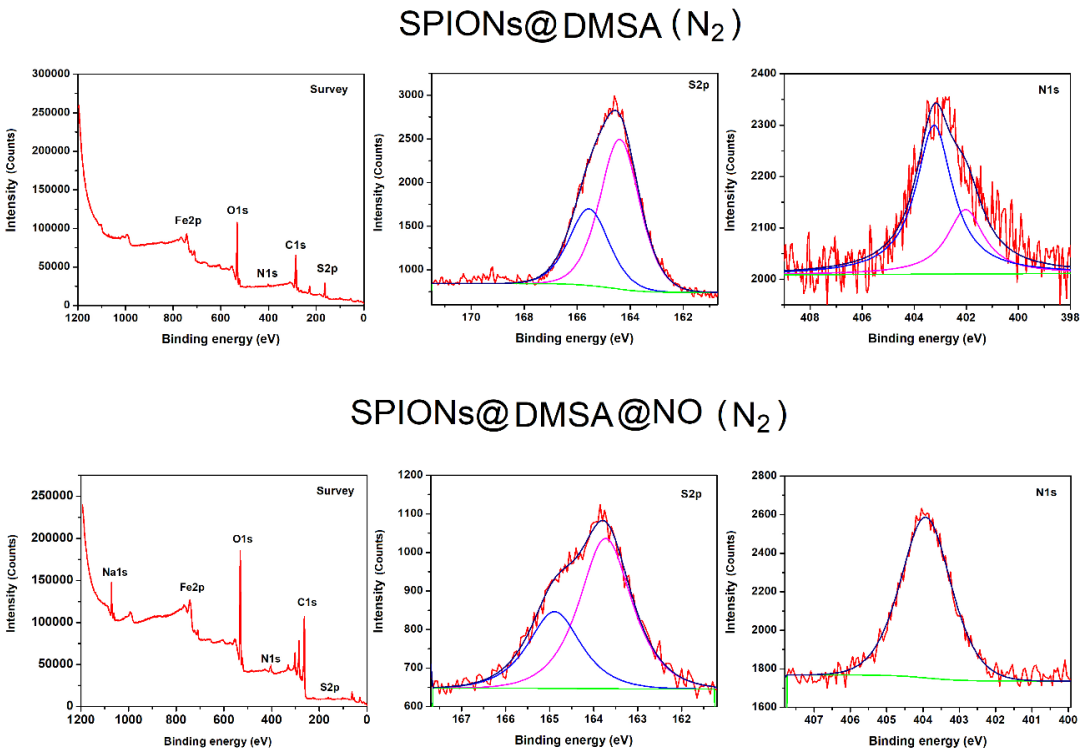

Figure 7.11 XPS peaks of SPION@DMSA (upper series) and SPION@DMSA@NO (lower series) under a nitrogen atmosphere

7.7.2.2 TOF-SIMS

Thiolation

Figure 7.12 and 7.13 indicate the presence of SH (39.98 Da), C-SH (48.98 Da) and C-SS (63.94 Da) for both series.

Nitrosation

The PEGdithiol series (Figure 7.14) does not exhibit either C-SN or SN-O peaks, while the DMSA series (Figure 7.15) exhibits a broad peak at the 61.97 Da position of SN-O. The appearance of SN-O_2 (77.96 Da) indicates that oxidation has occurred in both series

Table 7.2 XPS peak attributions of functionalized SPIONs under a nitrogen atmosphere

Comparison of PEGdithiol and DMSA XPS characterization				
Suggested Attribution	**PEG dithiol**		**DMSA**	
	SPION@PEGdithiol (eV)	**SPION@PEGdithiol@NO (eV)**	**SPION@DMSA (eV)**	**SPION@DMSA@NO (eV)**
SH, S-S	163.7 (1.2 at%)	163.5 (0.4 at%)	164.2 (7.2 at%)	163.7 (2.0 at%)
SO_3^{2-}	167.8 (0.2 at%)			
SO_4^{2-}		168.6 (0.2 at%)		
=C-NH	399.0 (0.7 at%)	399.1 (0.6 at%)		
$C - NH_2$	400.2 (0.4 at%)			
$C\text{-}NH_n^+$			402.0 (0.6 at%)	
NO			403.1 (1.5 at%)	
NO_2, SNO_2		403.8 (4.8 at%)		403.9 (4.7 at%)
NO_3	407.0 (2.0 at%)	407.6 (4.2 at%)		

7.8 Discussion

7.8.1 Thiolation and nitrosation under an oxygen atmosphere

The TEM images in Figure 7.1 and 7.2 display the successful formation of PEGdithiol and DMSA coatings around the nanoparticles, with the size distribution histograms showing large thickness variations for both systems. This indicates that the layers formed are not uniform, and that certain points might be free of functionalization, exposing the core nanoparticle.

XPS characterizations of both series (Figure 7.3 and 7.4), before nitrosation, show the presence of free -SH groups, indicating both successful SH functionalization and the presence of S-S bonds. On nitrosation, the N1s spectra (Figure 7.3, lower series) shows a shoulder on the $S2p_{3/2}$ peak, attributed to Fe-S, which may additionally be have a contribution from the presence of contaminant

S-Na, detected by TOF-SIMS. The presence of a peak attributed to SNO (403 eV) indicates that an oxygen atmosphere contributes to NO attachment but cannot avoid secondary reactions, such as the formation of amine groups. Figure 7.16 shows the XPS peak fittings used in this study; the actual Fe2p and C1s component peaks and attributions of the SPIONs used here are found in our previous article (Ikeda Y and Nagasaki Y, 2011), which concerns their surface analysis.

TOF-SIMS supports the identification of SNO. Nitrosation was carried out several times, and only the oxygen atmosphere was able to produce the successful attachment of NO (Figure 7.12 and 7.13). Because of low peak extinction coefficients and low concentrations, FTIR is not an appropriate characterization tool in the present case.

7.8.2 Thiolation and nitrosation under a nitrogen atmosphere

When carried out under a nitrogen atmosphere, both series (Figure 7.10 and 7.11) indicate the unexpected appearance of a N1s spectrum prior to nitrosation, as well as the oxidation of any SNO that was formed, to SNO_2.

The SNO peak is not displayed in the PEGdithiol TOF-SIMS spectrum (Figure 7.12); however, it appears (61.97 Da) in the SPIONs@DMSA-NO spectrum, as does the SNO_2 peak (77.96 Da, Figure 7.15), particularly intense in the negative SIMS spectrum. The presence of the SNO peak in SPIONs@DMSA-NO spectrum implies that some attachment of NO occurred, which was subsequently oxidized to SNO_2.

7.8.3 Generalities and comparison of the NO attachment process under oxygen and nitroge atmonpheres

The results of the two series, carried out under both oxygen and nitrogen atmospheres, are found in Table 7.3. The most surprising results pertain to the influences of the atmospheres under which the reactions occurred: nitrosation (SNO) is achieved only under an oxygen atmosphere, while the nitrogen atmosphere proves unexpectedly reactive, introducing N-containing species that, on subsequent exposure to air, oxidize to SNO_2.

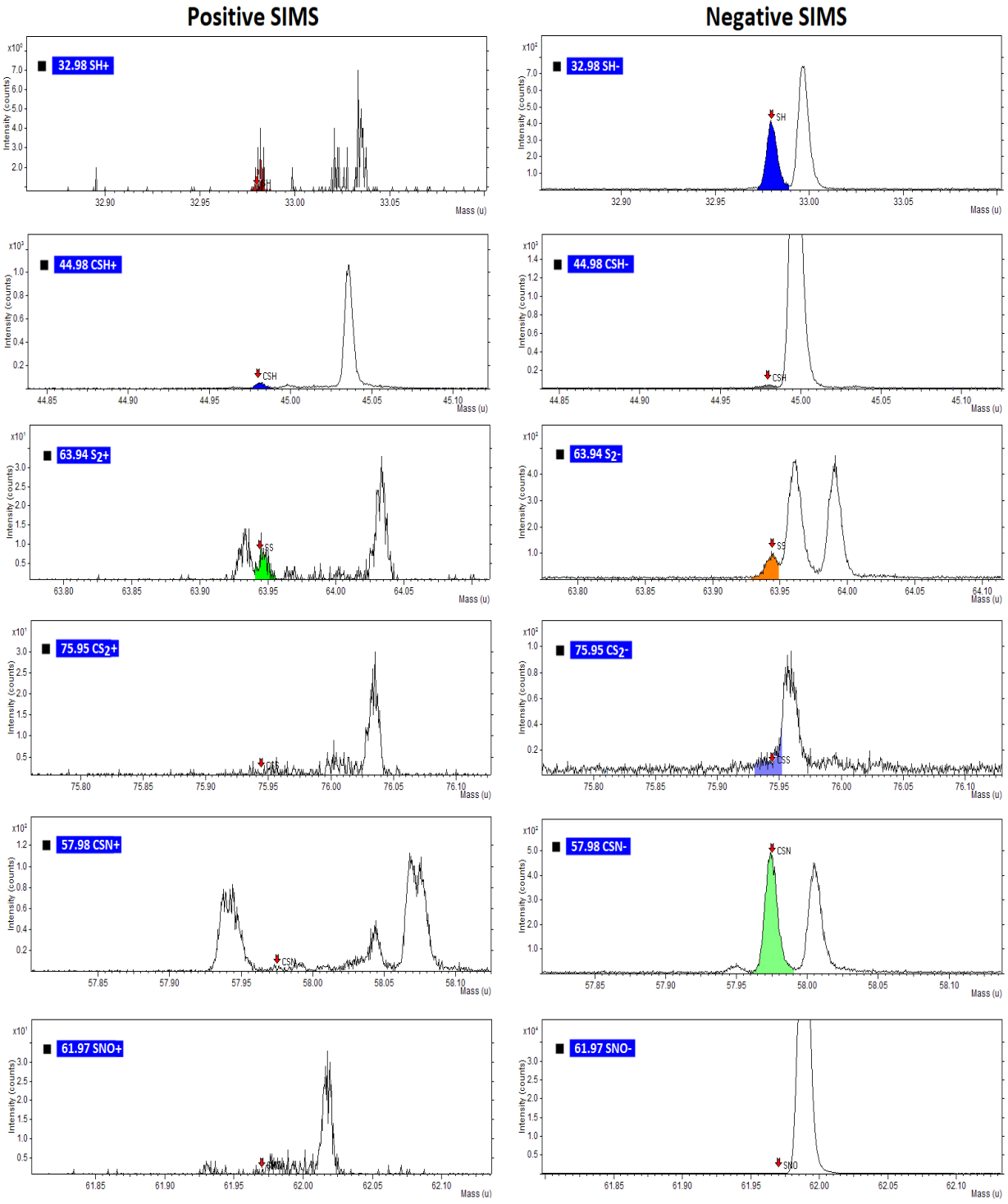

Figure 7.12 ToF-SIMS HR spectra of SPION@PEG dithiol under nitrogen atmosphere

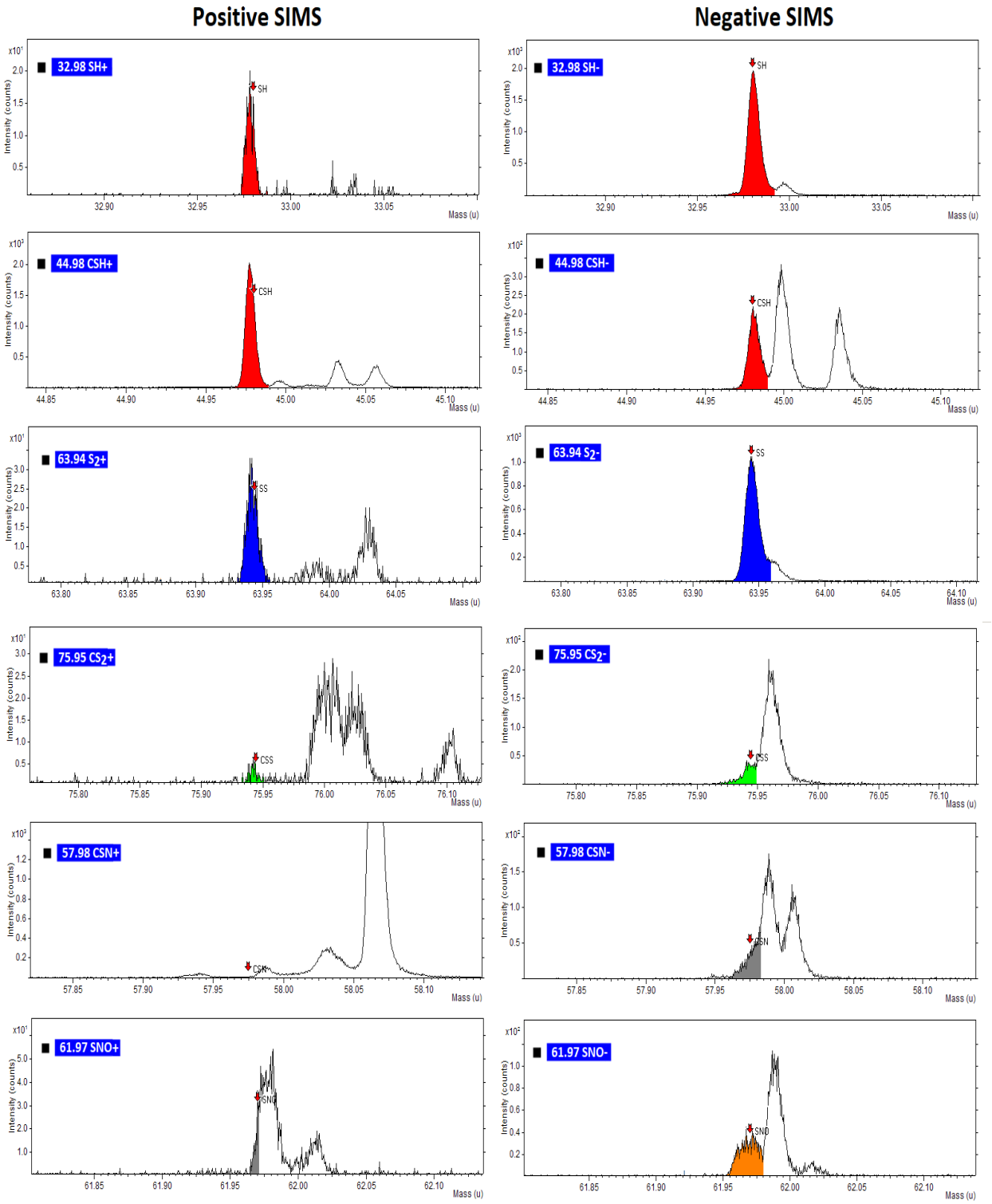

Figure 7.13 TOF-SIMS HR spectra of SPION@DMSA under a nitrogen atmosphere

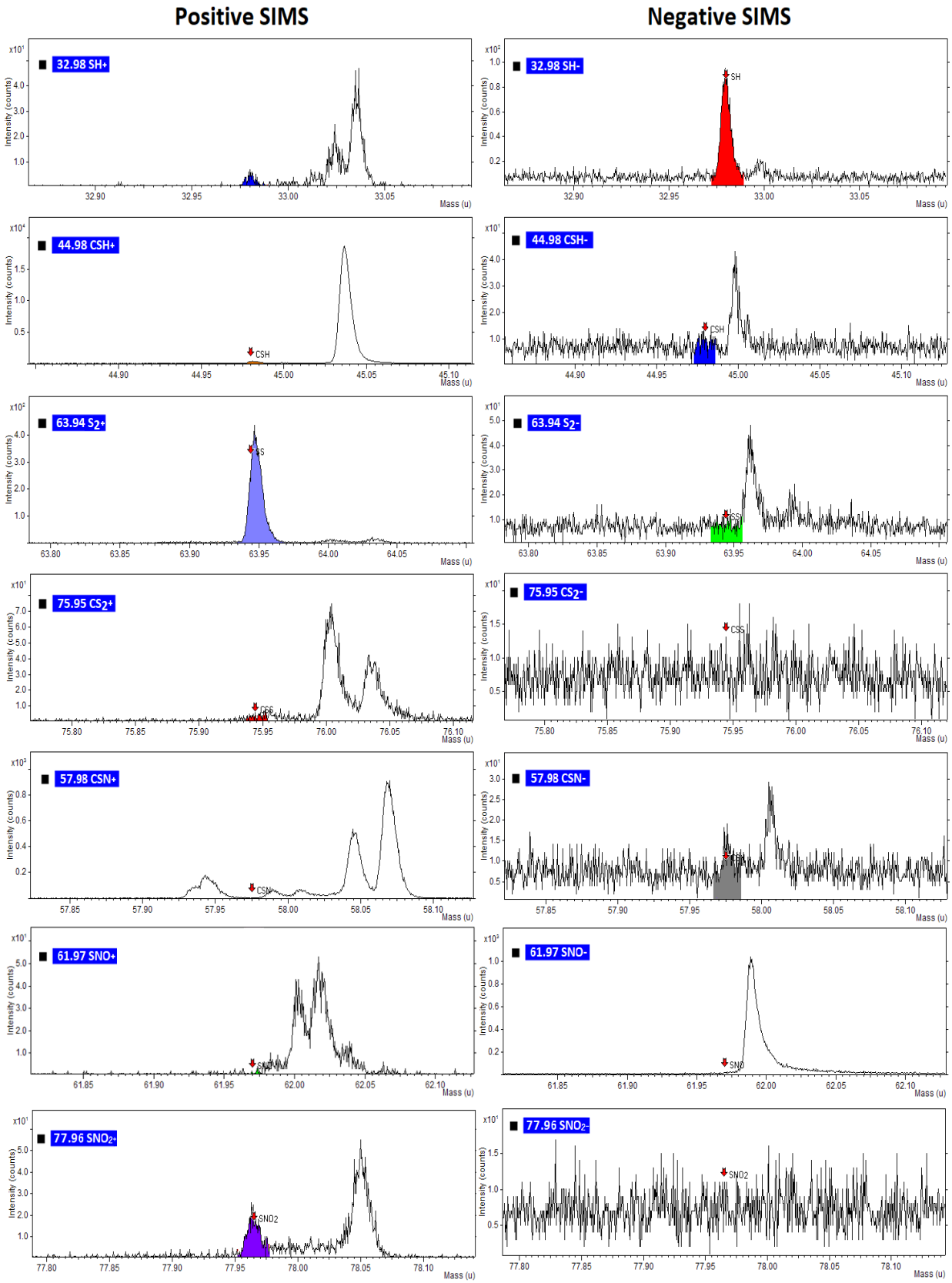

Figure 7.14 TOF-SIMS HR spectra of SPION@PEGdithiol@NO under a nitrogen atmosphere

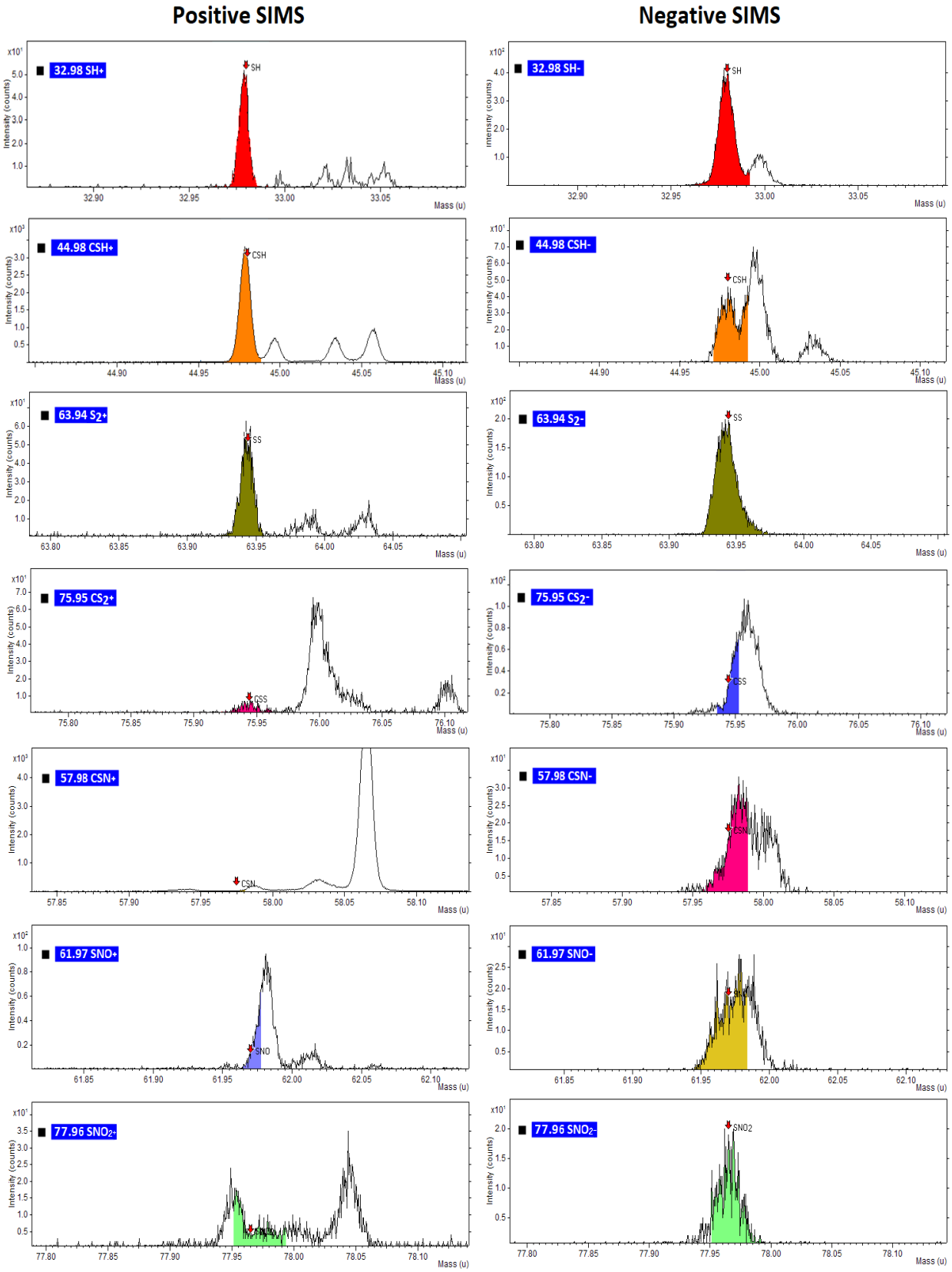

Figure 7.15 TOF-SIMS HR spectra of SPION@DMSA@NO under a nitrogen atmosphere

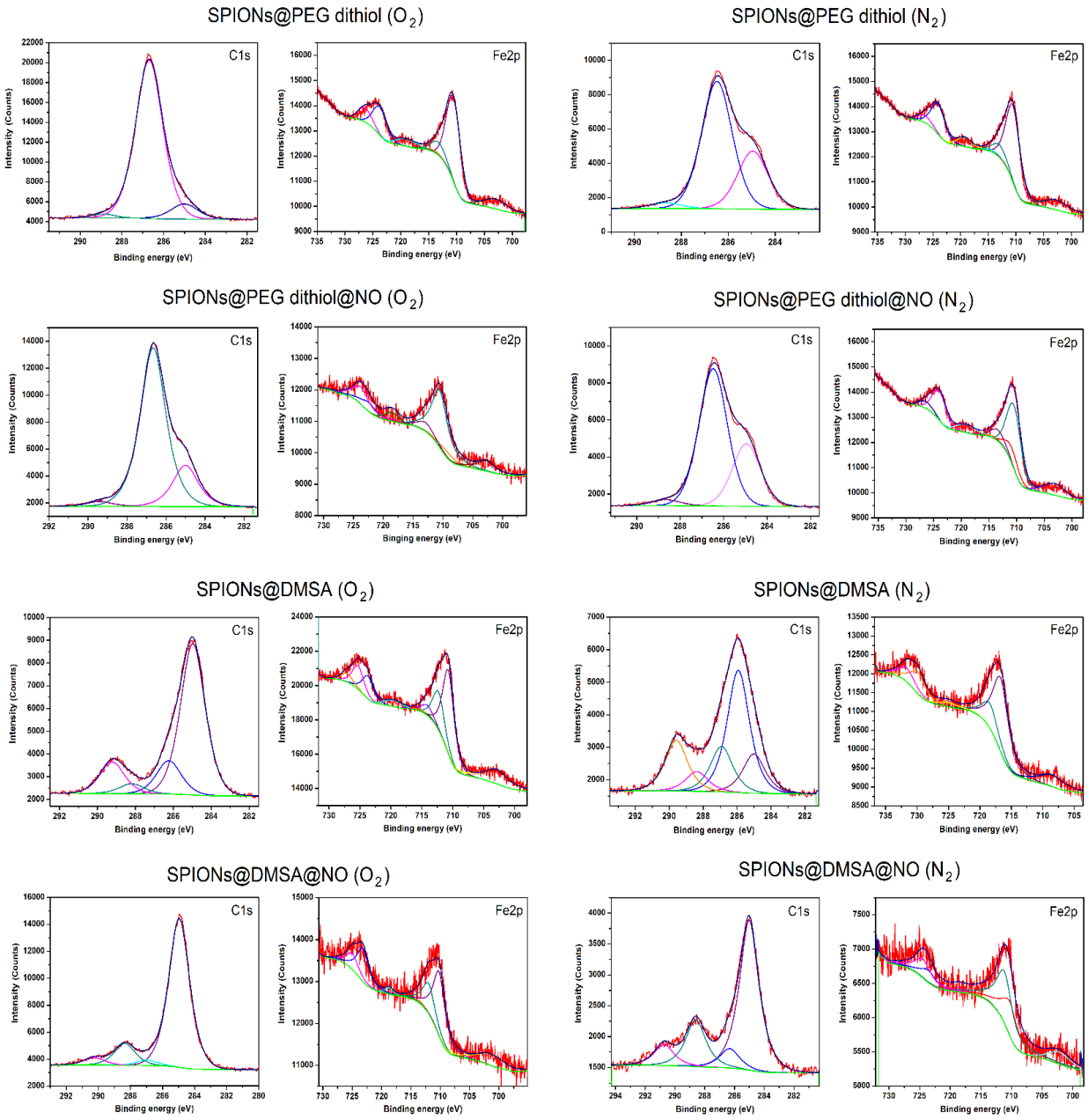

Figure 7.16 XPS peak fitting of C1s and Fe2p spectra

Table 7.3 A comparison of influences of oxygen and nitrogen atmospheres

O_2 atmosphere	N_2 atmosphere
X	N1s appear on thiolation (unexpected)
N1s appear on nitrosation	N1s appear on nitrosation
S-S bonds appear	S-S bonds appear
Fe- S peak found on SPIONs@PEGdithiol@NO	Fe- S peak found on SPIONs@PEGdithiol@NO
Fe- S peak found on SPIONs@DMSA@NO	X
amine group found on SPIONs@PEGdithiol-NO	amine group found on SPIONs@PEGdithiol-NO
amine group found on SPIONs@DMSA-NO	X
S-NO bond	S-NO_2 group
X	Oxidation of S2$p_{3/2}$ and N1s

7.9 Conclusions

We show the successful NO attachment to SPIONs for reactions occurring under an oxygen atmosphere, but not under a nitrogen atmosphere. In the latter case, the atmosphere influences the reaction, introducing species that ultimately oxidize on exposure to atmosphere. \

7.10 Acknowledgements

This work was supported by the Fonds de recherche du Québec-Nature et technologies (FRQNT), the Natural Sciences and Engineering Research Council of Canada (NSERC) and the Groupe de recherche en sciences et technologies biomédicales (GRSTB). It was also supported by the Fond National de la Recherche Scientifique (FNRS), UIAP VII, ARC Programs of the French Community of Belgium, COST Actions and the Walloon region (Gadolymph and Holocancer programs). We thank Josianne Lefebvre for assistance in processing the XPS and TOF-SIMs data, and Rafaella Oliveira do Nascimento for contributions during discussions.

References

Afkhami F, Taherkhani S, Mohammadi M, Martel S. Encapsulation of magnetotactic bacteria for targeted and controlled delivery of anticancer agents for tumor therapy, *Conf Proc IEEE Eng Med Biol Soc*., 2011, 6668 - 6671.

Bridot JL, Stanicki D, Laurent S, Boutry S, Gossuin Y, Leclère P, Lazzaroni R, Vander-Elst L, Muller RN. New carboxysilane-coated iron oxide nanoparticles for nonspecific cell labelling. *Contrast Media Mol. Imaging*, 2013; 8: 466–474.

França R, Zhang XF, Veres T., Yahia L'H, Sacher E. Core–shell nanoparticles as prodrugs: possible cytotoxicological and biomedical impacts of batch-to-batch inconsistencies, *J Colloid Interface Sci*., 2013, 1(389): 292–297.

Friedman AJ, Han G, Navati MS, Chacko M, Gunther L, Alfieri A, Friedman JM. 2008. Sustained release nitric oxide releasing nanoparticles: charac- terization of a novel delivery platform based on nitrite containing hydrogel/glass composites. *Nitric Oxide.*, 19:12–20.

Friedman A, Friedman J. New biomaterials for the sustained release of nitric oxide: past, present and future. *Exp. Opin. Drug Del*., 2009, 6(10): 1113 – 1122.

Gölander CG, J. N. Herron, K. Lim, P. Claesson, P. Stenius, and J. D. Andrade, Properties of Immobilized PEG Films and the Interaction with Proteins, *Biotechnical and Biomedical Applications*, J. M. Harris, Ed. New York: Plenum, 1992, pp. 221–45.

Gow AJ, Farkouh CR, Munson DA, Posencheg MA, Ischiropoulos H. Biological significance of nitric oxide- mediated protein modifications. *Am. J. Physiol. Lung Cell Moll. Physiol*., 2004, 287(2 31 – 2): L262 – L268.

Gupta AK, Wells S. Surface-modified superparamagnetic nanoparticles for drug delivery: preparation, characterization, and cytotoxicity studies. *IEEE Trans Nanobioscience*., 2004, 3(1): 66-73.

Howlin RP, Cathie K, Hall-Stoodley L, Cornelius V, Duignan C, Allan RN, Fernandez BO, Barraud N, Bruce KD, Jefferies J, Kelso M, Kjelleberg S, Rice SA, Rogers GB, Pink S, Smith C, Sukhtankar PS, Salib R, and Webb JS. Low-Dose Nitric Oxide as Targeted Anti-biofilm

Adjunctive Therapy to Treat Chronic *Pseudomonas aeruginos*a Infection in Cystic Fibrosis, *Mol. Ther*., 2017, 25(9): 2104 – 2116.

Jardeleza C, Thierry B, Rao S, Rajiv S, Drilling A, Miljkovic D, Paramasivan S, James C, Dong D, Thomas N, Vreugde S, Prestidge CA, Wormald PJ. An in vivo safety and efficacy demonstration of a topical liposomal nitric oxide donor treatment for Staphylococcus aureus biofilm–associated rhinosinusitis. *Transl Res*., 2015, 166 (6): 683-692

Koval IV. The chemistry of disulfides, *Russ. Chem. Rev., 1994, 63(9): 735 – 750.*

Laverty G, Gorman SP, Gilmore BF. Biomolecular mechanisms of Pseudomonas aeruginosa and Escherichia coli biofilm formation, *Pathogens.*, 2014, 3: 596–632.

Li YF, Chen C. Fate and toxicity of metallic and metal-containing nanoparticles for biomedical applications. *Small.*, 2011, 7: 2965–2980.

Liu R-t, Liu J, Tong J-q, Tang T. Kong WC, Wanga X-w, Lib Y, Tang J-t. Heating effect and biocompatibility of bacterial magnetosomes as potential materials used in magnetic fluid hyperthermia, *Pro Nat Sci- Mat*, 2012; 22(1): 31–39

MacMicking J, Xie QW, Nathan C. Nitric oxide and macrophage function, *Annu Rev Immunol.*, 1997, 15: 323-50.

Mancinelli RL, McKay CP. Effects of nitric oxide and nitrogen dioxide on bacterial growth, *Appl Environ Microbiol*., 1983, 46(1): 198-202.

Mbeh DA, França R, Merhi Y, Zhang XF, Veres T, Sacher E, Yahia, L'H. In vitro biocompatibility assessment of functionalized magnetite nanoparticles: biological and cytotoxicological effects, *J Biomed Mater Res A.*, 2012, 100(6):1637-46.

Mbeh DA, Mireles LK, Stanicki D, Tabet L, Maghni K, Laurent S, Sacher E and Yahia L'H. Human Alveolar Epithelial Cell Responses to Core−Shell Superparamagnetic Iron Oxide Nanoparticles (SPIONs), *Langmuir*., 2015, 31: 3829−3839.

Mejias R, Perez-Yague S, Gutierrez L, Cabrera LI, Spada R, Acedo P, Serna CJ, Lazaro FJ, Villanueva A, Morales Mdel P, Barber DF. Dimercaptosuccinic acid-coated magnetite nanoparticles for magnetically guided in vivo delivery of interferon gamma for cancer immunotherapy, *Biomaterials.*, 2011, 32: 2938-2952.

Mireles LK, Sacher E, Yahia L'H, Laurent S, Stanicki D. Acomparative physico chemical, morphological and magnetic study of silane-functionalized superparamagnetic iron oxide nanoparticles prepared by alkaline coprecipitation, *Int.J.Biochem. Cell Biol.*, 2016, 75: 203–211.

Mireles LK, Sacher E, Yahia L'H, Laurent S, Stanicki D. Washing effect on superparamagnetic iron oxide nanoparticles, *Data in Brief*., 2016b, 7: 1296–1301

Nablo BJ, Prichard HL, Butler RD, Klitzman B, Schoenfisch MH. Inhibition of implant associated infections via nitric oxide release, *Biomaterials.*, 2005, 26(34): 6984-90.

Naqvi S, Samim M, Abdin M, Ahmed FJ, Maitra A, Prashant C, Dinda AK. Concentration-dependent toxicity of iron oxide nanoparticles mediated by increased oxidative stress, *Int. J. Nanomedicine.*, 2010, 5: 983-989.

Privett BJ, Broadnax AD, Bauman SJ, Riccio DA, and Schoenfisch MH. Examination of Bacterial Resistance to Exogenous Nitric Oxide, *Nitric Oxide*., 2012; 26(3): 169–173.

Ruiz A, Morais PC, Bentes de Azevedo R, Lacava ZGM, Villanueva A, Del Puerto Morales M. Magnetic nanoparticles coated with dimercaptosuccinic acid: development, characterization, and application in biomedicine, *J Nanopart Res*., 2014, 16: 2589.

Ikeda Y and Nagasaki Y. PEGylation technology in nanomedicine, *Adv Polym Sci*., 2011, 247: 115–140.

Saraiva J, Marotta-Oliveira SS, Cicillini SA, Eloy JDO, Marchetti JM. Nanocarriers of nitric oxide delivery, *J. Drug Deliv*. 2011, 936438.

Tassa C, Shaw SY, Weissleder R. Dextran-coated iron oxide nanoparticles: a versatile platform for targeted molecular imaging, molecular diagnostics, and therapy. *Acc. Chem. Res*, 2011; 44(10): 842-52.

Trampuz A, Widmerm AF. Infections associated with orthopedic implants. *Clin. Infect. Dis.*, 2001, 2(33): S94.

Wattendorf U and Merkle HP. PEGylation as a tool for the biomedical engineering of surface modified microparticles, *J Pharm Sci*., 2008, 97: 4655–4669.

Wilcox M, Kite P, Mills K, Sugden S. In situ measurement of linezolid and vancomycin concentrations in intravascular catheter-associated biofilm. *J Antimicrob Chemother.*, 2001, 47: 171–175.

Worley BV, Schilly KM, Schoenfisch MH. 2015. Anti-biofilm efficacy of dual-action nitric oxide-releasing alkyl chain modified poly(amidoamine) dendrimers. *Mol Pharm* 12:1573–1583.

Zhang X, Mansouri S, Mbeh DA, Yahia L'H, Sacher E, Veres T. Nitric Oxide Delivery by Core/shell Superparamagnetic Nanoparticle Vehicles with Enhanced Biocompatibility. *Langmuir.*, 2012, 28 (35): 12879–12885.

.

CHAPTER 8 GENERAL DISCUSSION

8.1 Synthesis of nanoparticles

To compare and select the most appropriate magnetite (Fe_3O_4) SPIONs prepared by alkaline coprecipitation (Stanicki, D., Boutry, S, et al 2014), three batched of SPIONs differently functionalized were compared:

1) Bare SPIONs (precursor)

2) Coated positively SPIONs (-NH_2)

3) Coated negatively SPIONs (-COOH)

The synthesis of nanoparticles, such as the SPIONs, has been considered reproducible in the literature (Stanicki, D., Boutry, S, et al 2014) as well as being classified as potential candidates for use as prodrugs to target infected sites (Miroslava N, Borjana D, et al., 2017). However, the reality is that the general reproducibility of nanoparticle surface chemistry may be unfeasible. This presents a serious challenge for new materials in biomedical applications, with their safety related issues (like protein corona formation, hemocompatibilities, etc) that depend on the control of the chemical and physical properties of the surfaces.

The objective in the first article presented in this thesis (A comparative physicochemical, morphological and magnetic study of silane-functionalized superparamagnetic iron oxide nanoparticles prepared by alkaline coprecipitation) was the analysis and comparison of the three batches of nanoparticles received by our collaborator Sophie Laurent , such nanoparticles with different coatings were evaluated by physicochemical characterization techniques in order to verify their functionalization and guarantee their batch to batch reproducibility. In our research laboratory we had the experience observing variations in the reproducibility of iron oxide nanoparticles (Franca R, et al., 2013). Therefore, determining if batch to batch variations are persistent even when they were synthesized in the same laboratory and to identify the expected chemical groups on the surface as a result of functionalization, would be the first step to know the type of nanoparticles that were available in this project.

8.2 Characterization techniques

The selection of characterization techniques, played a very important role throughout the realization of this project, techniques such as TEM, VMS and FTIR were chosen to allow us to know the characteristics and properties of nanoparticles, in addition were using high-sensitivity techniques such as XPS and TOF SIMS to determine the chemical groups present on the surface SPIONs. The comparison of the results among the techniques chosen, gave guidelines to describe the morphology, size, magnetic properties and chemical composition of the SPIONs.

The step-by-step physicochemical characterization in each surface modification of the SPIONs identifies the chemical composition of the surface, detects batch to batch reproducibility inconsistencies, detects the presence of unexpected chemical groups, possibly due to cross contamination, indicating a protocol to achieve the thiolation and nitrosation of SPIONs. The prediction of the expected chemical reactions after the step by step characterization of the nanoparticles describing the function chemical groups, contribute to guarantee successful NO attachment, the possibility of demonstrating the S-NO covalent bond and determining the reproducibility of results, not previously observed.

8.2.1 Discriminant analysis through characterization results

8.2.1.1 HRTEM

The analysis performed in high resolution transmission electron microscopy (HRTEM), allowed the determination of shapes, sizes, distribution and thickness of the polymer layers that cover the nanoparticles. In the first article published (Chapter 5), images of the SPIONs (Figure 5.1) were observed with an average size of ~10 nm and good dispersion and no agglomeration of SPIONs, having a quasi-spherical shape pretty uniform, even when it is known that inorganic SPIONs often have high surface energies, facilitating surface oxidation, which leads to particle aggregation and clustering (Zhang Y, et al., 2004). However, the silane layers expected were not observed, forming a coating and increasing the size of Fe_3O_4@NH_2 and Fe_3O_4@COOH SPIONs compared with Fe_3O_4 SPIONs. The nanoparticle diameters were evaluated and it was found that the difference between the sizes of bare and coated SPIONs were ~ 0.4 and 0.55 nm, respectively.

The average standard deviation of NPs oscillates in the range of ± 1.4 nm, which suggests a narrow size distribution and the possible absence of functionalization of nanoparticles with TPED and TEPSA coatings. TEM characterization results of the SPIONs indicated that there was no successful surface modification and consequently it is not possible to consider chemical functionalization through the-NH_2 or -COOH functional groups. However, a second analysis through another characterization technique like XPS and FTIR would be useful to complement and corroborate the results.

The idea of considering nanoparticles with coatings for the implementation of nano-systems of nitric oxide release, is because the literature indicates that in biological applications, coated nanoparticles have major advantages over bare nanoparticles, leading to improved properties such as: 1) reduced agglomeration of SPIONs in a biological medium; 2) increased dispersion and biological cyto-compatibility; 3) better conjugation with other bioactive molecules; 4) greater thermal and chemical stability, 5) prevention of opsonization of SPIONs; 6) biocompatibility of SPIONs, etc (Mahmoudi M, et al., 2011, Sounderya N and Zhang Y, 2008).

8.2.1.2 FTIR, XPS and TOF SIMS

FTIR found the presence of silica peaks at ~ 1050 cm^{-1} (Si-O-Si) and 1100 cm^{-1} (Si-O-C) in the spectra of positive and negative SPIONs and the absence of silica of peaks on bare SPIONs. These results demonstrate the attachment of silane chains to the SPIONs surface, but considering that FTIR is not a quantitative technique, XPS characterization was required to quantify and determine the atomic percent (at%) of silane chains, according with XPS results (Table 5.1) indicating that only a monolayer of silica was deposited on SPIONs.

In summary XPS, FTIR and ToF SIMS explaining the presence of silane chains in Fe_3O_4@NH_2 and Fe_3O_4@COOH SPIONs, but also according with XPS (Table 5.1) the presence of silica corresponds to a very low amount.

XPS (Table 5.1) and ToF SIMS (Figure 5.9) show that amine and carboxylic acid groups, where found on SPIONs where not expected, meaning an obvious cross-contamination where -NH_2 groups were present on SPIONs coated with TEPSA and COOH groups were observed on SPIONs coated with TPED. The analysis of results was repeated on a second batch, and the

inconsistencies of results persisted, denoting a possible cross contamination and variations of batch to batch reproducibility. Given these results, we can say that the batch-to-batch surface homogeneity of the SPIONs is in doubt.

This variation of the chemical composition of the SPIONs appears to be unavoidable and can affect the expected surface charge of the SPIONs and it is risky to think about the biological application of these nanoparticles (*Mbeh D.A* et al. 2015) because it has been shown that the surface charge affects the characteristics of corona formation in physiological fluids and therefore its cytotoxicity could be affected (Gunawan C, et al., 2014; *Mbeh D.A* et al. 2015).

On the first full characterization of the three batches of nanoparticles, the inconsistencies in the functionalization of the surface could not be ignored; these inconsistencies can have a negative impact on biomedical applications. It was proposed to dialyse the SPIONs, hoping to eliminate contaminants, possibly generated during the manufacturing process, or to functionalize bare SPION with PEG to control the homogeneity of the surface.

8.2.2 Magnetic properties

Vibrating sample magnetometry (VSM) characterization of the magnetic properties of the SPIONs showed a magnetization plot (M vs H) indicating that the three batches of SPIONs with different coatings have superparamagnetic behavior, characterized by a magnetization curve without hysteresis, each batch having an average value of ~26 emu /g (reaching its Ms at ~ 10,000 Oe).

8.3 Washing effect – dialysis

As mentioned in the previous section, using SPIONs with non-uniform surfaces and cross-contamination is difficult for biomaterials, because it is the surface of the materials where the first interaction is made with the biological environment and the biocompatibility of such materials depends on this interaction. That is why it was decided to dialyse the nanoparticles to remove impurities. Centrifugation method of purification was attempted but ultimately the recovery of the filter edmaterial was low, and initially there was no sign of a ligand of the silane chains, as observed in TEM photomicrographs showing the absence of a visible layer of TEPSA or of TPED. Repeated centrifugation could be a good method of purification, offering no risk of aggregation if the material is well ligand-stabilized and on the other hand leads to losses by particles sticking to the filter.

However, the addition of silane chains on SPIONs apparently were minimal, as the XPS results suggested.

A routine does not exist to purify charge-stabilized colloids like Fe_3O_4@NH_2 and Fe_3O_4@COOH; even dialysis will often compromise their colloidal stability and lead to aggregation. This is in the nature of colloids and cannot be avoided since their stability as a dispersion depends on the presence of other factors in the system, for example ionic charge.

After testing centrifugation and observing the almost all the material was retained in the filters, we chose dialysis, performed for three days, using a 14 kD cutoff membrane, and changing the water repeatedly during the process. But when the dialysed data were obtain, the presence of impurities endured and, moreover, new impurities appeared, not previously observed (Mireles L.K et. al., 2016), indicating that the material is continuously reacting with the environment. The presence of impurities can determine whether SPIONs are suitable or not for use for human body applications, due to the appearance of hydroxyl groups (OH), which can seriously affect the cytotoxicity of SPIONs (Mbeh DA, et to 2015). Therefore, the consideration of the PEGylation of SPIONs in order to create a uniform surface suitable for the functionalization and nitric oxide attachment appeared to be the best option to continue with the nanocarriers design.

8.4 Surface contaminants

We have found that, in previous studies (Franca R, 2013) and throughout this thesis project, a variation in reproducibility and homogeneity on nanoparticle surfaces. The presence of contaminants on metallic oxide nanoparticle surfacess may be explained by chemical thermodynamics, which teaches that a reaction will occur if the change in Gibbs free energy, ΔG, is negative. In the case of two-dimensional surfaces, the Gibbs free energy, G, is replaced by the Helmholtz free energy, A, which is defined at constant volume; this is because the volume of the surface is taken to be constant, and equal to zero. Thus, reactions will occur at surfaces when ΔA is negative¨. (Bavand R, et al., 2018). Spontaneous reaction can occur at a surface when the reaction product has a lower surface tension; it is for this reason that surfaces oxidize, metals corrode, adventitious carbon forms.

The literature indicates that nanomaterials, because of the highly reactive nature of their surface, can adsorb molecules from the surrounding medium, to reduce surface free energy. As a

result, unintentional contaminants can be introduced to the surface of nanomaterials by adsorption of air or suspended solution compounds (Jones C.F and Grainger D.W 2009). But these aspects do not explain the presence of oxidative compounds on the surface and its inhomogeneity; the contaminants are not always the same, they vary according to the nature of the sample and numerous contaminants correspond to traces or residues of solvents or reagents used during the reaction. The process of dialysis is not enough to remove or eliminate completely all the residues, and techniques such as XPS and TOF SIMS are highly sensitive and can detect traces (0.01 at% for XPS and milli-amus for ToF SIMS).

8.5 S-NO attachment

Following surface analysis of SPIONs by XPS and TOF SIMS, the lack of NH_2 and COOH groups in nanoparticles was indisputable; these nanoparticles were subjected to a functionalization process in which it was expected that silane chains containing NH_2 (TPED) and COOH (TEPSA) surface groups, provide the possibility of reacting to these groups.

Finding NH_2 groups in nanoparticles with negative charge and vice versa were not expected, nor were trace contaminants and unwanted oxidized species, in addition to the failure to eliminate traces of surface chemical components ven after dialysis. It was necessary to propose a new strategy to achieve the objective: to cover the nanoparticles with polymer chains that favored anchoring and contributed with the safe application of the nanoparticles in biomedical devices increasing their biocompatibility (Laurent S, et al., 2011, Mbeh D.A, 2012, Mbeh D.A, 2015). Such polymeric coating, should be rich in thiol groups (thiolation) and subsequently forming covalent bonds S-NO by the reaction between thiol groups with $NaNO_2$ (nitrosation).

8.6 Coating selection – thiolation

Using SPIONs as vehicles of nitric oxide release has been a subject of research involving many research groups. However, the results published so far do not show evidence of a successful linkage of the molecule in which the appearance of the S-NO covalent bond is found.

The PEGylation of SPIONs has achieved successful results in different biomedical applications such as MRI contrast, cancer treatment, etc. (Fortes-Brollo ME, et l., 2017; Ruiz A, et al., 2019;

Pelegrino MT, et al., 2017; Ikeda Y and Nagasaki Y, 2011), which suggested that a functionalization using PEG would be a viable option to considerate during the SPION design of NO-releasing vehicles. In the search if reagents capable of coating SPIONs and having free thiol (-SH) groups, to react with nitric oxide, we found: PEG-dithiol and meso-2,3-dimercaptosuccinic acid (DMSA), which ones could be good choices for the thiolation of the SPIONs. (See chemical structure Figure 8.1)

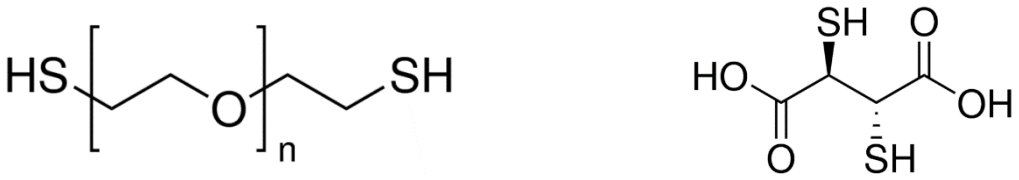

PEG-dithiol *meso*-2,3-Dimercaptosuccinic acid (DMSA)

Figure 8.1 Molecular schema of PEG-dithiol and DMSA

Figure 8.1 Chemical structure comparison of PEG-dithiol and meso 2,3 – Dimercaptosuccinic acid (DMSA)

DMSA in drug delivery has been previously used with efficacy (Mejias R, Perez-Yague S et al., 2011), with minimal cytotoxic effects (Naqvi S, Samim M, et al., 2010). PEG has been widely used as a coating material for magnetic nanoparticles; it is easily metabolized, having nonimmunogenic and nonantigenic properties, and can interact with cell membranes, resulting in an enhanced cellular response (Gölander CG, Herron JN, et al., 1992). However, it is not biodegradable, and its repeated dosage and accumulation can give rise to accelerated blood clearance. (Del Puerto *et al*. (Ruiz A, Morais PC, et al., 2014) and others (Ikeda Y and Nagasaki Y, 2011; Wattendorf U and Merkle HP, 2008), note that the use of PEG and DMSA, as magnetic nanoparticle coatings, reduces surface charge density, achieves long circulation times and maintains hydrodynamic sizes under 100 nm, avoiding agglomeration.

The coating with chains rich in thiol groups were formed around magnetite (Fe_3O_4) nanoparticles, but it should be emphasized that the layers are not uniform, in addition to varying

their thickness, (i.e: as shown in previous TEM results, after SPION functionalization with TEPSA and TPED in Figures 5.1, 5.2, 7.1, 7.2) and can leave exposed areas of the uncoated nanoparticles.

The surface chemistry of the SPIONs, revealed the presence of organic and inorganic nitroso groups on bare and positive SPIONs in both batches analyzed, even after having undergone dialysis. Only the second batch of nanoparticles with negative charge (SPIONs@TEPSA) was free of nitrogen components. Therefore, the use of SPIONs@TEPSA might would guarantee that all the nitrogen species observed were a consequence of functionalization.

8.7 Funcionalization – covalent bonds

Magnetite nanoparticles (Fe_3O_4) were functionalized by coatings: 1) dimercaptosuccinic acid (DMSA) and 2) poly(ethylene glycol) dithiol (PEGdithiol); both coatings formed shells containing free thiol (-SH) ligands on the SPION surface, subsequently used as reactive groups for nitrosation.

8.7.1 Thiolation: PEGdithiol/DMSA

The functionalizations of SPIONs were carried out using PEGdithiol and dimercaptosuccinic acid (DMSA) allowing thiolation. The PEGdithiol layer is seen thinner in the order of 2.7 ± 1.3 nm (Figure 7.1e), in comparison with DMSA at 3.1 ± 1.7 nm. Where the PEG chain is ~ 3x the size of the average thickness, indicating that the chains lie parallel to the SPION surface and the case of DMSA, the molecular length is ~ ¼ that the average thickness, indicating chain extension. These results indicate that the reaction conditions for thiolation probably favor thiolation for DMSA and consequently at a greater deposition of polymer chains on the surface of the nanoparticles, a greater number of SH groups could be found.

But what is the effect of thiolacion under nitrogen atmosphere and oxygen atmosphere?

Under O_2 atm and N_2 atm, SH and SS groups were found by XPS and TOF SIMS

When carrying out reactions under O_2 atm, it is known that it would be possible to generate the formation of SS groups which will eliminate the presence of free thiol groups, and no attachment of NO could be happen.

For XPS, the -SH and -SS peaks overlap at 164.0 eV, and therefore it is not possible to quantify the number of SH and SS groups. But it is found that for DMSA, the greater the deposition

of material, the greater concentration of $Si2p_{3/2}$ (2% at) has, compared to PEGdithion $Si2p_{3/}2$ (0.5-1.0 at%). A significant difference was clearly observed: (Figure 7.3 and 7.4, upper series) under N_2 atm, showing N1s contamination that should not appear. This means that N_2 interferes with the reaction.

8.7.2 Nitrosation: PEG-dithiol/DMSA

The addition of the NO groups, transforming the SH groups to -SNO, occurred by the reaction of the -SH functional groups with nitrite.

Under O_2 atm:

By XPS results, the N1s peak at 403-403.5 eV which corresponds to SNO, appeared after nitrotation, when the reaction was carried out under O_2 atmphere. ~0.3 at%. On nitrosation, ToF SIMS results of SPION@PEGdithiol-NO and SPION@DMSA-NO (Figure7.7 and 7.8) still display peaks of, SH, SS. This means that after reaction some free SH remains, available.The successful nitrosation of thiol groups on SPION@PEGdithiol-NO and SPION@DMSA-NO under N_2 atmosphere was shown by peaks at 57.98 Da (C-SN) and 61.97 Da (SN-O), again supporting the XPS attributions. The experiments where reproduced five times, and the same behavior persisted; it was found that DMSA react 3x more than PEGdithiol

Under N_2 atm:

The XPS spectra of SPIONs@PEGdithiol (Figure 7.10) shows $S2p_{3/2}$ peaks at 163.7 and 167.8 eV, attributed to SH and SO_3, respectively. N1s peaks appear, even when nitrosation was not carried out, at 399.0 (NH), 400.2 (NH_2) and 407eV (NO_3), indicating an unexpected reaction with the nitrogen atmosphere, since the subsequent use of an oxygen atmosphere gave no hint of glassware contamination.

Also, SPIONs@DMSA (Figure 7.11) shows free thiol at 164.2 (S-H), and unexpected N1s peaks at 402.0 and 403.1 eV. Clearly, the species introduced by the presence of a nitrogen atmosphere are reactive, subsequently oxidizing on exposure to air.

The SNO peak is not displayed in the PEGdithiol TOF-SIMS spectrum (Figure 7.12); however, it appears (61.97 Da) in the SPIONs@DMSA-NO spectrum, as does the SNO_2 peak (77.96 Da,

Figure 7.15), particularly intense in the negative SIMS spectrum. The presence of the SNO peak in SPIONs@DMSA-NO spectrum implies that some attachment of NO occurred, which was subsequently oxidized to SNO_2.

Thus,

The effect of the N2 atmosphere in each of the reactions were constant, interfering with oxidizing components in the thiolation and nitrosation and in the same way for PEG-dithiol and DMSA.

The hypothesis proposed: the thiolation of the SPIONs surfaces free of N1s compounds, will demonstrate the annulation of cross contamination, or will be identify the source of contamination, and under O_2 atmosphere the thiolation will generate thiol groups bonded to S-NO.

To estimate the efficienty of S-NO functionalization is considering that S-H, S-S and S-N they all have an XPS peak at the same position (Table 7.1), and is not possible to estimate a minimum value by assuming that the S-H contribution to the (S-H + S-S + S-N) peak is 100 %. As seen in the SPION@PEGdithiol-NO column of Table 7.1, the minimum value corresponds to 0.3/1.0 = 30 %; in the SPION@DMSA-NO column, the minimum value corresponds to 1.8/2.1 = 86 %.

8.8 Difficulties, challenges and contributions

This section in my thesis represents one of the most important bases that gave strength to this project, I would like to enumerate several important aspects of this work:

1) Management and interpretation of characterization techniques: to carry out the study and analysis of results through highly sentivite characterization techniques, lide XPS and TOF SIMS, which represented a great contribution to my knowledge and allowed me to carry out a critical and detailed analysis of my work

2) Lack of databases: within the critical analysis, I find important to mention: the comparison of resultswas difficults because at present there are not numerous publications that provide results regarding drug attachment with characterization techniques such as XPS and TOF SIMS, which ones are already demonstrated that, not all characterization techniques have the enought sensitivity

to show reliable results regarding the functionalization of nanoparticles, more specifically in the interpretation of surface chemistry and surface chemical bonds (attachments).

3) In the literature as mentioned in chapters above, the protocols proposed to molecular attachment (as NO to SPIONs), establish the necessity to maintain a $N_{2\ atm}$ to favor the conditions of better molecular attachment. However, the variation of parameters was crucial to understand the optimal concentrations, optimal parameters and finally when varying the nitrogen atmosphere to the iron atmosphere it was the key point and that defied the ideal parameters estimated according to laws of the quiba established, but it was surprising that the results were opposed to nanoscale.

4) The demonstration for the first time of the cross-link S-NO, was undoubtedly the most satisfactory result of this work, since for the first time it can be demonstrated with complementary characterization techniques, that the chemistry of the SPF superfine demonstrates clearly the anchor of NO.

Here, in this part of my thesis where, I wouldl like to answer the question at the beginning of this manuscript, based on the results obtained in this project:

Is it possible that after almost 60 years, since the beginning of the nanotechnology era, the chemical reactions and behaviors of nanomaterials are unpredictable today?

- Until now, nano-scale reactions require study to understand their behavior

CHAPTER 9 CONCLUSIONS AND RECOMMENDATIONS

9.1 Conclusions

This project showed step by step the successful attachment of nitric oxide molecules to SPIONs and demonstrated how the effect of the atmosphere in which the attachment reaction takes place determines the success of the anchoring; that is, nitric oxide is anchored to SPIONs when the reactions are carried out under an oxygen atmosphere, but the same reaction favors the introduction of species that oxidize when carried out under an atmosphere of nitrogen.

To design this nitric oxide release system, the physicochemical characterization of SPIONs was the key to developing the protocol of attachment. The first surface characterization on SPIONs with charges (neural, positive and negative) resulted in discarding the attachment using the silica chains on such surface nanoparticles, due to their surfaces inconsistencies and the various contaminants present in them.

Thiolation reactions using PEG-dithiol and DMSA generated a homogeneous surface with free thiols available to attach NO molecules. The amount of covalent S-NO bonds is greater in Fe_3O_4@DMSA because it has a greater number of thiol groups available compared to Fe_3O_4@PEG-dithiol. However, PEG-dithiol and DMSA, anchored NO molecules under oxygen atmosphere conditions successfully and both generate oxidize species under nitrogen atmosphere.

The demonstration of successful results of this thesis by different characterization techniques helps to make known with certainty that nano-scale reactions may have completely different mechanisms.

9.2 Recommendations

This work opens the way to extensive possibilities of continuing the study of SPION attached with NO; some recommendations are:

a) Extend the study of nitric oxide release, varying the concentrations of nitric oxide released and the time of release.

b) Biocompatibility and cytotoxicity studies of Fe_3O_4@PEG-dithiol@NO and Fe_3O_4@DMSA@NO

c) Perform NO release tests in the presence of common bateria found on implants (gram-positive and gram-negative) such as *Staphylococcus aureus*, *Staphylococcus epidermidis*, *Pseudomonas aeruginosa*, *etc*, to probe antibacterial effects and efficacy.

d) Perform NO release tests in contact with cancer cells and hyperthermia tests

e) Control and manipulate SPIONs under magnetic fields, to release nitric oxide at specific targets

f) Standardize the NO attachments protocol

REFERENCES

- Achike, F. I., & Kwan, C. Y. (2003). 1.1 Nitric oxide, human diseases and the herbal products that affect the nitric oxide signalling pathway. Clin Exp Pharmacol Physiol, 30 (9), 605-615.
- Allegranzi B, Nejad S.B, Combescure C, Graafmans W, Attar H, Donaldson L and Pittet D. Burden of endemic health-care-associated infection in developing countries: systematic review and meta-analysis. *The Lancet*. (2011) ;377(9761):228–241.
- Ankamwar B, Lai T. C, Huang J. H, Liu R. S, Hsiao M, Chen C. H and Hwu, Y. K. Biocompatibility of Fe3O4 nanoparticles evaluated by in vitro cytotoxicity assays using normal, glia and breast cancer cells. Nanotechnology. (2010); 21(7), 75102.
- Appelhans A. D and Delmore J. E. Comparison of polyatomic and atomic primary beams for secondary ion mass-spectrometry of organics. *Analytical Chemistry*, (1989). 61(10), 1087-1093.
- Arruebo M, Fernandez-Pacheco, Ibarra M. R and Santamaria J. Magnetic nanoparticles for drug delivery. *Nano Today*, (2007); 2(3): p. 22-32.
- Auffan M, Decome L, Rose J, Orsiere T, De Meo M, Briois V, Chaneac C, Olivi L, Berge-lefranc J.L Botta A, Wiesner M.R, Bottero J,Y. In vitro interactions between DMSA-coated maghemite nanoparticles and human fibroblasts: a physiolochemical and cyto-genotoxical study. *Environ. Sci. Technol*. (2006) 40, 4367–4373.
- Bavand R, Chen L, França R, Loran S, Yang D-Q, Yelon A, Zhang G.X and E. Sacher "Intensity modulation of the Shirley background of the Cr3p spectra with photon energies around the Cr2p edge", by A Herrera-Gomez, D Cabrera-German, A D Dutol et al, Surface Interface Anal, 2018;50:246-252. *Surf Interface Anal*. (2018); 50:683–685.
- Baumgartner J, Bertinetti L, Widdrat M, Hirt A.M and Faivre D. Formation of magnetite nanoparticles at low temperature: from superparamagnetic to stable single domain particles. *PLoS One*. (2013); 8(3): p. e57070.

- Beligni, M. V., & Lamattina, L. (2001). Nitric oxide in plants: the history is just beginning. Plant, Cell, and Environment , 24, 267-27.
- Bohme, G. A., Bon, C., Lemaire, M., Reibaud, M., Piot, O., Stutzmann, J., Doble, A., Blanchard, J. C. (1993). Altered Synaptic Plasticity and Memory Formation in Nitric Oxide Synthase Inhibitor-Treated Rats. Proc Natl Acad Sci USA, 90, 9191-9194.
- Bharde A.A, Parikh RY, Baidakova M, Jouen S, Hannoyer B, Enoki T, Prasad BL, Shouche YS, Ogale S and Sastry M. Bacteria-mediated precursor-dependent biosynthesis of superparamagnetic iron oxide and iron sulfide nanoparticles. *Langmuir*. (2008); 24(11): p. 5787-94.
- Bhattacharya K, Davoren M, Boertz J, Schins R P, Hoffmann E and Dopp E. Titanium dioxide nanoparticles induce oxidative stress and DNA-adduct formation but not DNA-breakage in human lung cells. *Part. Fibre Toxicol*. (2009); 6, 17.
- Birolini C, De Miranda J.S, Utiyama E.M, Rasslan S, Birolini D. Active *Staphylococcus aureus* infection: Is it a contra-indication to the repair of complex hernias with synthetic mesh? A prospective observational study on the outcomes of synthetic mesh replacement, in patients with chronic mesh infection caused by *Staphylococcus aureus. Int. J. Surg.* (2016), *28*, 56– 62.
- Boisseau P, Loubatonb B. "Nanomedicine, nanotechnology in medicine". *CR Physique* (2011). 12(7); 620-636.
- Bouwmeester H, Dekkers S, Noordam M, Hagens W, Bulder A., De Heer C, Ten Voorde S.E, Wijnhoven S.W, Marvin H.J, Sips A.J. "Review of health safety aspects of nanotechnologies in food production". *Regul Toxicol Pharmacol* (2009). 53(1); 52-62.
- Bozzola J.J and Russell L.D, Electron Microscopy, principles and techniques for biologist. *Jones & Bartlett Publishers*. (1999) 2nd Edition, IL, U.S.A
- Briggs D. Surface analysis of polymers by XPS and static SIMS. Cambridge: *Cambridge University Press*, (1998).

- Briggs D., Brown A. and Vickerman J.C. Handbook of static secondary ion mass spectrometry. *Chichester: Wiley and Sons Ltd*., (1989).
- Briggs D. and Seah M. Practical surface analysis volume 2 - ion and neutral spectroscopy. *Chichester: Wiley and Sons Ltd*., (1992).
- Bulte, J. W. M. In Vivo MRI Cell Tracking: Clinical Studies. *American Journal of Roentgenology.* (2009).193(2), 314-325.
- Cai L.L. Actively-Targeted LTVSPWY Peptide-Modified Magnetic Nanoparticles for Tumor Imaging. Int. J. Nanomed. (2012); 7, 3981–3989.
- Calatayud M.P, Sans B, Raffa V, Riggio C, Ibarra M.R and Goya G.F. The effect of surface charge of functionalized Fe3O4 nanoparticles on protein adsorption and cell uptake. *Biomaterials*. (2014); 35(24): p. 6389-99.
- Carvalho S.M, Leonel A.G, Mansur A.A.P, Carvalho I.C, Krambrock K and Mansur H.S. Bifunctional magnetopolymersomes of iron oxide nanoparticles and carboxymethylcellulose conjugated with doxorubicin for hyperthermo-chemotherapy of brain cancer cells. *Biomater. Sci*., (2019); 7, 2102-2122.
- Cedervall T, Lynch I, Foy M, Berggad T, Donnelly S. C, Cagney G and Dawson, K. A. Detailed identification of plasma proteins adsorbed on copolymer nanoparticles. *Angewandte Chemie-International Edition*. (2007) 46(30), 5754-5756.
- Chaves S.B, Lacava L.M, Lacava Z.G.M, Silvia O, Pelegrini F, Buske N, Gansau C, Morais P.C and Azevedo R.B. Light microscopy and magnetic resonance characterization of a DMSA-coated magnetic fluid in mice. *IEEE T Magn*. (2002) 38(5), 3231–3233.
- Chen, Z.P, et al., Preparation and characterization of water-soluble monodisperse magnetic iron oxide nanoparticles via surface double-exchange with DMSA. Colloids and Surfaces A: Physicochemical and Engineering Aspects, (2008); 316(1–3): p. 210-216.
- Chien-Chi L, Anseth KS. PEG Hydrogels for the Controlled Release of Biomolecules in Regenerative Medicine. *Pharmaceutical Research*. (2009). 26(3) 631–643
- Coppo J. “Nanotecnología, medicina veterinaria y producción agropecuaria”. Rev Vet. (2009). 20(1); 61-71.

- Crist B.V. Handbooks of Monochromatic XPS Spectra. *XPS International LLC*, Mountain View. (2004), Vol. 1-5, CA, USA.
- Davies I. R and Zhang X. Nitric Oxide Selective Electrodes. *Methods in Enzymology*. (2008); Vol. 436, 63-95.
- De Lima R, De Oliveira J.L, Ludescher A, Molina M.M, Itri R, Seabra A.B and Haddad P.S. Nitric oxide releasing iron oxide magnetic nanoparticles for biomedical applications: cell viability, apoptosis and cell death evaluations. Journal of Physics: Conference Series 429 (2013) 012034
- Dilnawaz F, Singh A and Mohanty C.S.S.K. Dual Drug Loaded Superparamagnetic Iron Oxide Nanoparticles for Targeted Cancer Therapy. Biomaterials (2010); 31, 3694–3706.
- Donahue, N. M. The reaction that wouldn't quit. *Nature Chemistry*. (2011); 3, 98- 99.
- Drexler K.E. Engines of Creation : The Coming Era of Nanotechnology. Anchor Books. (1986); downloaded from : http://www.foresight.org/EOC/EOC_Chapter_1.html
- Drury J.L and Mooney J.D. Hydrogels for tissue engineering: scaffold design variables and applications. *Biomaterials*. (2003) 24:4337–4351.
- Duffo G. Materiales y materias primas: Biomateriales. Ministerio de Educación, (2011); Buenos Aires, Argentina
- Dunlop D.J. and Ozdemir O.Z. Rock magnetism : fundamentals and frontiers. (1997); *Cambridge*: Cambridge University Press.
- Dupont, H. The empiric treatment of nosocomial intra-abdominal infections. *Int. J. Infect. Dis*. (2007), 11 (1); S1– S6.
- Ekmekcioglu, S., Tang, C. H., & Grimm, E. A. (2005). NO news is not necessarily good news in cancer. Curr Cancer Drug Targets , 5 (2), 103-115.
- Estall, L. B., Grant, S. J., & Cicala, G. A. (1993). Inhibition of nitric oxide (NO) production selectively impairs learning and memory in the rat. Pharmacol Biochem Behav , 46 (4), 959-62

- Estelrich J, Sánchez-Martín M.J and Busquets M.A. Magnetic properties of nanoparticles as a function of their spatial distribution on liposomes and cells. *Int. J. Nanomed.*, (2015), 10, 1727 -1741.

- Etheridge M.L, Campbell S.A, Erdam A.G, Haynes C.L, Wolf S.M, Mccullough J. "The big picture on nanomedicine: the state of investigational and approved nanomedicine products". *Nanomedicine*. (2013). 9(1); 1-14.

- Faghihzadeh F, Anaya N.M, Schifman L.A, Oyanedel-Craver V. Fourier transform infrared spectroscopy to assess molecular-level changes in microorganisms exposed to nanoparticles. *Nanotechnology for Environmental Engineering*. (2016); 1:1.

- Fang B, Gon S, Park M, Kumar K N, Rotello V M, Nusslein K and Santore M M. Bacterial adhesion on hybrid cationic nanoparticle–polymer brush surfaces: Ionic strength tunes capture from monovalent to multivalent binding. *Colloids and Surfaces B: Biointerfaces*. (2011); 87, 109.

- Fedorovich S, Alekseenko A., Waseem T. "Are synapses targets of nanoparticles?". *Biochem Soc Trans*. (2010) 38(2); 536-538.

- Feynman, R. P. There's Plenty of Room at the Bottom. (1959), http://www.zyvex.com/nanotech/feynman.html.

- Figuerola A, Di Corato R, Manna L, Pellegrin T. From iron oxide nanoparticles towards advanced iron-based inorganic materials designed for biomedical applications. *Pharmacol. Res.* (2010) 62, 126–143.

- Fiorillo F. Measurements of magnetic materials. *Metrologia,* (2010). 47; S114–S142

- Franca, R., Zhang, X.F., Veres, T., Yahia L'H, Sacher E. Core–shell nanoparticles as prodrugs: possible cytotoxicological and biomedical impacts of batch-to-batch inconsistencies. *J Colloid Interface Sci*. (2013) 1 (389), 292–297.

- Freitas R. “What is nanomedicine?”. *Nanomedicine: NBM*. (2005). 1(1); 2-9.

- Friedman AJ, Han G, Navati MS, Chacko M, Gunther L, Alfieri A, Friedman JM. 2008. Sustained release nitric oxide releasing nanoparticles: charac- terization of a novel delivery platform based on nitrite containing hydrogel/glass composites. *Nitric Oxide.,* 19:12–20.

- Friedman A, Friedman J. New biomaterials for the sustained release of nitric oxide: past, present and future. *Exp. Opin. Drug Del*., 2009, 6(10): 1113 – 1122.

- Fortes-Brollo M.E, Veintemillas-Verdaguer S, Menor-Salván C and Del Puerto-Morales M. Key Parameters on the Microwave Assisted Synthesis of Magnetic Nanoparticles for MRI Contrast Agents. Contrast Media & Molecular Imaging. (2017)

- Furchgott, R. F., & Zawadzki, J. V. (1980). The obligatory role of endothelial cells in the relaxation of arterial smooth muscle by acetylcholine. Nature, 373-376.

- Garcia M.P, Parca R.M, Chaves S.B, Silva L.P, Santos A.D, Lacava, Z.G, Morais P.C and Azevedo R.B Morphological analysis of mouse lungs after treatment with magnetite-based magnetic fluid stabilized with DMSA. *J.Magn. Magn. Mater*. (2005) 293, 277–282.

- Grams J. New trends and potentialities of ToF-SIMS in surface studies. New York: *Nova Science Publishers*, Inc.(2007).

- Grant J.T and Briggs D. Surface Analysis by Auger and X-ray Photoelectron Spectroscopy. *IM Publications*. (2003), Chichester, UK

- Gunawan C, Lim M, Marquis C. P and Amal R. Nanoparticle-protein corona complexes govern the biological fates and functions of nanoparticles. *Journal of Materials Chemistry B.* (2014); 2(15), 2060-2083.

- Gupta A.K. and M. Gupta, Cytotoxicity suppression and cellular uptake enhancement of surface modified magnetic nanoparticles. Biomaterials, 2005. 26(13): p. 1565-73.

- Gupta, A. K., & Gupta, M. Synthesis and surface engineering of iron oxide nanoparticles for biomedical applications. *Biomaterials. (2005)b; 26*(18), 3995-4021.

- Hall, C. N.; Garthwaite, J., What is the real physiological NO concentration in vivo? Nitric Oxide (2009); 21, 92-103.

- Heywood J. B. Internal Combustion Engine Fundamentals. McGraw Hill: New York, (1988); p 20.

- Hong, S. C, Lee J. H, Lee J, Kim H.Y, Park J. Y, Cho J and Han, D. W. Subtle cytotoxicity and genotoxicity differences in superparamagnetic iron oxide nanoparticles coated with various functional groups. *International journal of nanomedicine*. (2011) *6* 3219-3231.

- Huang, E. P. (1997). Synaptic plasticity: A role for nitric oxide in LTP. Curr Biol , 7, R141-R143.

- Hudgins P.A, Anzai Y, Morris M.R and Lucas M.A.Ferumoxtran-10, a superparamagnetic iron oxide as a magnetic resonance enhancement agent for imaging lymph nodes: a phase 2 dose study. AJNR Am J Neuroradiol, 2002. 23(4): p. 649-56.

- Ignarro L. J, Buga G. M, Wood K. S, Byrns R. E and Chaudhuri, G. Endothelium-derived relaxing factor produced and released from artery and vein is nitric oxide. *Proceeding of the National Academy of Science.* (1987); 84, 9265-9269.

- Ignarro L. J. Byrns, R. E.; Buga, G. M.; Wood, K. S., Endothelium-derived relaxing factor from pulmonary artery and vein possesses pharmacologic and chemical properties identical to those of nitric oxide radicals. *Circulation Research* (1987); 61, 866- 879.

- Iijima M and Kamiya H. Surface modification for improving the stability of nanoparticles in liquid media. KONA Powder and Particle Journal. (2009); 27, 119-129.

- Ikeda Y and Nagasaki Y. PEGylation technology in nanomedicine, *Adv Polym Sci*., (2011); 247: 115–140.

- Illés E, Szekeres M, Tóth I.Y, Szabó Á, Iván B, Turcu R, Vékás L, Zupkó I, Jaics G and Tombácz E. Multifunctional PEG-Carboxylate Copolymer Coated Superparamagnetic Iron Oxide Nanoparticles for Biomedical Application. J. Magn. Magn. Mater. (2018); 451, 710–720.

- Invernizzi N, Foladori G. "El despegue de las nanotecnologías". *Ciencia ergo sum*. (2005). 12(3); 321-327.

- Jones C. F and Grainger D. W. In vitro assessments of nanomaterial toxicity. *Advanced drug delivery review.* (2009); 61(6), 438-456.

- Kadiyala U, Kotov N.A and VanEpps J.S. Antibacterial metal oxide nanoparticles: challenges in interpreting the literature. *Curr Pharm Des*. (2018); 24(8): 896–903.

- Karlsson H. L, Cronholm P, Gustafsson J and Moller L. Copper oxide nanoparticles are highly toxic: a comparison between metal oxide nanoparticles and carbon nanotubes. *Chemical research in toxicology.* (2008) 21(9), 1726-1732.

- Kewal J. "Nanotechnology in clinical laboratory diagnostics". *Clin Chim Acta.* (2005) 358(1-2); 37-54.

- Kim J, Yung C, Kim W.J and Chen X. Combination of nitric oxide and drug delivery systems: tools for overcoming drug resistance in chemotherapy. *Journal of Controlled Release*, (2017); 263: 223-230

- Kroll A, Pillukat M. H, Hahn D and Schnekenburger, J. Current in vitro methods in nanoparticle risk assessment: Limitations and challenges. *European Journal of Pharmaceutics and Biopharmaceutics*, (2009);72 (2), 370-377.

- Kubinová S and Syková E. "Nanotechnology for treatment of stroke and spinal cord injury". *Nanomedicine* (2010). 5(1); 99-108.

- LaConte L.E, Nitin N, Zurkiya O, Caruntu D, O'Connor C.J, Hu X and Bao G. Coating Thickness of Magnetic Iron Oxide Nanoparticles Affects R2 Relaxivity. J. Magn. Reson. Imaging (2007); 26, 1634–1641.

- Lamarque, D., Kiss, J., Whittle, B., & Delchier, J. C. (1995). Role of nitric oxide in maintaining the mucosal integrity and in inflammatory gastrointestinal diseases. Gastroenterol Clin Biol , 20 (12), 1085-1098.

- Langer R. Drug delivery and targeting. *Nature*, (1998), 392, 6679

- Laocharoensuk R., Burdick J., Wang J. "Carbon-nanotube-induced acceleration of catalytic nanomotors" (2008). *ACS Nano*. 2(5); 1069-1075.

- Laurent S, Forge D, Port M, Roch A, Robic C, Vander Elst L and Muller RN. Magnetic iron oxide nanoparticles: synthesis, stabilization, vectorization, physicochemical characterizations, and biological applications. *Chem Rev.* (2008); 108(6): p. 2064- 110

- Laurent, S., Dutz, S., Hafeli, U. O., & Mahmoudi, M. Magnetic fluid hyperthermia: Focus on superparamagnetic iron oxide nanoparticles. *Advances in colloid and interface science.* (2011) *166*(1-2), 8-23.

- Lewis K. Persister cells and the riddle of biofilm survival. *Biochemistry*. (2005); 70(2): 267–274.

- Lin C.C and Metters A.T. Hydrogels in controlled release formulations: Network design and mathematical modeling. *Adv. Drug Deliv. Rev.* (2006). 58:1379–1408.

- Lin C, Liu Y, Yan H. "Designer DNA nanoarchitectures". *Biochemistry*. (2009) 48(8); 1663-1674.

- Lo C.T, Van Tassel P.R and Saltzman W.M. Simultaneous Release of Multiple Molecules from Poly(Lactide-co-Glycolide) Nanoparticles Assembled onto Medical Devices. *Biomaterials*. 2009 Oct; 30(28): 4889–4897.

- Mah T.F.C, O'Toole G.A. Mechanisms of biofilm resistance to antimicrobial agents. *Trends in Microbiology*. 2001;9(1):34–39.

- Mahmoudi M, Hofmann H, Rothen-Rutishauser B, Petri-Fink A. Assessing the in vitro and in vivo toxicity of superparamagnetic iron oxide nanoparticles. *Chem Rev*. (2012); 112(4): p. 2323-38.

- Mahmoudi M, Lynch I, Ejtehadi M. R, Monopoli M. P. Bombelli F. B and Laurent S. Protein-nanoparticle interactions: opportunities and challenges. *Chem Rev*. (2011); 111 (9), 5610-37.

- Mahmoudi M, Sant S, Wang B, Laurent S and Sen T. Superparamagnetic iron oxide nanoparticles (SPIONs): development, surface modification and applications in chemotherapy. *Advanced drug delivery reviews*. (2011); 63(1-2), 24-46.

- Mahmoudi M, Simchi A, Milani A S and Stroeve P. Cell toxicity of superparamagnetic iron oxide nanoparticles. J. Colloid Interface Sci. (2009); 336, 510.

- Mbeh D. A, Franca R, Merhi Y, Zhang XF, Veres T, Sacher E, Yahia L'H. In vitro biocompatibility assessment of functionalized magnetite nanoparticles: Biological and Cytotoxicological effects. *Journal of Biomedical Materials Research A*. (2012); 100(6):1637-46.

- Mbeh, D. A, Javanbakht T, Tabet L, Merhi Y, Maghni K, Sacher E and Yahia, L. H. Protein corona formation on magnetite nanoparticles: effects of culture medium composition, and its consequences on superparamagnetic nanoparticle cytotoxicity. *Journal of Biomedical Nanotechnology*.(2014); 11(5):828-40.

- Mbeh, D.A, Mireles L.K, Stanick D, Tabet L, Maghni K, Laurent S, Sacher E and Yahia L'H. Human alveolar epithelial cell responses to core–shellsuperparamagnetic iron oxide nanoparticles (SPIONs). *Langmuir*. (2015); 31,3829–3839.

- Mellott M.B, Searcy K, and Pishko M.V. Release of protein from highly cross-linked hydrogels of poly(ethylene glycol) diacrylate fabricated by UV polymerization. *Biomaterials*. (2001). 22:929–941

- Mohanty S, Jain K.G, Nandy S.B, Kakkar A, Kumar M, Dinda A.K, Singh H, Ray A. Iron oxide labeling does not affect differentiation potential of human bone marrow mesenchymal stem cells exhibited by their differentiation into cardiac and neuronal cells. *Mol Cell Biochem.* (2018); 448(1-2): 17-26.

- Molina M.M, Seabra A.B, De Oliveira M.G, Itri R, Haddad P.S. Nitric oxide donor superparamagnetic iron oxide nanoparticles. *Materials Science and Engineering: C*. (2013); 33(2): 746-751

- Monge-Fuentes V, Garcia M, Tavares M.C.H and Bentes-Azevedo R. Biodistribution and biocompatibility of DMSA-stabilized maghemite magnetic nanoparticles in nonhuman primates (Cebus spp.). Nanomedicine (Lond), 2011. 6(9): p. 1529-44.

- Mou, Y., et al., Effects of 2,3-dimercaptosuccinic acid modified Fe2O3 nanoparticles on microstructure and biological activity of cardiomyocytes. RSC Advances, 2015. 5(25): p. 19493- 19501.

- Murray C B, Norris D J and Bawendi M G. Synthesis and characterization of nearly monodisperse CdE (E = sulfur, selenium, tellurium) semiconductor nanocrystallites. J. Am. Chem. Soc. (1993); 115, 8706.

- Na H, Song I and Hyeon T. Inorganic Nanoparticles for MRI Contrast Agents. Adv. Mater. (2009); 21, 2133–2148.

- National Center for Health Statistics. Vital statistics of the United States. 119th ed. Washington: U.S. Census Bureau. Statistical abstract of the United States; (1999); 99.

- Nedyalkova M, Donkova B, Romanova J, Tzvetkova G, Madurga S, Simeonova V, Iron oxide nanoparticles – In vivo/in vitro biomedical applications and in silico studies. *Advances in Colloid and Interface Science*. (2017) 249; 192–212.

- Nguyen T K, Thanha L and Greena, A W. Functionalisation of nanoparticles for biomedical applications *Nano Today* (2002); 5, 213.

- Nuttelman CR, Rice MA, Rydholm AE, Salinas CN, Shah DN, and Anseth KS. Macromolecular monomers for the synthesis of hydrogel niches and their application in cell encapsulation and tissue engineering. *Prog. Polym. Sci*. (2018); 33:167–179.

- O'Connor D.J, Sexton B.A and Smart R.S.C. Surface analysis methods in materials science. (2003) 2nd ed. Berlin: Springer-Verlag.

- Oostingh G. J, Casals E, Italiani P, Colognato R, Stritzinger R, Ponti J and Boraschi D. Problems and challenges in the development and validation of human cell-based assays to determine nanoparticle-induced immunomodulatory effects. *Particle and Fibre Toxicology*. (2011); 8.

- Palmer R. M. J, Ferrige A. G and Moncada, S., Nitric oxide release account for the biological activity of endothelium-derived relaxing factor. *Nature* (1987); 327, 524-526.

- Pankhurst, Q A, Connolly J, Jones S K and Dobson J. pplications of magnetic nanoparticles in biomedicine. *J. Phys. D:Appl. Phys*. (2004) 2003: 36, R167.

- Park M.V, Annema W, Salvati A, Lesniak A, Elsaesser A, Barnes C, McKerr G, Howard C.V, Lynch I, Dawson K.A and others. In vitro developmental toxicity test detects inhibition of stem cell differentiation by silica nanoparticles. *Toxicol Appl Pharmacol* (2009); 240: 108–116.

- Passchier C.W and Trouw R.A.J. Microtectonics. (2005) V(1); Berlin: Springer-Verlag.

- Pastrana H., Avila A. “Nanomedicina: Estado del arte”. *Revista de Ingeniería Universidad de los Andes*. (2006); 25, 60-69.

- Pelegrino M.T, Silva L.C, Watashi C.M, Haddad P.S,, Rodrigues Tand Seabra A.B. Nitric oxide-releasing nanoparticles: synthesis, characterization, and cytotoxicity to tumorigenic cells. *Journal of Nanoparticle Research*. *(*2017); 19:57

- Peppas N.A, Hilt J.Z, Khademhosseini A, and Langer R. Hydrogels in biology and medicine: From molecular principles to bionanotechnology. *Adv. Mater*. (2006) 18:1345–1360.

- Pisanic T.R., 2nd, et al., Nanotoxicity of iron oxide nanoparticle internalization in growing neurons. Biomaterials, 2007. 28(16): p. 2572-81.

- Poulin, S., Franca, R., Moreau-Belanger, L., & Sacher, E. Confirmation of X-ray Photoelectron Spectroscopy Peak Attributions of Nanoparticulate Iron Oxides, Using 145 Symmetric Peak Component Line Shapes. *Journal of Physical Chemistry C*. (2010); 114(24), 10711-10718.

- Puurunen K, Vasara P. “Opportunities for utilising nanotechnology in reaching near-zero emissions in the paper industry”. (2007). J Clean Prod. 15(13-14); 1287-1294.

- Rahman M, Laurent S, Tawil N, Yahia L’H. Mahmoudi, M., Protein-Nanoparticle Interactions. *The Bio-Nano Interface*. (2013); Vol. 15.

- Roco M. “Nanotechnology: convergence with modern biology and medicine”. *Curr Opin Biotechnol.* (2003) 14(3); 337-346.

- Romanò C.L, Tsuchiya H, Morelli I, Battaglia A,G and Drago L. Antibacterial coating of implants: are we missing something?. *Bone Joint Res.* (2019); 8(5): 199–206.

- Rosen J E and Gu F X. Surface functionalization of silica nanoparticles with cysteine: a low-fouling zwitterionic surface. *Langmuir*. (2011); 27, 10507.

- Ross A.E, Bengani L.C, Tulsan R, Maidana D.E, Salvador-Culla B, Kobashi H, Kolovou P.E, Zhai H, Taghizadeh K, Kuang L, Mehta M, Vavvas D.G, Kohane D.S.B. Topical sustained drug delivery to the retina with a drug-eluting contact lens. *Biomaterials*. (2019); 217 -119285

- Ruiz A, Beola L, Rubio C, Gavilán H, Marciello M, Rodríguez-Ramiro I, Ciordia S, Morris C.J and Del Puerto Morales M. Understanding the Influence of a Bifunctional Polyethylene Glycol Derivative in Protein Corona Formation around Iron Oxide Nanoparticles. Materials (Basel). (2019); Jul; 12(14): 2218

- Saavedra J. E and Keefer L. K. Nitrogen-Based Diazeniumdiolates: Versatile Nitric Oxide-Releasing Compounds in Biomedical Research and Potential Clinical Applications. *Journal of Chemical Education* (2002); 79 (12), 1427-1434.

- Sahoo S, Parveen S, Panda J. "The present and future of nanotechnology in human health care". *Nanomedicine: NBM.* (2007). 3(1); 20-31.

- Schierholz, J. M.; Beuth, J. Implant infections: a haven for opportunistic bacteria. *J. Hosp Infect*. (2001); 49(2); 87– 93.

- Seabra A.B, de Lima R, Calderón M, Nitric oxide releasing nanomaterials for cancer treatment: current status and perspectives. *Curr Top Med Chem*. 2015;15(4):298-308.

- Seah M.P and Briggs D. Practical Surface Analysis by Auger and X-ray Photoelectron Spectroscopy. *Wiley & Sons*, (1992). 2nd edition, Chichester, UK

- Soler M. A. G, Báo S. N, Alcântara G. B, Tibúrcio V. H. S, Paludo G. R, Santana J.F. B, Guedes M. H, Lima E. C. D, Lacava Z. G. M and Morais P.C. Interaction of erythrocytes with magnetic nanoparticles. *J.Nanosci Nanotechnol*. (2007) 7(3), 1069–1071.

- Sounderya N and Zhang Y. Brevet Singapore no. F. o. E. Division of Bioengineering, National University of Singapore. (2008).

- Sprigge J. S. Sir Humphry Davy; his researches in respiratory physiology and his debt to Antoine Lavoisier. *Anaesthesia*. (2002); 357-364.

- Stanicki D, Boutry S, Laurent S, Wacheul L, Nicolas E, Crombez D and Muller R. N. Carboxy-silane coated iron oxide nanoparticles: a convenient platform for cellular and small animal imaging. *Journal of Materials Chemistry B,* (2014) 2(4), 387-397.

- Thorek D.L, Chen A.K, Czupryna J, Tsourkas A. Superparamagnetic iron oxide nanoparticle probes for molecular imaging. Ann *Biomed Eng* (2006); 34(1): p. 23-38. 4

- Tkachenko A.G, Xie H, Liu Y, Coleman D, Ryan J, Glomm W.R, Shipton M.K, Franzen S and Feldheim D.L. Cellular Trajectories of Peptide-Modified Gold Particle Complexes: Comparison of Nuclear Localization Signals and Peptide Transduction Domains. Bioconjug. Chem. (2004); 15, 482–490.

- Vangijzegem T, Stanicki D and Laurent S. Magnetic iron oxide nanoparticles for drug delivery: applications and characteristics. *Expert Opinion on drug delivery*. (2018); 18-1

- Vickerman J.C and Briggs D. ToF-SIMS: Materials Analysis by Mass Spectrometry. IM Publications. (2013). 2nd edition. Manchester, UK: SurfaceSpectra

- Wahajuddin and S. Arora, Superparamagnetic iron oxide nanoparticles: magnetic nanoplatforms as drug carriers. *Int J Nanomedicine*. (2012); 7: p. 3445-71.

- Wang J. “Can man-made nanomachines compete with nature biomotors?”. ACS Nano. (2009) 3(1); 4-9.

- Wattendorf U and Merkle HP. PEGylation as a tool for the biomedical engineering of surface modified microparticles, *J Pharm Sci*., (2008); 97: 4655–4669.

- Watts J.F and Wolstenholme J. An Introduction to Surface Analysis by XPS and AES. *Wiley & Sons*, (2003), Chichester, UK

- Wenzel RP, Edmond MB. The Impact of Hospital-Acquired Bloodstream Infections. Emerg Infect Dis. (2001); 7(2):174-177.

- Wilhelm C., et al., Intracellular uptake of anionic superparamagnetic nanoparticles as a function of their surface coating. Biomaterials, 2003. 24(6): p. 1001-11.

- Wu W, He Q, and Jiang C. Magnetic iron oxide nanoparticles: synthesis and surface functionalization strategies. *Nanoscale Res Lett*, (2008); 3(11): p. 397-415

- Yadav H.K.S, Alsalloum G.A and Halabi N.A.A. Nanobiotics and nanoengineered prosthetics. Nanostructures for the engineering of cells, tissues and organs - From design to applications. (2018); 513 – 587.

- Yang H.W, Hua M.Y, Liu H.L, Huang C.Y and Wei K.C. Potential of magnetic nanoparticles for targeted drug delivery. Nanotechnol. Sci. Appl. (2012); 5, 73–86.

- Yang, L. Endotoxin contamination: An interference for nanosafety studies. *NanoToes*. (2014)

- Yang, W, Peters J. I and Williams R. O. Inhaled nanoparticles a current review. *International Journal of Pharmaceutics.* (2008); *356*(1-2), 239-247.

- Yokoyama M. Drug targeting with nano-sized carrier systems. *J. Artif. Organs*. (2011); 8, 238.

- Uhrich K E, Cannizzaro S M, Langer R S and Shakesheff K M. Polymeric systems for controlled drug release. (2011); *Chem. Rev*., 99, 3181.

- Zhang Y, Sun C, Kohler N and Zhang, M. Self-assembled coatings on individual monodisperse magnetite nanoparticles for efficient intracellular uptake. *Biomedical microdevices.* (2004); *6*(1), 33-40.

- Zabow G, Dodd S, Moreland J, Koretsky A. Micro-engineered local field control for high-sensitivity multispectral MRI. *Nature* (2008); 2008:1058–1063

- Zarb P, Coignard B, Griskeviciene J, Muller A, Vankerckhoven V, Weist K, Goossens M, Vaerenberg S, Hopkins S, Catry B, Monnet D, Goossens H, Suetens C. The European Centre f or Disease Prevention and Control (ECDC) pilot point prevalence survey of healthcare-associated infections and antimicrobial use. *Euro Surveillance*. (2012);17(46)

- Zhu M T, Feng W Y, Wang B, Wang T C, Gu Y Q, Wang M, Wang Y, Ouyang H, Zhao Y L and Chai Z F. Comparative study of pulmonary responses to nano- and submicron-sized ferric oxide in rats. *Toxicology*. (2008); 247, 102-111